

Washington University in St. Louis

Washington University Open Scholarship

All Theses and Dissertations (ETDs)

5-24-2010

Structural And Functional Studies On Thrombin Allostery

Prafull Gandhi

Washington University in St. Louis

Follow this and additional works at: <https://openscholarship.wustl.edu/etd>

Recommended Citation

Gandhi, Prafull, "Structural And Functional Studies On Thrombin Allostery" (2010). *All Theses and Dissertations (ETDs)*. 848.

<https://openscholarship.wustl.edu/etd/848>

This Dissertation is brought to you for free and open access by Washington University Open Scholarship. It has been accepted for inclusion in All Theses and Dissertations (ETDs) by an authorized administrator of Washington University Open Scholarship. For more information, please contact digital@wumail.wustl.edu.

WASHINGTON UNIVERSITY IN ST. LOUIS

Division of Biology and Biomedical Sciences

Department of Biochemistry and Molecular Biophysics

Dissertation Examination Committee:

Enrico Di Cera, Co-chairperson

Carl Frieden, Co-chairperson

Eric Galburt

Roberto Galletto

Kathleen Hall

Katherine Henzler-Wildman

John Majors

STRUCTURAL AND FUNCTIONAL STUDIES ON THROMBIN ALLOSTERY

by

Prafull Subhash Gandhi

A dissertation presented to the Graduate School of Arts and Sciences of
Washington University in partial fulfillment of the requirements for the degree of
Doctor of Philosophy

May 2011
Saint Louis, Missouri

ABSTRACT OF THE DISSERTATION

Structural and functional studies on thrombin allostery

by

Prafull Subhash Gandhi

Doctor of Philosophy in Biology and Biomedical Sciences (Molecular Biophysics)

Washington University in St. Louis, 2010

Enrico Di Cera, Co-chairperson

Carl Frieden, Co-chairperson

Thrombin is an allosteric serine protease endowed with important physiological functions in the blood. Once activated, α -thrombin plays procoagulant, prothrombotic, and anticoagulant functions in blood. Its important role in blood coagulation can be emphasized by the fact that thrombin interacts with numerous substrates, cofactors, ligands, and inhibitors. Two well-documented allosteric pathways, involving the Na^+ binding site and the exosite I, regulate thrombin catalytic efficiency and substrate specificity. Identifying structural epitopes of substrate binding, the exact pathway and the molecular basis of allosteric regulation remains challenging.

The case of protease-activated receptor (PAR_1) is particularly relevant in view of the plethora of biological effects associated with its activation by thrombin. We present the crystal structure of thrombin in complex with a 30-residue long

uncleaved extracellular fragment of PAR₁. The structure reveals novel and unexpected features of thrombin-PAR₁ interaction, paving the way for future protein engineering studies. Furthermore, thrombin mutants D102N and WE are stabilized in a self-inhibited conformation, E*, where access to the active site is occluded by a collapse of the entire 215-219 β -strand. Binding of PAR₁ fragment to exosite I, 30-Å away from the active site region, causes a large conformational change and restores access to the active site, akin to the E form in the D102N mutant but not the WE mutant. Using a network of polar interactions, we propose the structural basis of a likely long-range allosteric communication in thrombin. These structural findings, along with kinetic and calorimetry data, indicate that WE is strongly stabilized in the E* form and reveals the molecular basis of its potent anticoagulant property *in vivo*.

We have developed a new expression system using *E. coli* to label thrombin for solution based structural studies. ¹⁹F-NMR results indicate that α -thrombin is a highly dynamic and flexible molecule. Binding of Na⁺, an exosite I ligand, and an irreversible inhibitor induces significant and unique structural and dynamic changes. A zymogen form of thrombin, prethrombin-2, displays unique structural signatures when compared to α -thrombin. ¹⁹F-NMR results corroborate our recent crystallographic data, expand the repertoire obtained from previous x-ray structural studies and highlight the unprecedented and previously undocumented plasticity endowed to a thrombin molecule. Taken together, results presented in

this thesis fill a significant gap in our understanding of the molecular mechanisms of substrate recognition by thrombin and its allosteric regulation.

Dedication

This work is dedicated to my family for their unwavering love, support and encouragement.

Acknowledgements

I would like to acknowledge my advisor Professor Enrico Di Cera. It was his vision, enthusiasm and support that made this work possible. I am forever grateful to you for providing opportunities to learn and advance in my career. Thanks a lot.

I would like to thank all the members of the Di Cera lab with whom I have shared numerous exciting, challenging and fun moments. I would like to thank the members of my thesis committee as well as other faculty members in the department for sharing their insight and guiding me through my thesis work and graduate studies. I would like to thank all the people who have been either directly or indirectly involved with my thesis work. I would like to thank all my friends for the wonderful time that I have had in St. Louis.

I would like to acknowledge the sacrifices my family has made over several years which has allowed me to continue my graduate studies away from home. Thana shivay mein PhD nahi kar sakto tho!

| | |
|--|------------|
| Title Page..... | i |
| Abstract of the Dissertation..... | ii |
| Dedication..... | v |
| Acknowledgements..... | vi |
| Table of Contents..... | vii |
| List of Figures..... | x |
| List of Tables..... | xi |
| Abbreviations..... | xii |

Table of Contents

| | |
|---|-----------|
| 1. Introduction..... | 1 |
| 1.1. Blood coagulation..... | 1 |
| 1.2. Platelet biology..... | 4 |
| 1.3. Thrombin mediated platelet activation..... | 6 |
| 1.4. Thrombin..... | 11 |
| 1.4.1. Structural features of E*..... | 15 |
| 1.4.2. Structural studies of thrombin..... | 16 |
| 1.5. References..... | 21 |
| 2. Crystal structure of thrombin bound to PAR₁..... | 30 |
| 2.1. Prelude..... | 30 |
| 3. Identification of an allosteric pathway..... | 38 |
| 3.1. Prelude..... | 38 |

| | | |
|-----------|--|-----------|
| 3.2. | E* to E transition can be triggered by other exosite I binding ligands... | 38 |
| 3.3. | Evidence from stopped-flow fluorescence studies..... | 40 |
| 4. | Mechanism of the anticoagulant activity of the thrombin mutant WE | |
| 4.1. | Prelude..... | 49 |
| 5. | Expression of thrombin catalytic domain in <i>E. coli</i> | 58 |
| 5.1. | Need for a new recombinant expression system..... | 58 |
| 5.2. | <i>E. coli</i> expression protocol..... | 59 |
| 5.3. | Functional and structural characterization of thrombin expressed in the <i>E. coli</i> expression system..... | 61 |
| 6. | Application of ¹⁹F-NMR to study thrombin structure and allostery | 64 |
| 6.1. | Prelude..... | 64 |
| 6.2. | Introduction..... | 65 |
| 6.3. | Results..... | 67 |
| 6.3.1. | Assignment of ¹⁹ fluorine resonances..... | 67 |
| 6.3.2. | Binding of Na ⁺ , exosite I ligand hirugen, and an irreversible inhibitor PPACK induce significant and distinct structural and dynamic changes..... | 69 |
| 6.3.3. | ¹⁹ F-NMR spectra of prethrombin-2..... | 71 |
| 6.3.4. | Thermodynamics of ligand induced allostery in thrombin..... | 72 |
| 6.4. | Discussions..... | 73 |
| 6.4.1. | ¹⁹ F-tryptophan as a probe to study thrombin allostery..... | 74 |
| 6.4.2. | Is the thrombin scaffold flexible?..... | 76 |

| | |
|---|------------|
| 6.4.3. How different is the zymogen from the α -thrombin?..... | 80 |
| 6.4.4. Conundrum of substituting wild-type by mutant thrombin..... | 83 |
| 6.5. Materials and Methods..... | 84 |
| 6.6. References..... | 92 |
| 7. Future | |
| directions..... | 99 |
| 7.1. Protein Engineering..... | 100 |
| 7.2. Crystal structure of thrombin bound to PAR ₄ | 101 |
| 7.3. Structural studies of E* and E..... | 101 |
| 7.4. NMR studies of thrombin..... | 102 |
| Curriculum Vitae | 104 |

List of Figures

| | |
|--|----|
| 1.1. The blood coagulation cascade..... | 2 |
| 1.2. Mechanism of PAR ₁ cleavage by thrombin..... | 7 |
| 1.3. The three forms of thrombin..... | 11 |
| 1.4. Prothrombin proteolytic derivatives..... | 12 |
| 1.5. X-ray crystal structure of the catalytic domain of α -thrombin..... | 13 |
| 1.6. Structural features of E* | 15 |
| 3.1. E* to E transition can be triggered by other exosite I ligands..... | 39 |
| 3.2. Effect of hirugen on the dependence of k_{obs} on [Na ⁺]..... | 41 |
| 5.1. Structural Crystal structure of α -thrombin expressed in <i>E. coli</i> | 63 |
| 6.1. Alignment of <i>E. coli</i> expressed wild-type ¹⁹ F-thrombin and BHK expressed wild-type thrombin bound to PPACK..... | 87 |
| 6.2. ¹⁹ F-NMR spectra of apo wild-type (black) and WE mutant (blue) in α -thrombin and prethrombin-2 forms..... | 88 |
| 6.3. ¹⁹ F-NMR spectra of wild-type α -thrombin and prethrombin-2 in the apo form, in presence of Na ⁺ , in presence of hirugen, and in presence of Na ⁺ , hirugen and PPACK..... | 89 |
| 6.4. Argatroban binding to thrombin variants using isothermal titration calorimetry..... | 90 |

List of Tables

| | |
|--|----|
| 3.1. Summary of the crystallographic parameters..... | 40 |
| 5.1. Catalytic efficiency of thrombin expressed in BHK and E. coli expression systems towards FPR..... | 62 |
| 6.1. Catalytic efficiency, k_{cat}/K_m ($\mu\text{M}^{-1}\cdot\text{sec}^{-1}$), of ^{19}F labeled wild-type and unlabeled wild-type for different substrates..... | 87 |
| 6.2. Crystallographic parameters..... | |
| 6.3. Sequence alignment of thrombin from 27 different species. | 91 |

Abbreviations

k_{cat} Catalytic constant

K_m Michaelis constant

s k_{cat}/K_m

Å Angstrom unit (1 Å = 0.1nm)

ChCl Choline Chloride

NaCl Sodium Chloride

PC Protein C

aPC Activated protein C

TM Thrombomodulin

TF Tissue factor

PAR₁ Protease-activated receptor 1

FPR D-Phenylalanine-Proline-Arginine-p-nitroanalide

FPK D-Phenylalanine-Proline-Lysine-p-nitroanalide

FXa Activated coagulation factor X (similar for other coagulation proteases)

PEG Polyethylene glycol

Tris-HCl Tris(hydroxymethyl)aminomethane hydrochloride

1. Introduction

1.1. Blood coagulation:

The process of blood coagulation involves several proteins that act together following vascular injury to generate a clot that prevents severe loss of body fluids and/or pathogenic invasion. The initiation and termination of the clotting process is timely and localized, otherwise uncontrolled clot formation will result in the occlusion of blood vessels and thrombosis, which can lead to cardiovascular diseases such as ischemic strokes and heart attacks. Thus, a tightly-regulated coagulation process is essential for survival to prevent excessive bleeding or widespread clot deposits. The cascade of events leading to the formation of a blood clot can be initiated through two pathways known as the intrinsic (contact) and extrinsic (tissue factor) pathways. Each pathway consists of a series of zymogen activation steps where a newly activated enzyme catalyzes the activation of the next zymogen in the series until prothrombin is converted to α -thrombin (1).

Laboratory and clinical data have shown that the primary route of initiating the coagulation cascade after vascular injury is the extrinsic pathway (1). The central event of the coagulation cascade is the formation of thrombin, and can be divided into three distinct phases (initiation, propagation and termination). Vascular lesion causes the exposure of tissue factor to the blood stream forming a complex with factor VIIa. This results in the generation of small quantities of factors IXa and Xa (2, 3). This small concentration of Xa produces minute amounts of

thrombin (initial phase) that can activate factor XI and cofactors VIII and V. During the

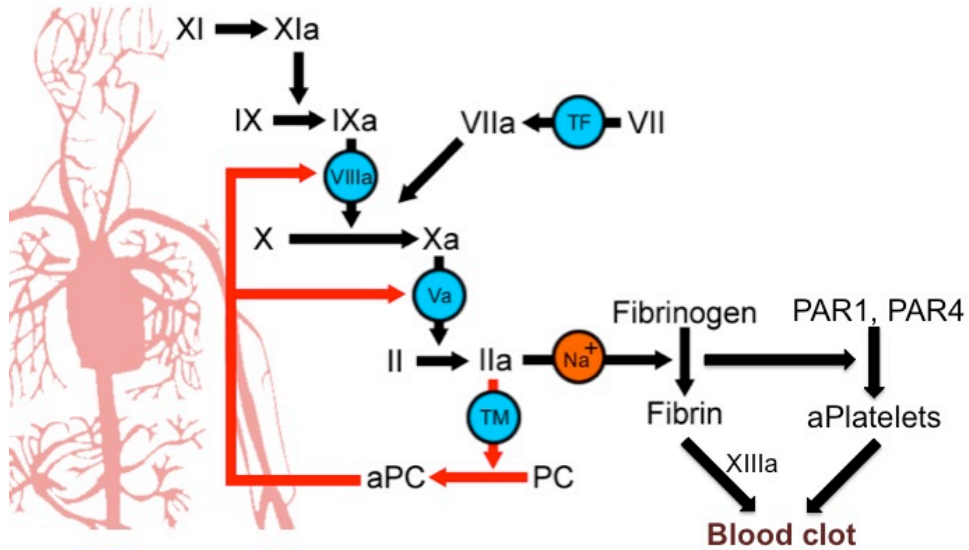


Figure 1.1. The Blood Coagulation Cascade. Shown are the intrinsic (contact) and extrinsic (tissue factor, TF) pathways of initiating the coagulation cascade. Lower case “a” denotes the activated form of the clotting factors.

propagation phase, the procoagulant complexes are assembled, and they enhance the generation of factor Xa and thrombin in the tenase (IXa, VIIIa, Ca²⁺, phospholipids, X) and prothrombinase (Xa, Va, Ca²⁺, phospholipids, prothrombin) complexes by ~5 orders of magnitude relative to their free enzymes. The termination phase involves the coordination of stoichiometric and dynamic inhibitors that down regulate the explosive generation of thrombin to halt the progression of the coagulation cascade. Although antithrombin III (AT-III) and the tissue factor pathway inhibitor (TFPI) are the principal stoichiometric inhibitors,

heparin cofactor II, α_2 -macroglobulin, α_1 -antitrypsin, and activated protein C inhibitor are essential inhibitors that contribute in regulating the coagulation cascade as well (4, 5). AT-III is a potent neutralizer of all the procoagulant enzymes while TFPI shuts down the generation of factors IXa and Xa by effectively inhibiting the tissue factor VIIa-Xa complex.

Once activated, thrombin plays a central role in blood coagulation by acting as a procoagulant, prothrombotic and as an anticoagulant agent in the blood (6, 7). As a procoagulant, thrombin cleaves fibrinogen in blood plasma and activates factor XIII, creating monomers of fibrin that then polymerize into a mesh, assisted by factor XIIIa, across a wound in a blood-vessel wall. As a prothrombotic agent, thrombin activates platelets by cleaving protease-activated receptors (8). Activated platelets and the fibrin meshwork form a stable clot that prevents bleeding long enough for healing to occur. In addition, thrombin down regulates the fibrinolytic system by activating Thrombin-Activatable Fibrinolysis Inhibitor (TAFI). TAFIa removes C-terminal lysine and arginine residues from fibrin, hence reducing the ability of fibrin to initiate the fibrinolytic response. As an anticoagulant, thrombin activates protein C (9). Binding of the cofactor thrombomodulin, suppresses the ability of thrombin to cleave PARs or fibrinogen but enhances > 1000-fold the specificity toward the zymogen protein C (10, 11). Activated protein C (aPC) cleaves and inactivates factors Va and VIIIa, two essential cofactors of coagulation factors Xa and IXa that are required for thrombin generation, thereby down regulating

both the amplification and progression of the coagulation cascade. Efficiency of the coagulation system requires that the response be rapid, localized at the injury site, and then readily terminated. Insufficient amounts of thrombin may result in hemorrhage whereas overproduction or failure to efficiently inhibit thrombin activity results in thrombosis.

1.2. Platelet Biology:

Accumulation of platelets at the site of vascular injury is the first step in the formation of hemostatic plug and plays a key role in the prevention of blood loss after injury. However, excessive or uncontrolled platelet activation may lead to the formation of pathogenic thrombi that can result in atherothrombotic condition (12). A detailed understanding of platelet biology is therefore required.

Platelets are produced by megakaryocytes as anucleate cells that lack genomic DNA but contain megakaryocyte-derived messenger RNA (mRNA) and the translational machinery needed for protein synthesis. Pre-mRNA splicing, a typical nuclear function, has been detected in the cytoplasm of platelets, and the platelet transcriptome contains approximately 3000 to 6000 transcripts. After leaving the bone marrow, platelets circulate in the blood in a quiescent state for about 10 days. Their activation is inhibited by nitric oxide and prostaglandin I₂ released from endothelial cells. However, once activated, platelets primary function is to stop bleeding after tissue trauma and vascular injury. Platelets are essential for primary

hemostasis and repair of the endothelium, but they also play a key role in the formation of pathogenic thrombi/plaques in patients with atherothrombotic disease, such as acute coronary syndromes, ischemic stroke, and peripheral artery disease (13).

There are at least five unique platelet activation pathways (14) mediated by a) adenosine diphosphate (ADP), b) thromboxane A₂ (TXA₂), c) serotonin, d) collagen, and e) thrombin. Two ADP receptors P₂Y₁ and P₂Y₁₂ are responsible for change in platelet shape, transient aggregation, and signaling cascade that culminate in platelet aggregation and thrombus growth and stabilization. P₂Y₁₂ plays a critical growth in the amplification of platelet aggregation induced by other agents, including TXA₂, serotonin, and thrombin. Once activated, platelets release TXA₂ that promotes amplification of platelet adhesion response by binding to TP α and TP β receptors. Binding to these receptors results in change of shape and enhancement of recruitment and aggregation of platelets to the primary platelet plug. It is also responsible for contraction of microvessels downstream to disturb blood flow. Serotonin is a vasoconstrictor that binds its receptors and amplifies the platelet response by stimulating shape change and aiding platelet recruitment to sites of injury. It may also play a procoagulant role by promoting retention of the procoagulant proteins, fibrinogen, and thrombospondin on the platelet surface. Under high shear conditions, collagen interacts with GpIb via vWF and activates GPIIb/IIIa eventually leading to stable vWF-mediated platelet aggregates. Under

low shear conditions, collagen serves as an adhesive substrate for platelets via the GPIa/IIa ($\alpha_2\beta_1$ integrin) and GPVI collagen receptors. GPVI is the major collagen receptor mediating the platelet activation that is necessary for adhesion, aggregation, deregulation, and coagulation activity of the matrix protein. Binding of collagen to GPVI triggers intracellular signals that shift platelet integrins to a high-affinity state and induces release of ADP and TXA₂. Finally, serine proteases including trypsin, tryptase, fVIIa, fXa, and thrombin activate platelets through protease-activated receptors (PARs).

There are several existing strategies to inhibit or slow down platelet activation and aggregation with proven clinical benefits (15). Aspirin is used to inhibit expression of TXA₂, while P₂Y₁₂ receptor antagonist is used to interfere with ADP binding. Although beneficial, the residual morbidity and mortality among those receiving these medications still remain significantly high. Furthermore, existing antiplatelet interventions are associated with bleeding risk most likely due to inhibition of platelet activation pathway required for normal hemostasis. As a result, there is a need to develop novel and efficacious strategies. Amongst various possibilities, inhibition of PARs mediated platelet activation pathway has emerged as a promising strategy.

1.3. Thrombin mediated platelet activation:

Thrombin is a very potent platelet agonist that activates platelets at extremely low concentrations. Thrombin-mediated platelet activation contributes to pathological thrombosis through the formation of an occlusive platelet-rich thrombus. Platelets express protease-activated receptors (PARs) on their surface. Besides playing an important role in blood coagulation, PARs have been implicated in vascular homeostasis, inflammation, cancer, and embryogenesis (16-19). PARs are conventionally placed within a large family of cell-surface receptors that work

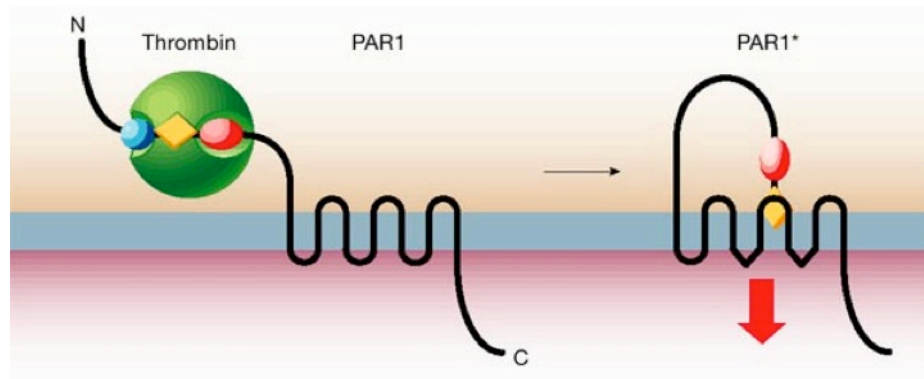


Figure 1.2. Mechanism of PAR₁ cleavage by thrombin. Thrombin recognizes the N-terminal exodomain of PAR₁ by interacting with sites both amino (blue sphere) and carboxyl terminal (red oval). Thrombin cleaves the peptide bond between receptor residues Arg₄₁ and Ser₄₂ (peptide bond between blue sphere and yellow diamond). This serves to unmask a new amino terminus beginning with the sequence SFLLRN (yellow diamond) that functions as a tethered ligand, docking intramolecularly with the body of the receptor to effect transmembrane signaling eventually leading to platelet aggregation.

through intracellular switches called G protein coupled receptors (GPCR). Four members of the PAR family have been identified: PAR 1 – 4 and they all share the basic mechanism of activation (20, 21). Thrombin – PARs interaction leads to platelet activation and eventual aggregation. Thrombin cleaves PAR 1, PAR 3, and PAR 4 but not PAR 2 (19, 22-24). The finding that simultaneous blockade of PAR 1 and PAR 4 abolishes the ability of human platelets to respond to thrombin (25) suggests that human platelets express PAR 1 and PAR 4 on their surface. Thrombin recognizes the N – terminal exodomain of PAR 1 and cleaves the peptide bond between receptor residues Arg₄₁ and Ser₄₂. This serves to unmask a new amino terminus beginning with the sequence ⁴²SFLLRN (diamond) that functions as a tethered ligand, docking intramolecularly with the body of the receptor to effect transmembrane signaling and eventual platelet aggregation. It is well documented that PAR 1 is a better substrate for thrombin than PAR 4 (26-28). When both are present cleavage of PAR 1 presumably precedes cleavage of PAR 4 as thrombin accumulates (25, 29). On the other hand, once PAR 4 is cleaved, it appears to signal for longer (30). Activation of PAR 1 and PAR 4 promotes platelet aggregation in humans and unfolds the prothrombotic role of thrombin in the blood.

Because of its central role in thrombotic disorders, thrombin has emerged as a key target for drug discovery. Current strategies aimed at providing safer alternatives to vitamin K antagonists and antithrombin activators (heparinoids) are based on the inhibition of thrombin (and factor Xa) at the active site (31-33). However, an

active-site inhibitor of thrombin shuts down procoagulant, prothrombotic and anticoagulant activities of the enzyme and often poses serious problems with safety. A more promising strategy would be to generate anticoagulant activity in the circulation that can be overwhelmed, when needed, by hemostatic thrombin generation at the immediate site of vessel wall injury. In this regard, mutant thrombins with compromised procoagulant activity, but that retain the ability to activate PC may offer a significant therapeutic advantage (34-36). Once administered in the circulation, these anticoagulant thrombin mutants (ATMs) can maintain high levels of aPC and temper the coagulation response. For such a possibility, it is crucial to delineate thrombin – PARs interactions so that it can be exploited for rational drug design. For drugs targeting PARs, it is therefore obvious that both PAR₁ and PAR₄ should be targeted for better efficacy.

In the first half of this thesis, we present the crystal structure of thrombin bound to an extracellular fragment of hPAR 1. Our model depicts a productive binding mode with numerous H bond and van der Waals (vdW) interactions. Our model corroborates previous site-directed mutagenesis results as well as reveals novel intermolecular interactions. These novel interactions could be exploited to engineer thrombin devoid of any prothrombotic activity in order to improve the anticoagulant potency of engineered thrombin mutants.

Thrombin allostery:

Allostery is widely regarded as the second secret of life, second only to the genetic code. Allostery is a common mechanism of regulation of enzyme activity and specificity. For the purposes of this thesis, we define an allosteric event such that events occurring at a given site of the protein can be transmitted long-range to affect affinity or catalytic efficiency at a distant site. It was convincingly shown that thrombin is a Na^+ -activated (37), allosteric serine protease. While Na^+ improves the catalytic efficiency of thrombin towards fibrinogen and PARs, it is dispensable for its activity toward protein C. Instead, thrombomodulin, a cofactor that binds at thrombin exosite I, enhances its catalytic efficiency towards protein C by ~ 1000 fold. Besides thrombomodulin, there are several peptides that bind to exosite I and allosterically modulate thrombin catalytic efficiency towards synthetic substrates. Two well documented distinct long-range allosteric pathways are known, a) one employing the Na^+ binding site and b) the other employing the exosite I form the basis of thrombin's opposing functions (38, 39). X-ray crystal structures of thrombin free of Na^+ , E, and bound to Na^+ , E: Na^+ , have been solved and display subtle but important structural differences (40-42). It was recently established that in addition to the E and the E: Na^+ forms of thrombin, there is a third form of the enzyme, E*, that can neither bind/cleave substrates nor bind Na^+ (43, 44). Using stopped-flow to monitor fluorescence change upon Na^+ binding to wild-type thrombin, it was reported that at 15 °C the ratio between E* to E is 1:3. The physiological concentration of Na^+ (140 mM) is not enough to saturate thrombin (K_d for Na^+ binding to thrombin is 110 mM at 37 °C). As a result, both the E and

$E:Na^+$ forms of thrombin are significantly populated (2:3 ratio) while the E^* state is populated $< 1\%$ *in vivo*.

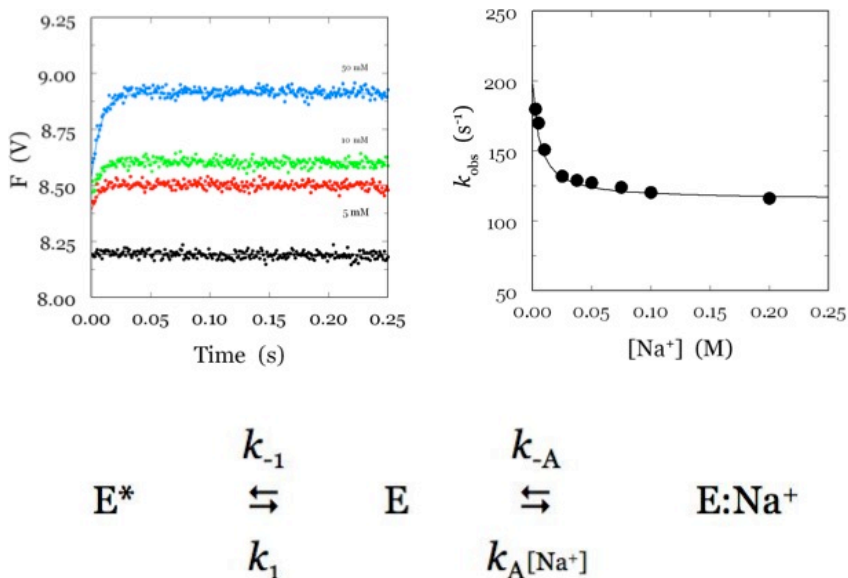


Figure 1.3. The three forms of thrombin. Stopped-flow fluorescence experiments reveal the mechanism of Na^+ binding to thrombin. Na^+ binds to thrombin in a two-step mechanism with a rapid phase occurring within the dead time of the spectrometer (< 0.5 ms) followed by a single-exponential slow phase whose k_{obs} decreases hyperbolically with increasing Na^+ . The rapid phase is due to Na^+ binding to the enzyme E to generate the $E:Na^+$ form. The slow phase is due to the interconversion between E^* and E , where E^* is a form that cannot bind Na^+ .

1.4. Thrombin:

Prothrombin is the most abundant of the vitamin K-dependant proteases and it circulates in the plasma at a concentration of 1-2 μM . Prothrombin is the zymogen precursor of thrombin and has no catalytic activity. It is mainly synthesized in the liver, expressed as a 622 amino acid protein from which a 43 amino acid prepropeptide is excised during extracellular secretion. The remainder of the 579 amino

acids can be divided into the following domains as shown in the figure 1.4, Gla domain (res. 1-40), Kringle 1 (res. 41-155), Kringle 2 (res. 156-271), and catalytic domain (res. 272-579). Prothrombin contains 10 carboxyglutamic acids, forming the Gla domain, and 3 carbohydrate side chains incorporated at three Asp residues. The calcium bound conformation of the Gla domain in PT greatly enhances binding to the phospholipid membrane during activation. Lack of glutamic acid modification prevents activation with the prothrombinase complex. A number of thrombin derivatives can be formed depending on the site of cleavage by the activation complex.

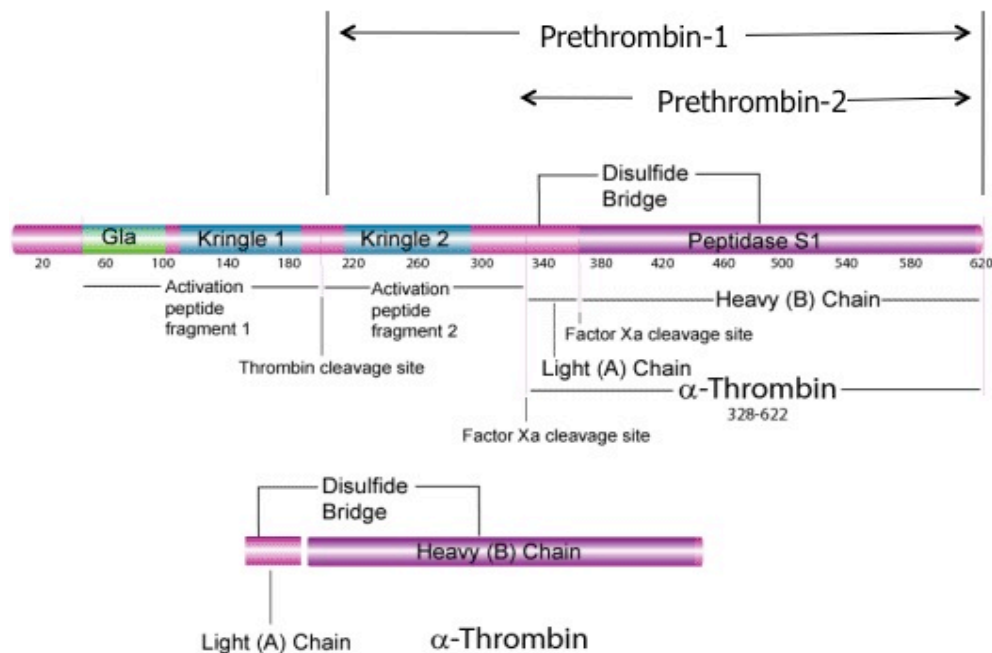


Figure 1.4. Prothrombin proteolytic derivatives.

There is no clear evidence of any specific intermediate being favored along the activation pathway. The closest zymogen form of thrombin is the prothrombin-2.

Prethrombin-2 is a single chain protein. Cleavage of the Arg₁₅-Ile₁₆ peptide bond, within prethrombin-2, exposes the N-terminus of Ile₁₆. This new N-terminus inserts into the core of the protein where it engages the Asp₁₉₄ and confers catalytic activity. The catalytically active form of thrombin is referred to as α -thrombin.

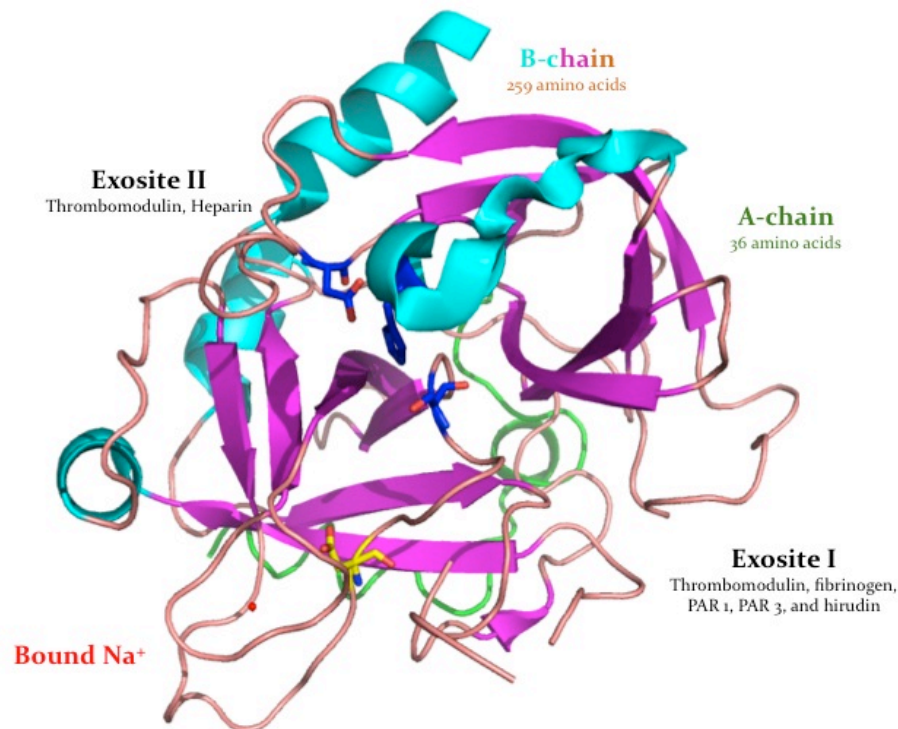


Figure 1.5. X-ray crystal structure of the catalytic domain of α -thrombin. The catalytic domain of α -thrombin is composed of two chains, the A-chain and the B-chain connected by a single disulfide bond. Important domains and loops are highlighted. Residues belonging to the catalytic triad, His₅₇, Asp₁₀₂, and Ser₁₉₅, are shown in stick model (blue). Asp₁₈₉ (yellow) is shown at the bottom of the primary specificity pocket that confers specificity of thrombin towards substrates carrying a positively charged residue (70).

α -thrombin is a member of the chymotrypsin family and folds in a typical trypsin-like architecture consisting of two six-stranded beta barrels with the active site housed at their interface. The catalytic triad is made of His₅₇, Asp₁₀₂, and Ser₁₉₅. The nomenclature used for residue numbering in this work is based on the chymotrypsin numbering as described by Bode, W. et al., 1992. Active thrombin, a 33.8 kDa serine protease, is composed of two polypeptide chains of 36 (A chain) and 259 (B chain) residues that are covalently linked by a single disulfide bond (Cys₁-Cys₁₂₂). There are three other disulfide bonds in the B chain (Cys₄₂-Cys₅₈, Cys₁₆₈-Cys₁₈₂, and Cys₁₉₁-Cys₂₂₀). While the exact role of the A chain in thrombin remains to be elucidated, the B chain carries the functional epitopes of the enzyme. While neutral at physiological conditions, thrombin carries two positively charged patches in the east and north rims, exosite I and II respectively, and a negatively charged portion surround the catalytic pocket. The majority of these charged residues are surface exposed and a number of them form salt bridges and ion clusters. The uneven charge distribution on the surface helps in the orientation of approaching ligands in solution through long-range electrostatic forces. The active site of thrombin forms a deep canyon groove, and is strategically located between the Na⁺ binding site, exosite I and exosite II. There are several loops that confer upon thrombin its substrate specificity. Of the various loops, the autolysis loop has been thought to be extremely flexible.

1.4.1. Structural features of E*: Significant progress in the field was achieved by

solving the crystal structure of the thrombin mutant D102N (PDB: 2GP9), (46). The D102N crystal structure was solved at 1.87-Å, free of Na⁺ and any active site inhibitors, and shows an occluded active site and a collapsed Na⁺ binding site. The crystal structure documents a drastic rearrangement in the active site architecture where the 215-219 β-strand collapses into the primary specificity pocket. W215 rotates 130° at the C_β and causes the indole ring to pack against the hydrophobic pocket in the active site formed by W60d, Y60a, H57, and L99. Such a conformation of W215 essentially abrogates substrate binding at the active site.

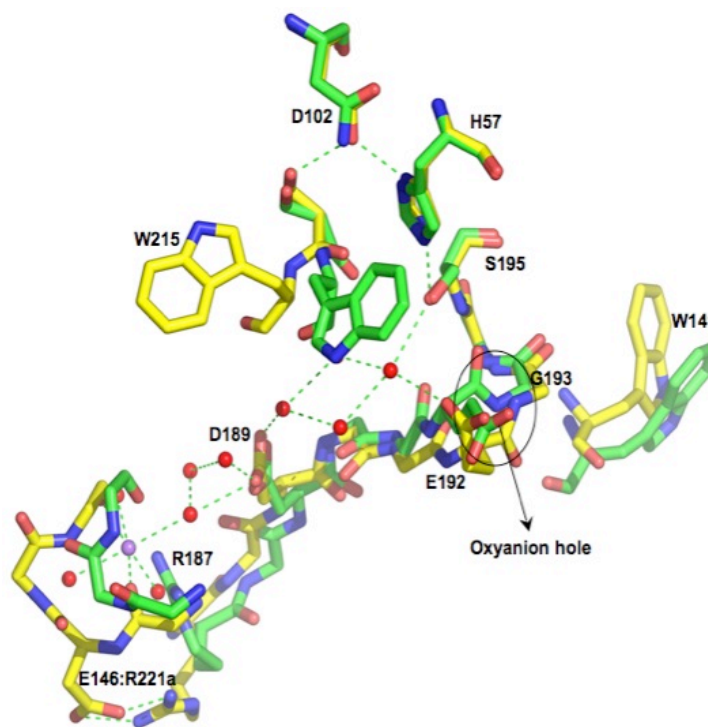


Figure 1.6. Structural features of E*. The crystal structure E* form of thrombin documents a collapse in the active site, an abrogated Na⁺ binding site as well as a disrupted oxyanion hole.

Further downstream, the twist in W₂₁₅ results in movement of the entire 220-loop disrupting the Na⁺ binding site. By occupying the Na⁺ binding site, R₁₈₇ disrupts the crosstalk between the Na⁺ binding site and S₁₉₅. Furthermore, the oxyanion hole is disrupted because of the flip in the peptide bond between the E₁₉₂ and the G₁₉₃ residues. There is a substantial movement in the side-chain of W₁₄₁ close to the active site. The crystal structure of D_{102N} presents all the properties expected of E* and documents a self-inhibited conformation unable to bind either substrate or Na⁺. Indeed, stopped-flow fluorescence analysis of this mutant showed that the ratio of E* to E is 1:1 at 15 °C. The crystal structure of E* was later confirmed when I was able to crystallize the D_{102N} mutant at even higher resolution of 1.55-Å (PDB: 3BEI) (47). Further studies have revealed two unique mutants, the autolysis loop deletion mutant and N_{143P}, adopting an E* like conformation. The relevance of E* is underscored by the fact that similar collapse, although to a lesser extent, in the active site and the Na⁺ binding site has been observed in other anticoagulant thrombin mutants, WE and E_{217K} mutants (48-50). More recently, it was shown that the zymogen form of thrombin, prethrombin-1, adopts an E* like structure (51).

1.4.2. Structural studies of thrombin:

X-ray crystallography has revealed remarkable secrets about macromolecular recognition and substrate specificity in thrombin. Tracking allosteric changes in the thrombin scaffold as a result of ligand interaction is still challenging. Several

crystal structures of thrombin bound to various ligands have been reported in the literature with a lack of significant conformational transitions. This was interpreted as thrombin fold being rather rigid (52).

Extensive biochemical studies on thrombin have shown that the active site, Na⁺ binding site and exosite I are energetically linked (53-56). Similar sites in other serine proteases (activated Protein C, fXa) are also known to be linked energetically (57, 58). X-ray crystallography has shown that, thrombin crystallized in presence of an active-site inhibitor, and devoid of Na⁺, essentially adopts the same conformation as thrombin crystallized in presence of Na⁺, free of any active site inhibitors. The two most striking examples are the crystal structures of thrombin bound to thrombomodulin and hirugen respectively. The crystal structure of thrombin bound to thrombomodulin represented a remarkable achievement in the field but showed no conformational changes in thrombin as a result of thrombomodulin binding (59). The free and the thrombomodulin bound structures of thrombin are so similar that the authors suggested that maybe the action of thrombomodulin is not to change allosterically the conformation of the enzyme, but rather to provide a scaffold for optimal protein C diffusion. Critics of this structure have pointed out that it was solved in the presence of an active site inhibitor, EGR-chloromethylketone, that could abrogate potential structural changes induced by thrombomodulin binding within the active site of the enzyme. The second example is the structure of thrombin bound to hirugen, where the

acidic C-terminal tail of hirudin binds specifically to exosite I and elicits changes in activity and specificity toward substrates and active site inhibitors. The hirugen complex was solved without any inhibitor in the active site, but like the thrombomodulin complex, it failed to reveal any significant changes within the active site of the enzyme. Critics of this structure point out that it was crystallized in presence of 187 mM NaCl, 13.5 % PEG 8000, 0.5 mM sodium azide, and 75 mM sodium phosphate buffer pH = 7.3 (60). The monovalent cation Na^+ acts as an allosteric regulator and can potentially mask the conformational change that hirugen could have induced. Therefore, to observe allosteric changes in thrombin structure, it is vital to crystallize the complex in the absence of any active site probes and any other modulators (like the monovalent cations Na^+ or K^+).

Lack of conformational change in the previous structures can be attributed to a variety of reasons ranging from crystal contacts to the presence of thrombin effectors in the crystallization conditions. It is very difficult to predict the correct and optimum buffer conditions that will aid in crystal nucleation and its growth. Often, crystallization conditions need to include functionally unnecessary reagents to induce crystallization with little information on their effects on thrombin function. Furthermore, a homogeneous protein sample does not guarantee diffraction quality crystals, which is often the bottleneck in structural studies based on x-ray crystallography. Finally, crystal packing can potentially mask the true conformation of the enzyme.

Unambiguous interpretation of the allosteric effect requires crystals of thrombin with the ligand under consideration in absence of any other thrombin effectors. Often this turns out to be a non-trivial endeavor. In contrast, NMR not only offers structural information of the lowest energy conformation, like x-ray crystallography does, but also provides information on protein dynamics in solution (61). Information on the lowest energy conformers and possible transitions among them is crucial to our understanding. Such experiments can easily be scaled to study allosteric communication by performing similar experiments with different ligands or effectors to gather information on conformational transitions resulting from ligand binding. The biggest advantage of NMR is that it allows access to structural information under desired solution conditions as long as the protein remains stable and allows one to ask physiologically relevant questions in relevant buffer conditions.

NMR has been successfully applied to thrombin substrates including PAR₁ (62), PAR₄ (63), fXIII activation peptide (64-66), and γ' peptide (67) as well as thrombomodulin (TM), a thrombin cofactor (68, 69). NMR studies on PAR₁ documented a major conformational transition in PAR₁ peptide upon thrombin cleavage while studies on γ' peptide revealed formation of a significant secondary structure upon binding to thrombin exosite II. NMR studies of TM revealed a correlation between backbone dynamics and anticoagulant cofactor activity. NMR

studies on thrombin substrates and cofactor have elegantly captured the conformational transitions upon thrombin binding/cleavage and have underscored the role of protein dynamics in macromolecular recognition.

In the present thesis, I have employed molecular biology, various biophysical techniques and structural biology including x-ray crystallography and ^{19}F -NMR to probe properties of thrombin. Chapter 1 presents a brief introduction to relevant aspects of thrombin biology. A detailed description of our current understanding of thrombin is provided. Chapter 2 presents the crystal structure of thrombin in complex with the uncleaved extracellular fragment of PAR₁ depicting a productive binding mode. Our model reveals a wealth of novel interactions that could be exploited for protein engineering studies. Chapter 3 presents crystallographic evidence of long-range allosteric communication in thrombin upon cleaved PAR₁ binding at exosite I. Our model reveals the molecular basis of allosteric communication between the two sites. In chapter 4, we extend our study to a clinically relevant thrombin mutant, W₂₁₅A/E₂₁₇A, and explain the basis of its anticoagulant potency using isothermal titration calorimetry and x-ray crystallography. Chapter 5 provides the details of our new expression system using *E. coli*. Our kinetic and structural data show that thrombin expressed using *E. coli* expression system has similar properties to thrombin expressed using the mammalian expression system. Chapter 6 provides the details on the technique to label thrombin with ^{19}F -tryptophan. Using ^{19}F -NMR spectroscopy, we show for the

first time that apo wild-type α -thrombin is a highly dynamic and flexible molecule when compared to its closest zymogen form prethrombin-2. Further, we show that binding of Na^+ and hirugen brings about significant and distinct changes in the α -thrombin scaffold not observed in crystal structures.

1.6. References:

1. Mann KG (2003) Thrombin formation. *Chest* 124(3 Suppl):4S-10S.
2. Gailani D & Broze GJ, Jr. (1991) Factor XI activation in a revised model of blood coagulation. *Science* 253(5022):909-912.
3. Girard TJ, *et al.* (1990) Inhibition of factor VIIa-tissue factor coagulation activity by a hybrid protein. *Science* 248(4961):1421-1424.
4. Gettins PG (2002) Serpin structure, mechanism, and function. *Chem Rev* 102(12):4751-4804.
5. Tollefsen DM (2007) Heparin cofactor II modulates the response to vascular injury. *Arteriosclerosis, thrombosis, and vascular biology* 27(3):454-460.
6. Davie EW & Kulman JD (2006) An overview of the structure and function of thrombin. *Seminars in thrombosis and hemostasis* 32 Suppl 1:3-15.
7. Di Cera E (2003) Thrombin interactions. *Chest* 124(3 Suppl):11S-17S.
8. Coughlin SR (2005) Protease-activated receptors in hemostasis, thrombosis and vascular biology. *J Thromb Haemost* 3(8):1800-1814.
9. Esmon CT (2000) Regulation of blood coagulation. *Biochim Biophys Acta* 1477(1-2):349-360.

10. Esmon CT (1989) The roles of protein C and thrombomodulin in the regulation of blood coagulation. *J Biol Chem* 264(9):4743-4746.
11. Sadler JE (1997) Thrombomodulin structure and function. *Thromb Haemost* 78(1):392-395.
12. Jennings LK (2009) Role of platelets in atherothrombosis. *Am J Cardiol* 103(3 Suppl):4A-10A.
13. Angiolillo DJ, Ueno M, & Goto S (2010) Basic principles of platelet biology and clinical implications. *Circ J* 74(4):597-607.
14. Jennings LK (2009) Mechanisms of platelet activation: need for new strategies to protect against platelet-mediated atherothrombosis. *Thrombosis and haemostasis* 102(2):248-257.
15. Gaglia MA, Jr., Manoukian SV, & Waksman R (2010) Novel antiplatelet therapy. *Am Heart J* 160(4):595-604.
16. Cunningham MA, *et al.* (2000) Protease-activated receptor 1 mediates thrombin-dependent, cell-mediated renal inflammation in crescentic glomerulonephritis. *J Exp Med* 191(3):455-462.
17. Fiorucci S, *et al.* (2001) Proteinase-activated receptor 2 is an anti-inflammatory signal for colonic lamina propria lymphocytes in a mouse model of colitis. *Proc Natl Acad Sci U S A* 98(24):13936-13941.
18. Leger AJ, Covic L, & Kuliopulos A (2006) Protease-activated receptors in cardiovascular diseases. *Circulation* 114(10):1070-1077.

19. Sambrano GR, Weiss EJ, Zheng YW, Huang W, & Coughlin SR (2001) Role of thrombin signalling in platelets in haemostasis and thrombosis. *Nature* 413(6851):74-78.
20. Brass S (2001) Cardiovascular biology. Platelets and proteases. *Nature* 413(6851):26-27.
21. O'Brien PJ, Molino M, Kahn M, & Brass LF (2001) Protease activated receptors: theme and variations. *Oncogene* 20(13):1570-1581.
22. Ishihara H, *et al.* (1997) Protease-activated receptor 3 is a second thrombin receptor in humans. *Nature* 386(6624):502-506.
23. Nakanishi-Matsui M, *et al.* (2000) PAR3 is a cofactor for PAR4 activation by thrombin. *Nature* 404(6778):609-613.
24. Vu TK, Wheaton VI, Hung DT, Charo I, & Coughlin SR (1991) Domains specifying thrombin-receptor interaction. *Nature* 353(6345):674-677.
25. Kahn ML, *et al.* (1998) A dual thrombin receptor system for platelet activation. *Nature* 394(6694):690-694.
26. Ayala Y & Di Cera E (1994) Molecular recognition by thrombin. Role of the slow-->fast transition, site-specific ion binding energetics and thermodynamic mapping of structural components. *J Mol Biol* 235(2):733-746.
27. Coughlin SR (2001) Protease-activated receptors in vascular biology. *Thromb Haemost* 86(1):298-307.

28. Kataoka H, *et al.* (2003) Protease-activated receptors 1 and 4 mediate thrombin signaling in endothelial cells. *Blood* 102(9):3224-3231.
29. Xu WF, *et al.* (1998) Cloning and characterization of human protease-activated receptor 4. *Proc Natl Acad Sci U S A* 95(12):6642-6646.
30. Covic L, Gresser AL, & Kuliopulos A (2000) Biphasic kinetics of activation and signaling for PAR₁ and PAR₄ thrombin receptors in platelets. *Biochemistry* 39(18):5458-5467.
31. Adang AE, *et al.* (2002) Unique overlap in the prerequisites for thrombin inhibition and oral bioavailability resulting in potent oral antithrombotics. *J Med Chem* 45(20):4419-4432.
32. Brady SF, *et al.* (1998) Discovery and development of the novel potent orally active thrombin inhibitor N-(9-hydroxy-9-fluorene-carboxy)prolyl trans-4-aminocyclohexylmethyl amide (L-372,460): coapplication of structure-based design and rapid multiple analogue synthesis on solid support. *J Med Chem* 41(3):401-406.
33. Feng DM, *et al.* (1997) Discovery of a novel, selective, and orally bioavailable class of thrombin inhibitors incorporating aminopyridyl moieties at the P₁ position. *J Med Chem* 40(23):3726-3733.
34. Gibbs CS, *et al.* (1995) Conversion of thrombin into an anticoagulant by protein engineering. *Nature* 378(6555):413-416.
35. Griffin JH (1995) Blood coagulation. The thrombin paradox. *Nature* 378(6555):337-338.

36. Grinnell BW (1997) Tipping the balance of blood coagulation. *Nat Biotechnol* 15(2):124-125.
37. Wells CM & Di Cera E (1992) Thrombin is a Na(+)-activated enzyme. *Biochemistry* 31(47):11721-11730.
38. Di Cera E, Page MJ, Bah A, Bush-Pelc LA, & Garvey LC (2007) Thrombin allostery. *Phys Chem Chem Phys* 9(11):1291-1306.
39. Huntington JA (2005) Molecular recognition mechanisms of thrombin. *J Thromb Haemost* 3(8):1861-1872.
40. Huntington JA & Esmon CT (2003) The molecular basis of thrombin allostery revealed by a 1.8 Å structure of the "slow" form. *Structure* 11(4):469-479.
41. Pineda AO, *et al.* (2004) Molecular dissection of Na⁺ binding to thrombin. *The Journal of biological chemistry* 279(30):31842-31853.
42. Pineda AO, Savvides SN, Waksman G, & Di Cera E (2002) Crystal structure of the anticoagulant slow form of thrombin. *The Journal of biological chemistry* 277(43):40177-40180.
43. Bah A, Garvey LC, Ge J, & Di Cera E (2006) Rapid kinetics of Na⁺ binding to thrombin. *The Journal of biological chemistry* 281(52):40049-40056.
44. Lai MT, Di Cera E, & Shafer JA (1997) Kinetic pathway for the slow to fast transition of thrombin. Evidence of linked ligand binding at structurally distinct domains. *The Journal of biological chemistry* 272(48):30275-30282.

45. Bode W & Stubbs MT (1993) Spatial structure of thrombin as a guide to its multiple sites of interaction. *Seminars in thrombosis and hemostasis* 19(4):321-333.
46. Pineda AO, *et al.* (2006) Crystal structure of thrombin in a self-inhibited conformation. *The Journal of biological chemistry* 281(43):32922-32928.
47. Gandhi PS, Chen Z, Mathews FS, & Di Cera E (2008) Structural identification of the pathway of long-range communication in an allosteric enzyme. *Proceedings of the National Academy of Sciences of the United States of America* 105(6):1832-1837.
48. Carter WJ, Myles T, Gibbs CS, Leung LL, & Huntington JA (2004) Crystal structure of anticoagulant thrombin variant E217K provides insights into thrombin allostery. *The Journal of biological chemistry* 279(25):26387-26394.
49. Gandhi PS, Page MJ, Chen Z, Bush-Pelc L, & Di Cera E (2009) Mechanism of the anticoagulant activity of thrombin mutant W215A/E217A. *The Journal of biological chemistry* 284(36):24098-24105.
50. Pineda AO, *et al.* (2004) The anticoagulant thrombin mutant W215A/E217A has a collapsed primary specificity pocket. *The Journal of biological chemistry* 279(38):39824-39828.
51. Chen Z, Pelc LA, & Di Cera E (2010) Crystal structure of prethrombin-1. *Proceedings of the National Academy of Sciences of the United States of America* .

52. Stubbs MT & Bode W (1993) A player of many parts: the spotlight falls on thrombin's structure. *Thrombosis research* 69(1):1-58.
53. Di Cera E, Hopfner KP, & Dang QD (1996) Theory of allosteric effects in serine proteases. *Biophysical journal* 70(1):174-181.
54. Fredenburgh JC, Stafford AR, & Weitz JI (1997) Evidence for allosteric linkage between exosites 1 and 2 of thrombin. *The Journal of biological chemistry* 272(41):25493-25499.
55. Kroh HK, Tans G, Nicolaes GA, Rosing J, & Bock PE (2007) Expression of allosteric linkage between the sodium ion binding site and exosite I of thrombin during prothrombin activation. *The Journal of biological chemistry* 282(22):16095-16104.
56. Verhamme IM, Olson ST, Tollefsen DM, & Bock PE (2002) Binding of exosite ligands to human thrombin. Re-evaluation of allosteric linkage between thrombin exosites I and II. *The Journal of biological chemistry* 277(9):6788-6798.
57. Schmidt AE, *et al.* (2002) Thermodynamic linkage between the S₁ site, the Na⁺ site, and the Ca²⁺ site in the protease domain of human activated protein C (APC). Sodium ion in the APC crystal structure is coordinated to four carbonyl groups from two separate loops. *The Journal of biological chemistry* 277(32):28987-28995.
58. Underwood MC, Zhong D, Mathur A, Heyduk T, & Bajaj SP (2000) Thermodynamic linkage between the S₁ site, the Na⁺ site, and the Ca²⁺ site

- in the protease domain of human coagulation factor xa. Studies on catalytic efficiency and inhibitor binding. *The Journal of biological chemistry* 275(47):36876-36884.
59. Fuentes-Prior P, *et al.* (2000) Structural basis for the anticoagulant activity of the thrombin-thrombomodulin complex. *Nature* 404(6777):518-525.
 60. Vijayalakshmi J, Padmanabhan KP, Mann KG, & Tulinsky A (1994) The isomorphous structures of prethrombin₂, hirugen-, and PPACK-thrombin: changes accompanying activation and exosite binding to thrombin. *Protein Sci* 3(12):2254-2271.
 61. Henzler-Wildman KA, *et al.* (2007) Intrinsic motions along an enzymatic reaction trajectory. *Nature* 450(7171):838-844.
 62. Seeley S, *et al.* (2003) Structural basis for thrombin activation of a protease-activated receptor: inhibition of intramolecular liganding. *Chemistry & biology* 10(11):1033-1041.
 63. Cleary DB, Trumbo TA, & Maurer MC (2002) Protease-activated receptor 4-like peptides bind to thrombin through an optimized interaction with the enzyme active site surface. *Archives of biochemistry and biophysics* 403(2):179-188.
 64. Isetti G & Maurer MC (2004) Thrombin activity is unaltered by N-terminal truncation of factor XIII activation peptides. *Biochemistry* 43(14):4150-4159.

65. Isetti G & Maurer MC (2004) Probing thrombin's ability to accommodate a V₃₄F substitution within the factor XIII activation peptide segment (28-41). *J Pept Res* 63(3):241-252.
66. Trumbo TA & Maurer MC (2003) V₃₄I and V₃₄A substitutions within the factor XIII activation peptide segment (28-41) affect interactions with the thrombin active site. *Thrombosis and haemostasis* 89(4):647-653.
67. Sabo TM, Farrell DH, & Maurer MC (2006) Conformational analysis of gamma' peptide (410-427) interactions with thrombin anion binding exosite II. *Biochemistry* 45(24):7434-7445.
68. Prieto JH, *et al.* (2005) Dynamics of the fragment of thrombomodulin containing the fourth and fifth epidermal growth factor-like domains correlate with function. *Biochemistry* 44(4):1225-1233.
69. Wood MJ, Sampoli Benitez BA, & Komives EA (2000) Solution structure of the smallest cofactor-active fragment of thrombomodulin. *Nature structural biology* 7(3):200-204.
70. Prasad S, *et al.* (2004) Residue Asp-189 controls both substrate binding and the monovalent cation specificity of thrombin. *The Journal of biological chemistry* 279(11):10103-10108.

2. Crystal structure of thrombin bound to

PAR₁

2.1. Prelude:

PARs play critical roles in coagulation, inflammation, and vascular homeostasis (Cunningham et al, 2000; Sambrano et al, 2001; Fiorucci et al, 2001; Leger et al, 2006). Four members of the PAR family have been identified: PAR₁ – 4 and they all share the basic mechanism of activation (O'Brien et al, 2001; Brass, 2001). Thrombin – PARs interaction leads to platelet aggregation. The finding that simultaneous blockade of PAR₁ and PAR₄ abolishes the ability of human platelets to respond to thrombin (Kahn et al, 1999) suggests that human platelets express PAR₁ and PAR₄ on their surface. Thrombin recognizes the N – terminal exodomain of PAR₁ and cleaves the peptide bond between receptor residues Arg₄₁ and Ser₄₂. This serves to unmask a new amino terminus beginning with the sequence ⁴²SFLLRN (diamond) that functions as a tethered ligand, docking intramolecularly with the body of the receptor to effect transmembrane signaling and eventual platelet aggregation. It is well documented that PAR₁ is a better substrate for thrombin than PAR₄ (Coughlin 2001; Ayala et al, 2001; Kataoka et al, 2003). When both are present cleavage of PAR₁ presumably precedes cleavage of PAR₄ as thrombin accumulates (Kahn et al, 1998; Xu et al, 1998). Activation of PAR₁ and PAR₄ promotes platelet aggregation in humans and unfolds the prothrombotic role of thrombin in the blood. In case of drugs targeting PARs for

therapeutic intervention in patients with acute coronary syndromes, it is therefore obvious that both PAR₁ and PAR₄ should be targeted for better efficacy. I was able to co-crystallize thrombin mutant S₁₉₅A (catalytically inactive) with uncleaved extracellular fragment of PAR₁. The complex validates previous mutagenesis data as well as sheds light on novel interactions and mechanism that the receptor utilizes for interaction with thrombin.

Crystal Structure of Thrombin Bound to the Uncleaved Extracellular Fragment of PAR1*

Received for publication, February 17, 2010, and in revised form, March 10, 2010. Published, JBC Papers in Press, March 17, 2010, DOI 10.1074/jbc.M110.115337

Prafull S. Gandhi, Zhiwei Chen, and Enrico Di Cera¹

From the Department of Biochemistry and Molecular Biology, Saint Louis University School of Medicine, St. Louis, Missouri 63104

Abundant structural information exists on how thrombin recognizes ligands at the active site or at exosites separate from the active site region, but remarkably little is known about how thrombin recognizes substrates that bridge both the active site and exosite I. The case of the protease-activated receptor PAR1 is particularly relevant in view of the plethora of biological effects associated with its activation by thrombin. Here, we present the 1.8 Å resolution structure of thrombin S195A in complex with a 30-residue long uncleaved extracellular fragment of PAR1 that documents for the first time a productive binding mode bridging the active site and exosite I. The structure reveals two unexpected features of the thrombin-PAR1 interaction. The acidic P3 residue of PAR1, Asp³⁹, does not hinder binding to the active site and actually makes favorable interactions with Gly²¹⁹ of thrombin. The tethered ligand domain shows a considerable degree of disorder even when bound to thrombin. The results fill a significant gap in our understanding of the molecular mechanisms of recognition by thrombin in ways that are relevant to other physiological substrates.

Thrombin is a trypsin-like protease endowed with important physiological functions that are mediated and regulated by interaction with numerous macromolecular substrates, receptors, and inhibitors (1). Fenton (2) was the first to recognize that thrombin selectivity toward macromolecular substrates depends on interactions with exosites that extend beyond the active site. Exosite I is positioned some 15 Å away from the active site (3) and occupies a domain analogous to the Ca²⁺-binding loop of trypsin and chymotrypsin (4). Recognition of macromolecular substrates or receptors responsible for the procoagulant, prothrombotic, signaling, and anticoagulant functions of thrombin depends on the structural integrity of this exosite (1). In general, exosite-dependent binding is kinetically limiting as a recognition strategy of macromolecular targets by enzymes involved in blood coagulation (5). Structural and site-directed mutagenesis data document the important role of exosite I in the interaction of thrombin with fibrinogen (6–9) and the protease-activated receptors (PARs)² PAR1 (7,

10–13) and PAR3 (7, 14, 15). Likewise, abundant structural and functional data document how thrombin recognizes substrates at the active site (3, 16, 17), including fibrinogen (18), PAR4 (15, 19), and factor XIII (20, 21). On the other hand, structural elucidation of how substrates bridge the active site and exosite I in their binding to thrombin has been challenging.

PAR1 is a premiere prothrombotic and signaling factor (22), the most specific physiological substrate of thrombin in terms of k_{cat}/K_m values (7), and a most relevant target for crystallization studies. PARs are members of the G-protein-coupled receptor superfamily and play important roles in blood coagulation, inflammation, cancer, and embryogenesis (23–28). Four PARs have been cloned, and they all share the same mechanism of activation (22, 26, 29): thrombin and other proteases derived from the circulation and inflammatory cells cleave at a specific site within the extracellular N terminus to expose a new N-terminal tethered ligand domain, which binds to and activates the cleaved receptor (30). Thrombin activates PAR1 (10), PAR3 (14, 24), and PAR4 (31–33) in this manner but has no specificity toward PAR2, which is the target of other proteases. Cleaved PAR1 also acts as a cofactor for PAR4 activation on human platelets (34).

Major progress has been made recently in our structural understanding of how thrombin recognizes the extracellular domain of PAR4 and how cleaved PAR3 acts as a cofactor for PAR4 cleavage on murine platelets (15). On the other hand, our structural information on the binding mode of PAR1 remains confined to the acidic hirugen-like domain, which recognizes exosite I (12, 13) as predicted by mutagenesis data (7, 10). In a previous structure of thrombin bound to an extracellular fragment of PAR1, the cleavage site at Arg⁴¹ was directed toward the active site of a second thrombin molecule in the crystal lattice in a nonproductive binding mode (12). No details could be gleaned on the contacts made by the P1–P4 residues (35) of PAR1 with the active site of thrombin or on the precise conformation of the tethered ligand domain bound to the enzyme. That information is presented here for the first time.

MATERIALS AND METHODS

The human thrombin mutant S195A was constructed, expressed, and purified to homogeneity as described previously (36). A soluble extracellular fragment of human PAR1, ³³ATNATLDPR ↓ SFLLRNPNDKYEPFWEDEEKN⁶² (where the arrow indicates the site of cleavage between Arg⁴¹ and Ser⁴²), was synthesized by solid phase, purified to homogeneity by high pressure liquid chromatography, and tested for purity by mass spectrometry. Thrombin S195A was concentrated to 9 mg/ml in 50 mM choline chloride and 20 mM Tris (pH 7.4). The

* This work was supported, in whole or in part, by National Institutes of Health Grants HL49413, HL58141 HL73813, and HL95315 (to E. D. C.).

The atomic coordinates and structure factors (code 3LU9) have been deposited in the Protein Data Bank, Research Collaboratory for Structural Bioinformatics, Rutgers University, New Brunswick, NJ (<http://www.rcsb.org/>).

¹ To whom correspondence should be addressed. Tel: 314-977-9201; Fax: 314-977-1183; E-mail: enrico@slu.edu.

² The abbreviations used are: PAR, protease-activated receptor; w, water molecule.

Thrombin-PAR1 Complex

PAR1 fragment, also in the same buffer, was added to maintain the molar ratio at 1:11. Initial crystal screening was done using the PEGs Suite (Qiagen, Valencia, CA) containing 0.2 M Na⁺/K⁺ tartrate. Vapor diffusion with hanging drops was used to generate crystals. For each of the 96 screen conditions, a hanging drop was prepared by mixing 1 μ l of thrombin-PAR1 complex and 1 μ l of reservoir solution, and the drop was allowed to equilibrate with 500 μ l of crystallization buffer at 22 °C. Diffraction quality crystals were obtained in 2 weeks. The crystals were triclinic, with space group P1 and unit cell parameters $a = 46.3$ Å, $b = 50.2$ Å, and $c = 85.5$ Å and $\alpha = 76.4^\circ$, $\beta = 83.9^\circ$, and $\gamma = 73.7^\circ$, with two molecules in the asymmetric unit. Crystals were cryoprotected with the appropriate buffer and 15% glycerol prior to flash-freezing. X-ray data were collected to 1.8 Å resolution at 100 K on an ADSC Quantum-315 CCD detector at beamline 14-BM-C of the Advanced Photon Source at Argonne National Laboratory (Argonne, IL). Data processing including indexing, integration, and scaling was performed using the HKL2000 software package (37). The crystal structure of thrombin S195A bound to the extracellular fragment of PAR1 was solved by molecular replacement using the coordinates of thrombin bound to *H*-D-Phe-Pro-Arg-CH₂Cl (Protein Data Bank code 1SHH) (17) as the search model. Refinement and electron density generation were performed with REFMAC from the CCP4 Suite (38), and 5% of the reflections were selected randomly as a test for cross-validation. Model building was performed with COOT (39). In the final refinement stage, TLS (translation/libration/screw) tensors modeling rigid body anisotropic temperature factors were calculated and applied to the model. Statistics for data collection and refinement are summarized in Table 1. Atomic coordinates and structure factors have been deposited in the Protein Data Bank (code 3LU9).

RESULTS

It has long been recognized that the extracellular fragment of PAR1 carries all determinants for thrombin recognition (7, 10) and that these are the site of cleavage around Arg⁴¹, ³⁸LDPR⁴¹, contacting the active site and the acidic hirugen-like motif ⁵¹KYEPF⁵⁵ engaging exosite I. It was therefore expected that PAR1 would interact with thrombin by bridging the active site and exosite I (10, 40), as first observed for the potent natural inhibitor hirudin (41). Results from structural investigation of the thrombin-PAR1 interaction have documented the expected binding mode to exosite I (12, 13) but not the way PAR1 contacts the active site. Specifically, a previous low (3.1 Å) resolution structure of thrombin bound to a 23-residue long fragment of PAR1 encompassing the cleavage site revealed an artifactual conformation of the tethered ligand downstream of Arg⁴¹ resulting into nonproductive contacts with a second thrombin molecule in the crystal lattice (12). The artifactual conformation documented for PAR1 bound to thrombin in this previous structure (12) is not surprising because thrombin was used in its active wild-type form. Productive binding of the PAR1 fragment to the active site would have resulted in cleavage and either failure to crystallize or crystallization of a complex with the cleaved peptide bound. The structure presented here was solved using thrombin inactivated with the S195A mutation and reveals a binding mode of PAR1 to the E:Na⁺ (fast) form of

TABLE 1

Crystallographic data for the thrombin-PAR1 complex

PEG, polyethylene glycol; PDB, Protein Data Bank; APS, Advanced Photon Source; r.m.s.d., root mean square deviation; mm, main chain-main chain; ms, main chain-side chain; ss, side chain-side chain.

| | |
|---|---|
| Buffer/salt | 0.2 M potassium/sodium tartrate |
| PEG | 20%, 3350 |
| PDB code | 3LU9 |
| Data collection | |
| Beamline | APS 14-BM-C |
| Wavelength (Å) | 0.9 |
| Space group | P1 |
| Unit cell dimensions | $a = 46.3$ Å, $b = 50.2$ Å, $c = 85.5$ Å; $\alpha = 76.4^\circ$, $\beta = 83.9^\circ$, $\gamma = 73.7^\circ$ |
| Molecules/asymmetric unit | 2 |
| Resolution range (Å) | 40–1.8 |
| Observations | 196,399 |
| Unique observations | 63,011 |
| Completeness (%) | 96.0 (93.4) |
| R_{sym} (%) | 5.8 (28.0) |
| $I/\sigma(I)$ | 17.6 (3.8) |
| Refinement | |
| REFMAC | |
| Resolution (Å) | 40–1.8 |
| $ F /\sigma(F)$ | >0 |
| R_{cryst} , R_{free} | 0.193, 0.236 |
| Reflections (working/test) | 57,541/3162 |
| Protein atoms | 5242 |
| Solvent molecules | 698 |
| Na ⁺ /glycerol | 2/1 |
| r.m.s.d. bond length (Å) ^a | 0.013 |
| r.m.s.d. angles ^a | 1.5° |
| r.m.s.d. ΔB (Å ² ; mm/ms/ss) | 3.18/2.09/3.40 |
| $\langle B \rangle$ protein (Å ²) | 35.7 |
| $\langle B \rangle$ solvent (Å ²) | 24.4 |
| $\langle B \rangle$ Na ⁺ /glycerol | 26.9/35.3 |
| Ramachandran plot | |
| Most favored (%) | 98.8 |
| Generously allowed (%) | 0.7 |
| Disallowed (%) | 0.5 |

^a r.m.s.d. from ideal bond lengths and angles and r.m.s.d. in B -factors of bonded atoms.

thrombin that is consistent with all functional and mutagenesis data (7, 10).

The relatively high (1.8 Å) resolution of the present structure yields good electron density for the entire complex (Fig. 1). The extracellular fragment of PAR1 is bound to a single thrombin molecule in the crystal, and the surface of recognition bridges the active site and exosite I, as expected (7, 10, 40). Interestingly, the tethered ligand connecting the domains of PAR1 interacting with the active site and exosite I is for the most part disordered. Electron density is strong for Arg⁴¹ and Ser⁴² at the cleavage site, vouching for an intact PAR1 peptide, but becomes weaker for sequence ⁴⁴LLRNP⁴⁸ immediately downstream (Fig. 2). A solution structure of the cleaved fragment of human PAR1 captured the entire tethered ligand, ⁴²SFLLRNPND⁵⁰, in a stable S-like conformation predicted to fold away from the thrombin surface (42). Recent crystallographic data were unable to detect strong electron density for fragments ³⁸SFNGGP⁴³ and ⁴²SFLLRNP⁴⁸, corresponding to the tethered ligands of murine PAR3 and human PAR1 (13, 15). These findings, along with the current structure of the thrombin-PAR1 complex, suggest that the tethered ligand may be “under tension” in the uncleaved form of PAR1, ready to snap back onto the receptor surface and away from the enzyme as soon as cleavage at Arg⁴¹ takes place.

Intramolecular interactions stabilize the architecture of the extracellular fragment of PAR1 bound to thrombin. In the N-terminal portion upstream of the cleavage site, OH of Thr³⁴

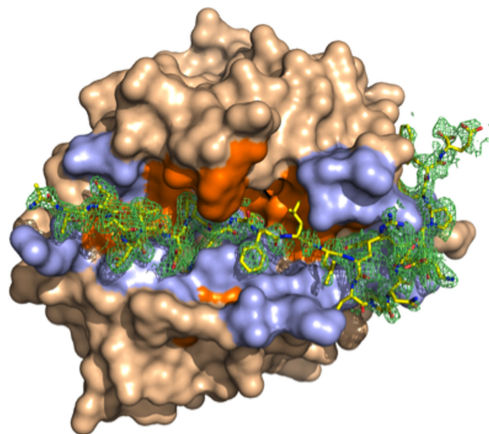


FIGURE 1. X-ray crystal structure of thrombin in complex with the un-cleaved extracellular fragment of PAR1. Thrombin is shown in the standard Bode orientation (3), with the active site in the center and exosite I on the right. Thrombin is rendered in surface representation (wheat), and PAR1 is rendered in stick representation (yellow). The $2F_o - F_c$ electron density map (light green mesh) for the un-cleaved PAR1 fragment is contoured at 0.9σ . Residues of thrombin interacting with PAR1 through molecular contacts within 4 Å are colored in orange (hydrophobic contacts) and marine (polar contacts). The un-cleaved extracellular fragment of PAR1 engages both the active site and exosite I in productive binding modes.

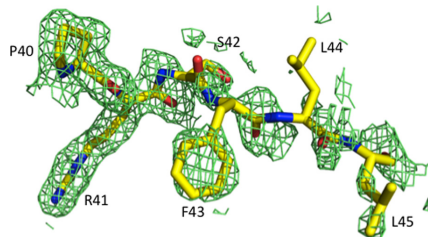


FIGURE 2. Details of the cleavage site and tethered ligand of PAR1. Fragment $^{40}\text{PRSFLL}^{45}$, spanning the P2–P4' positions, is shown with its $2F_o - F_c$ electron density map (light green mesh) contoured at 0.9σ . The peptide bond between Arg⁴¹ and Ser⁴² can be assigned with confidence, vouching for an intact PAR1 fragment. Downstream of Phe⁴³, the electron density becomes weaker, underscoring disorder in most of the tethered ligand.

H-bonds to the backbone N of Ala³⁶. The water molecule at position 166 (w166) mediates an intramolecular interaction for the backbone Os of Ala³⁶ and Leu³⁸ with Oδ1 of Asp³⁹. A second water molecule, w167, links the backbone O of Thr³⁴ to the backbone N and OH of Thr³⁷. The backbone O of Asn³⁵ engages the backbone N of Leu³⁸. These intramolecular interactions result in a single 3_{10} -helix turn reminiscent of the architecture seen in fragments of fibrinogen and factor XIII bound to thrombin (18, 20). The C-terminal portion of the cleavage site presents the tethered ligand within 4 Å from the thrombin surface. Pro⁴⁸ constrains Asn⁴⁹ and Asp⁵⁰ to fold toward the thrombin surface. An H-bond between the backbone O of Arg⁴⁶ and the backbone Ns of Asn⁴⁹ and Asp⁵⁰ stabilizes the architecture of PAR1 in this region, along with H-bonds

TABLE 2

H-bonding interactions between PAR1 and thrombin

NA, not applicable.

| PAR1 | Thrombin | Distance | |
|--------------------------------|--------------------------------|------------|------------|
| | | Molecule 1 | Molecule 2 |
| | | Å | |
| Thr ³⁴ N | Arg ¹⁷³ O | 3.5 | 4.7 |
| Thr ³⁷ Oγ1 | Glu ²¹⁷ Oε2 | 2.6 | 2.6 |
| Asp ³⁹ Oδ2 | Gly ²¹⁹ N | 2.8 | 3 |
| Asp ³⁹ N | Gly ²¹⁶ O | 2.9 | 2.9 |
| Asp ³⁹ O | Gly ²¹⁶ N | 3.1 | 3.1 |
| Arg ⁴¹ NH1, NH2 | Asp ¹⁸⁹ Oδ1, Oδ2 | 2.9, 2.9 | 2.8, 2.8 |
| Arg ⁴¹ NH2 | Ala ¹⁹⁰ O | 3.4 | 3.5 |
| Arg ⁴¹ NH2 | Gly ²¹⁹ O | 3 | 3.1 |
| Arg ⁴¹ N | Ser ²¹⁴ C | 2.9 | 2.9 |
| Arg ⁴¹ O | Ala ¹⁹⁹ N | 3 | 2.9 |
| Arg ⁴¹ O | Asp ¹⁹⁴ N | 3.4 | 3.5 |
| Arg ⁴¹ O | Gly ¹⁹³ N | 2.7 | 2.9 |
| Ser ⁴² OH | Leu ⁴⁵ O | 2.3 | 2.8 |
| Arg ⁴⁶ Ne, NH2 | Gln ³⁸ O | 3.1, 4.4 | 2.6, 3.1 |
| Asn ⁴⁷ Nδ2 | Lys ^{149c} O | 3.2 | NA |
| Asn ⁴⁷ Oδ1 | Lys ^{149c} Nε | 2.9 | NA |
| Tyr ⁵² OH | Arg ³⁸ NH1 | 3.2 | 2.5 |
| Tyr ⁵² O | Gln ³⁸ Ne2 | 3.0 | 7.2 |
| Glu ⁵¹ Oe1, Oe2 | Arg ⁷⁵ NH1 | 3.3, 3.2 | 7.8, 7.1 |
| Glu ⁵¹ Oe1 | Tyr ⁷⁶ N | 3.1 | 3.2 |
| Glu ⁵¹ N | Thr ⁷⁴ O | 2.9 | 3.0 |
| Phe ⁵⁵ benzene ring | Arg ⁶⁷ NH1, NH2, Ne | Cation-π | Cation-π |

between OH of Tyr⁵² and the backbone O of Leu⁴⁵ and between the backbone O of Asp⁵⁰ and the side chain of Arg⁴⁶. The H-bonding network likely provides a spring-loaded mechanism to trigger the conformational transition of the tethered ligand following cleavage at Arg⁴¹ required to engage the receptor for activation and signaling.

The extracellular fragment of PAR1 engages the active site and exosite I of thrombin with a number of polar and hydrophobic interactions (Fig. 1) that are summarized in Table 2. The N terminus of the peptide is solvent-exposed. The backbone N of Thr³⁴ interacts with the backbone O of Arg¹⁷³, and the side chain of Thr³⁷ contacts Glu²¹⁷. The aryl-binding site of thrombin (3) formed by Trp²¹⁵, Ile¹⁷⁴, and Leu⁹⁹ cages Leu³⁸ at the P4 position of PAR1 (Fig. 3). The backbone N and O of the P3 residue Asp³⁹ engage the backbone O and N of Gly²¹⁶ in the canonical antiparallel β-strand conformation expected for a bound substrate (43–45). The side chain of Asp³⁹ points away from the thrombin surface, but Oδ2 forms an H-bond with the backbone N of Gly²¹⁹ (Fig. 3). w271 strategically bridges the backbone O of Thr³⁷, Oδ2 of Asp³⁹, and the backbone N of Gly²¹⁹ and acts in concert with w166 to stabilize the side chain of Asp³⁹. The P2 residue of PAR1, Pro⁴⁰, fits snugly into a hydrophobic pocket formed by the benzyl ring of Tyr^{60a}, the indole of Trp^{60d}, the imidazole of catalytic His⁵⁷, and the side chain of Leu⁹⁹ (Fig. 3). These interactions are analogous to those observed for Pro residues at the P2 positions of PAR4 (15), factor XIII (20), and *H*-D-Phe-Pro-Arg-CH₂Cl (3, 17). The P1 residue of PAR1, Arg⁴¹, is involved in extensive H-bonding interactions that are observed in practically all trypsin-like proteases bound to substrate (43–45). Two water molecules contribute to the network. w40 links NH1 of Arg⁴¹ to Phe²²⁷, and w59 connects the backbone O of Asp³⁹ and Ne and NH2 of Arg⁴¹ to Oε2 of Glu¹⁹² and the backbone O of Gly²¹⁹. The guanidinium group of Arg⁴¹ engages the side chain of Asp¹⁸⁹ in a strong bidentate H-bonding interaction and also the backbone Os of Ala¹⁹⁰ and Gly²¹⁹. The backbone N of Arg⁴¹ inter-

Thrombin-PAR1 Complex

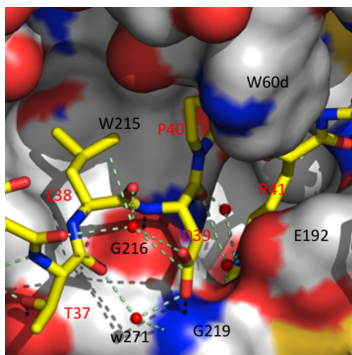


FIGURE 3. Molecular contacts at the active site for the thrombin-PAR1 complex. Thrombin is rendered in surface representation color-coded according to atom type (carbon, white; nitrogen, blue; oxygen, red; and sulfur, yellow), and PAR1 is rendered in stick representation (yellow). Residues of thrombin within 4 Å of PAR1 are labeled in black. PAR1 residues are labeled in red. Arg⁴¹ penetrates the primary specificity pocket and is partially covered in this view by the side chain of Glu¹⁹². Pro^{60b} at the P2 position makes strong hydrophobic interactions with Pro^{60b}, Pro^{60c}, and Trp^{60d}, and Leu³⁸ at the P4 position occupies the aryl-binding site formed by Trp²¹⁵, Ile¹⁷⁴, and Leu⁹⁹. Asp³⁹ at the P3 position makes a polar interaction with the backbone N of Gly²¹⁹, which is reinforced by a water-mediated contact contributed by w271. H-bonds between thrombin and PAR1 are listed in Table 2.

acts with the backbone O of Ser²¹⁴, whereas the backbone O of Arg⁴¹ occupies the oxyanion hole by engaging the backbone Ns of the mutated Ala¹⁹⁵ and Gly¹⁹³.

Downstream of the scissile bond, Leu⁴¹ of thrombin engages the side chain of Ser⁴² at the P1' position of PAR1. Lys^{60f} in the 60-loop of the enzyme bridges the backbone O and OH of Ser⁴² via w306 and w573. At the P2' position, the benzyl ring of Phe⁴³ is in van der Waals interaction with C β and C γ of Glu¹⁹². Leu⁴⁴ at P3' stacks against Leu⁴¹, Ne of Arg⁴⁶ at P5' interacts with the backbone O of Gln³⁸ in the 30-loop of thrombin, and Asn⁴⁷ at P6' makes a polar contact with Lys^{149e} in the autolysis loop of the enzyme. Pro⁴⁸ induces a β -turn in the extracellular fragment of PAR1 that exposes the entire segment ⁴⁸PNDK⁵¹ to solvent. The rest of the interactions are identical to those documented in previous structures (12, 13). The OH and backbone O of Tyr⁵² interact with NH1 of Arg⁷³ and Ne2 of Gln³⁸, respectively. The side chain of Glu⁵³ is engaged by the side chain of Arg⁷⁵ and the backbone N of Tyr⁷⁶ in exosite I. The backbone N of Glu⁵³ interacts with the backbone O of Thr⁷⁴. w217 links the backbone N and O of Glu⁵³ with NH1 and NH2 of Arg⁶⁷ and the backbone O of Thr⁷⁴. Finally, Phe⁵⁵ is involved in a weak cation- π interaction with the side chain of Arg⁶⁷. Trp⁵⁶ and Glu⁵⁷ are solvent-exposed, and no electron density is detected for the rest of PAR1 fragment ⁵⁸DEEKN⁶², in agreement with a previous structure (13) and mutagenesis data (10).

DISCUSSION

Information on how thrombin recognizes substrate at the active site has come from the structure bound to the irreversible active site inhibitor *H*-D-Phe-Pro-Arg-CH₂Cl (3). Arg at P1 ion pairs to Asp¹⁸⁹ in the primary specificity pocket; Pro at P2 fits snugly against Pro^{60b}, Pro^{60c}, and Trp^{60d} in the 60-loop; and

Phe at P3, in the *D*-enantiomer, makes an edge-to-face interaction with Trp²¹⁵ in the aryl-binding site. This interaction, although energetically very strong (46, 47), is present because of the *D*-enantiomeric form of the P3 residue. A residue at this position in the natural *L*-enantiomeric form would be directed to the solvent and away from the aryl-binding site. Indeed, the catalytic activity of thrombin depends little on the nature of the P3 residue (48). Nonetheless, the *H*-D-Phe-Pro-Arg-CH₂Cl-inhibited structure reveals interactions that are relevant to recognition of natural substrates like fibrinogen (18), PAR4 (15, 19), and factor XIII (20, 21). The structure of thrombin in complex with the potent natural inhibitor hirudin has revealed how thrombin recognizes ligands that bridge the active site and exosite I (41). Hirudin blocks access to the active site of thrombin using its compact N-terminal domain and binds to exosite I via its extended acidic C-terminal domain. The mode of interaction of the C-terminal domain of hirudin was later documented in the structures of thrombin bound to hirugen (49), fibrinogen (8, 9, 50), PAR1 (12, 13), PAR3 (15), and thrombomodulin (51). The structure presented here in the complex with the extracellular fragment of PAR1 expands our knowledge of how thrombin recognizes macromolecular substrates at both the active site and exosite I.

The P1–P4 sequence ³⁸LDPR⁴¹ of PAR1 is similar to the P1–P4 sequence ¹⁶⁶VDPR¹⁶⁹ of the anticoagulant substrate protein C. Because no structure of the thrombin-protein C complex is currently available, the conformation of Asp³⁹ of PAR1 becomes relevant to recognition of protein C. It was originally believed that the presence of an acidic residue at the P3 position of protein C would account for the poor specificity of thrombin toward this anticoagulant substrate in the absence of the cofactor thrombomodulin (52). It was argued that Asp at this position would clash with the side chain of Glu¹⁹² lining the thrombin active site (3). Indeed, thrombin mutants E192Q and E192A show slightly enhanced activity toward protein C (52, 53), and the protein C mutant in which the P3 residue Asp¹⁶⁷ is mutated to Phe is activated more rapidly by thrombin (54). These observations support the idea that Asp at the P3 position of protein C hinders binding to the enzyme by electrostatically clashing with the side chain of Glu¹⁹². Whether thrombomodulin moves Glu¹⁹² of thrombin or Asp¹⁶⁷ of protein C to produce a 1000-fold enhancement of protein C activation has long been the subject of debate (51–53, 55–60) and will likely remain so until a structure of thrombin bound to protein C is solved in the presence and absence of thrombomodulin. PAR1 carries an Asp residue at the P3 position but, unlike protein C, is the physiological substrate cleaved by thrombin with the highest k_{cat}/K_m value (7). Therefore, the presence of Asp³⁹ in PAR1 is not expected to provide much hindrance to binding to the active site of thrombin. Indeed, mutation of Asp³⁹ to Ala compromises PAR1 cleavage by thrombin to an extent comparable with that seen with the L38A and P40A mutations (61), supporting the conclusion that the side chain of Asp³⁹ interacts with the thrombin active site in a way that is energetically significant. Furthermore, the thrombin mutant E192Q has normal activity toward PAR1 (7).

The structure presented here shows that the side chain of Asp³⁹ makes direct and water-mediated H-bonds with the

backbone N of Gly²¹⁹ of thrombin. This is an important observation for two reasons. First, it demonstrates that an acidic residue at the P3 position of substrate can be accommodated favorably within the active site of the enzyme, thereby explaining the very high specificity of thrombin toward PAR1. Second, it draws renewed attention to the way thrombin recognizes protein C and proves that Asp¹⁶⁷ at the P3 position of protein C cannot contact thrombin as seen for Asp³⁹ of PAR1. Mutagenesis data have shown that the recognition surface between thrombin and protein C changes upon thrombomodulin binding (53) and is reduced to only a few residues within the active site in the presence of cofactor. It is quite likely then that protein C approaches the active site of thrombin in a conformation that does not resemble the extended architecture seen for PAR1. The structure of thrombin bound to PAR4 has revealed how substrate can fold in a way to redirect itself away from exosite I to enable cofactor binding to that domain (15). That strategy may be used by protein C to leave exosite I free for thrombomodulin binding.

Gly²¹⁹ assumes a potentially important role as a protein engineering target to construct thrombin variants with selective specificity toward macromolecular substrates. The interaction between Oδ2 of Asp³⁹ and the backbone N of Gly²¹⁹ is unique to PAR1. In murine PAR4, the P3 residue is Asn instead of Asp, the δ2 atom is N instead of O, and the side chain rotates by 39° to point away from the backbone N of Gly²¹⁹ (15). Removing the H-bonding interaction between Oδ2 of Asp³⁹ and the backbone N of Gly²¹⁹ with the G219P mutation, as done recently for the N143P mutant of thrombin (62), would be of significant interest. The G219P mutant may feature selective loss of PAR1 recognition and could afford a unique reagent devoid of prothrombotic and signaling functions.

REFERENCES

- Di Cera, E. (2008) *Mol. Aspects Med.* **29**, 203–254
- Fenton, J. W., 2nd (1986) *Ann. N.Y. Acad. Sci.* **485**, 5–15
- Bode, W., Turk, D., and Karshikov, A. (1992) *Protein Sci.* **1**, 426–471
- Bartunik, H. D., Summers, L. J., and Bartsch, H. H. (1989) *J. Mol. Biol.* **210**, 813–828
- Bock, P. E., Panizzi, P., and Verhamme, I. M. (2007) *J. Thromb. Haemost.* **5**, Suppl. 1, 81–94
- Tsiang, M., Jain, A. K., Dunn, K. E., Rojas, M. E., Leung, L. L., and Gibbs, C. S. (1995) *J. Biol. Chem.* **270**, 16854–16863
- Ayala, Y. M., Cantwell, A. M., Rose, T., Bush, L. A., Arosio, D., and Di Cera, E. (2001) *Proteins* **45**, 107–116
- Pechik, I., Madrazo, J., Mosesson, M. W., Hernandez, I., Gilliland, G. L., and Medved, L. (2004) *Proc. Natl. Acad. Sci. U.S.A.* **101**, 2718–2723
- Pechik, I., Yakovlev, S., Mosesson, M. W., Gilliland, G. L., and Medved, L. (2006) *Biochemistry* **45**, 3588–3597
- Vu, T. K., Wheaton, V. I., Hung, D. T., Charo, I., and Coughlin, S. R. (1991) *Nature* **353**, 674–677
- Myles, T., Le Bonniec, B. F., and Stone, S. R. (2001) *Eur. J. Biochem.* **268**, 70–77
- Mathews, II, Padmanabhan, K. P., Ganesh, V., Tulinsky, A., Ishii, M., Chen, J., Turck, C. W., Coughlin, S. R., and Fenton, J. W., 2nd (1994) *Biochemistry* **33**, 3266–3279
- Gandhi, P. S., Chen, Z., Mathews, F. S., and Di Cera, E. (2008) *Proc. Natl. Acad. Sci. U.S.A.* **105**, 1832–1837
- Ishihara, H., Connolly, A. J., Zeng, D., Kahn, M. L., Zheng, Y. W., Timmons, C., Tram, T., and Coughlin, S. R. (1997) *Nature* **386**, 502–506
- Bah, A., Chen, Z., Bush-Pelc, L. A., Mathews, F. S., and Di Cera, E. (2007) *Proc. Natl. Acad. Sci. U.S.A.* **104**, 11603–11608
- Bode, W. (2006) *Blood Cells Mol. Dis.* **36**, 122–130
- Pineda, A. O., Carrell, C. J., Bush, L. A., Prasad, S., Caccia, S., Chen, Z. W., Mathews, F. S., and Di Cera, E. (2004) *J. Biol. Chem.* **279**, 31842–31853
- Stubbs, M. T., Oschkinat, H., Mayr, I., Huber, R., Anglikar, H., Stone, S. R., and Bode, W. (1992) *Eur. J. Biochem.* **206**, 187–195
- Cleary, D. B., Trumbo, T. A., and Maurer, M. C. (2002) *Arch. Biochem. Biophys.* **403**, 179–188
- Sadasivan, C., and Yee, V. C. (2000) *J. Biol. Chem.* **275**, 36942–36948
- Isetti, G., and Maurer, M. C. (2007) *Biochemistry* **46**, 2444–2452
- Coughlin, S. R. (2005) *J. Thromb. Haemost.* **3**, 1800–1814
- Cunningham, M. A., Rondeau, E., Chen, X., Coughlin, S. R., Holdsworth, S. R., and Tipping, P. G. (2000) *J. Exp. Med.* **191**, 455–462
- Sambrano, G. R., Weiss, E. J., Zheng, Y. W., Huang, W., and Coughlin, S. R. (2001) *Nature* **413**, 74–78
- Fiorucci, S., Mencarelli, A., Palazzetti, B., Distrutti, E., Vergnolle, N., Hollenberg, M. D., Wallace, J. L., Morelli, A., and Cirino, G. (2001) *Proc. Natl. Acad. Sci. U.S.A.* **98**, 13936–13941
- Leger, A. J., Covic, L., and Kuliopulos, A. (2006) *Circulation* **114**, 1070–1077
- Even-Ram, S., Uziely, B., Cohen, P., Grisar-Granovsky, S., Maoz, M., Ginzburg, Y., Reich, R., Vlodaysky, I., and Bar-Shavit, R. (1998) *Nat. Med.* **4**, 909–914
- Griffin, C. T., Srinivasan, Y., Zheng, Y. W., Huang, W., and Coughlin, S. R. (2001) *Science* **293**, 1666–1670
- Brass, L. F. (2003) *Chest* **124**, 185–255
- Coughlin, S. R. (2000) *Nature* **407**, 258–264
- Kahn, M. L., Zheng, Y. W., Huang, W., Bigornia, V., Zeng, D., Moff, S., Farese, R. V., Jr., Tam, C., and Coughlin, S. R. (1998) *Nature* **394**, 690–694
- Nakanishi-Matsui, M., Zheng, Y. W., Sulciner, D. J., Weiss, E. J., Ludeman, M. J., and Coughlin, S. R. (2000) *Nature* **404**, 609–613
- Xu, W. F., Andersen, H., Whitmore, T. E., Presnell, S. R., Yee, D. P., Ching, A., Gilbert, T., Davie, E. W., and Foster, D. C. (1998) *Proc. Natl. Acad. Sci. U.S.A.* **95**, 6642–6646
- Leger, A. J., Jacques, S. L., Badar, J., Kaneider, N. C., Derian, C. K., Andrade-Gordon, P., Covic, L., and Kuliopulos, A. (2006) *Circulation* **113**, 1244–1254
- Schechter, I., and Berger, A. (1967) *Biochem. Biophys. Res. Commun.* **27**, 157–162
- Krem, M. M., and Di Cera, E. (2003) *Biophys. Chem.* **100**, 315–323
- Otwinowski, Z., and Minor, W. (1997) *Methods Enzymol.* **276**, 307–326
- Bailey, S. (1994) *Acta Crystallogr. D Biol. Crystallogr.* **50**, 760–763
- Emsley, P., and Cowtan, K. (2004) *Acta Crystallogr. D Biol. Crystallogr.* **60**, 2126–2132
- Qiu, X., Padmanabhan, K. P., Carperos, V. E., Tulinsky, A., Kline, T., Manganore, J. M., and Fenton, J. W., 2nd (1992) *Biochemistry* **31**, 11689–11697
- Rydel, T. J., Tulinsky, A., Bode, W., and Huber, R. (1991) *J. Mol. Biol.* **221**, 583–601
- Seeley, S., Covic, L., Jacques, S. L., Sudmeier, J., Baleja, J. D., and Kuliopulos, A. (2003) *Chem. Biol.* **10**, 1033–1041
- Hedstrom, L. (2002) *Chem. Rev.* **102**, 4501–4524
- Page, M. J., and Di Cera, E. (2008) *Cell. Mol. Life Sci.* **65**, 1220–1236
- Perona, J. J., Hedstrom, L., Rutter, W. J., and Fletterick, R. J. (1995) *Biochemistry* **34**, 1489–1499
- Arosio, D., Ayala, Y. M., and Di Cera, E. (2000) *Biochemistry* **39**, 8095–8101
- Vindigni, A., Dang, Q. D., and Di Cera, E. (1997) *Nat. Biotechnol.* **15**, 891–895
- Lottenberg, R., Hall, J. A., Blinder, M., Binder, E. P., and Jackson, C. M. (1983) *Biochim. Biophys. Acta* **742**, 539–557
- Vijayalakshmi, J., Padmanabhan, K. P., Mann, K. G., and Tulinsky, A. (1994) *Protein Sci.* **3**, 2254–2271
- Rose, T., and Di Cera, E. (2002) *J. Biol. Chem.* **277**, 18875–18880
- Fuentes-Prior, P., Iwanaga, Y., Huber, R., Pagila, R., Rumennik, G., Seto, M., Morser, J., Light, D. R., and Bode, W. (2000) *Nature* **404**, 518–525
- Le Bonniec, B. F., and Esmon, C. T. (1991) *Proc. Natl. Acad. Sci. U.S.A.* **88**, 7371–7375
- Xu, H., Bush, L. A., Pineda, A. O., Caccia, S., and Di Cera, E. (2005) *J. Biol.*

Thrombin-PAR1 Complex

- Chem.* **280**, 7956–7961
54. Richardson, M. A., Gerlitz, B., and Grinnell, B. W. (1992) *Nature* **360**, 261–264
55. Gerlitz, B., and Grinnell, B. W. (1996) *J. Biol. Chem.* **271**, 22285–22288
56. Hayashi, T., Zushi, M., Yamamoto, S., and Suzuki, K. (1990) *J. Biol. Chem.* **265**, 20156–20159
57. Vindigni, A., White, C. E., Komives, E. A., and Di Cera, E. (1997) *Biochemistry* **36**, 6674–6681
58. Yang, L., Bae, J. S., Manithody, C., and Rezaie, A. R. (2007) *J. Biol. Chem.* **282**, 25493–25500
59. Yang, L., Manithody, C., and Rezaie, A. R. (2006) *Proc. Natl. Acad. Sci. U.S.A.* **103**, 879–884
60. Yang, L., Prasad, S., Di Cera, E., and Rezaie, A. R. (2004) *J. Biol. Chem.* **279**, 38519–38524
61. Nieman, M. T., and Schmaier, A. H. (2007) *Biochemistry* **46**, 8603–8610
62. Niu, W., Chen, Z., Bush-Pelc, L. A., Bah, A., Gandhi, P. S., and Di Cera, E. (2009) *J. Biol. Chem.* **284**, 36175–36185

3. Identification of an allosteric pathway

3.1. Prelude: Crystal structure of E*, as exemplified by thrombin mutant D102N, shows an occluded active site, a collapsed Na⁺ binding but documents an unperturbed exosite I architecture. In principle, this should allow binding of exosite I ligands. To understand ligand recognition, I co-crystallized thrombin mutant D102N with the cleaved extracellular fragment of PAR₁. The 2.1-Å crystal structure of D102N complexed with PAR₁ documents a massive conformational change in D102N upon ligand binding and elucidates the molecular basis of E* to E transition. Binding of a PAR₁ fragment to exosite I, 30-Å away from the active site region, causes a massive conformational change that corrects the position of the 215-219 β-strand and restores access to the active site. The crystal structure of the thrombin-PAR₁ complex reveals the details of this long-range allosteric communication in terms of a network of polar interactions.

3.2. E* to E transition can be triggered by other exosite I binding ligands:

Thrombin exosite I contains several positively charged residues that provide electrostatic steering and optimal pre-orientation for multiple ligands including thrombomodulin, fibrinogen, the natural inhibitor hirudin, PAR₁, PAR₃, and hirugen to facilitate productive complex upon binding (Bode & Stubbs, 1993; Vindigni *et al*, 1997). To test the hypothesis that the E* to E conformational change is independent of the ligand, we co-crystallized thrombin mutant D102N in

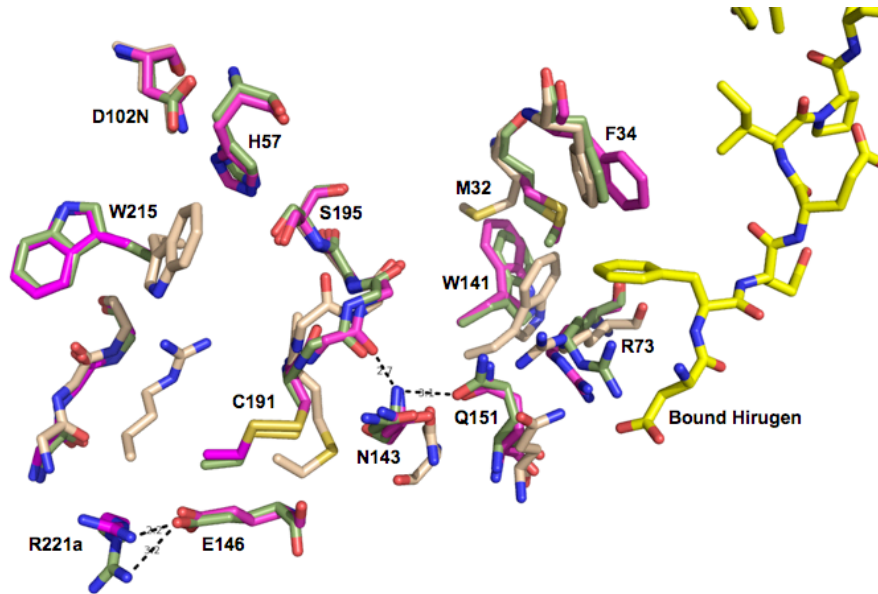


Figure 3.1. E* to E transition can be triggered by other exosite I ligands. Hirugen and PAR₃ can trigger similar E* to E transition as documented by the PAR₁ bound structure. Molecular basis of the allosteric communication between exosite I and the active site as documented in the D₁₀₂N-PAR₁ (magenta) and the D₁₀₂N-hirugen (green) crystal structures. The structure in wheat is the apo-form of the thrombin mutant D₁₀₂N. The structure of D₁₀₂N bound to PAR₃ was omitted for clarity. Identical pathway can be deduced from the two crystal structures crystallized in different conditions validating our proposed allosteric model.

presence of hirugen and PAR₃. The D₁₀₂N-hirugen and the D₁₀₂N-PAR₃ complex co-crystallized at 3.5-Å and 3.2-Å respectively are free of Na⁺. Figure 3.1 shows the overlay of critical residues from the apo-D₁₀₂N (wheat), D₁₀₂N bound to PAR₁ fragment (magenta), and D₁₀₂N bound to hirugen (green). Residues of D₁₀₂N bound to PAR₃ were omitted for clarity. Conformational changes observed in D₁₀₂N because of hirugen, PAR₃ and PAR₁ binding are almost identical. This

shows that notwithstanding the different crystallization conditions and the space groups of the complexes (D102N-PAR₁, D102N-hirugen, and D102N-PAR₃), the structures document near-identical conformational changes. We conclude that the E* to E transition can be triggered by any exosite I binding ligand. Crystallographic parameters are summarized in table 3.1.

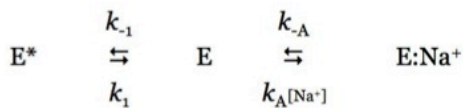
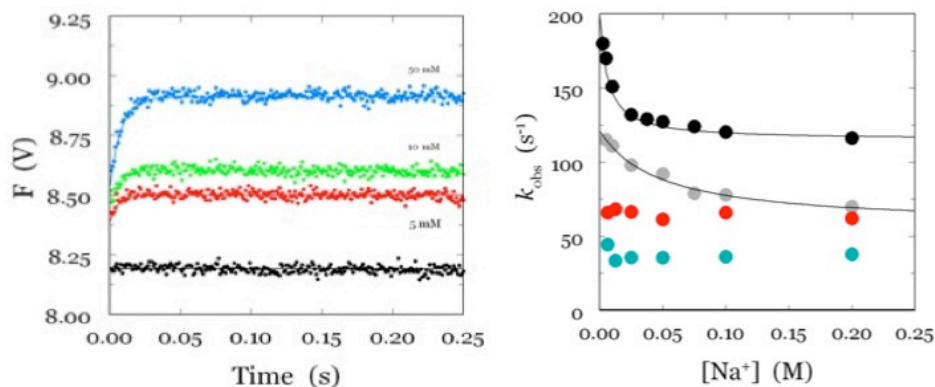
| | D102N free | D102N-PAR1 | D102N-hirugen | D102N-PAR3 |
|------------------------|---|---|--|---|
| Wavelength, Å | 0.9 | 0.9 | 0.9 | 0.9 |
| Space group | P4(3) | P1 | P2(1)2(1)2 | P4(3) |
| Unit cell dimension, Å | 57.9, 57.9, 119.9 | 46.1, 50.3, 85.1 | 154.8, 75.2, 57.2 | 88.9, 88.9, 159.1 |
| Angles | 90, 90, 90 | 76.9, 84.3, 73.7 | 90, 90, 90 | 90, 90, 90 |
| Rcryst, Rfree | 0.2(0.22) | 0.207, 0.248 | 0.236, 0.287 | 0.21(0.30) |
| Completeness | 99.2(92.8) | 94(87.7) | 84.4(68.1) | 95.1(90.5) |
| Rmerge | 5.2(34.3) | 6.1(22.1) | 13.8(26.7) | 11.1(28.7) |
| Molecules/asu | 1 | 2 | 2 | 3 |
| Resolution, Å | 1.87 | 2.2 | 3.5 | 3.2 |
| Crystal conditions | Protein: 20 mM Tris pH = 7.5, 50 mM ChCl; Reservoir: 0.1 M HEPES pH = 7.5, 18 % PEG 20000 | Protein: 20 mM MES pH = 6, 50 mM ChCl; Reservoir: 0.1 M MES pH = 6.5, 30 % PEG 4000 | Protein: 20 mM MES pH = 6, 50 mM ChCl; Reservoir: 0.1 M MES pH = 6.5, 15 % PEG 20000 | Protein: 20 mM MES pH = 6, 50 mM ChCl; Reservoir: 0.1 M Tris pH = 8.5, 30 % PEG 400 |

Table 3.1. Summary of crystallographic parameters. Different crystallization conditions and the space groups of the D102N complexes yield identical conformational change upon ligand binding. This validates our allosteric transition model first documented with the D102N in complex with fragment of PAR₁ crystal structure.

3.3. Evidence from stopped-flow studies: Stopped-flow analysis has proven very useful to understand thrombin equilibrium. Figure 3.2.a shows the time course of fluorescence change upon Na⁺ binding to thrombin wild-type. Stopped-flow fluorescence measurements were carried out with an Applied Photophysics SX20 spectrometer, using an excitation of 280 nm and a cutoff filter at 305 nm. Concentration of thrombin variants used in this study was 50 nM. Solution conditions were 50 mM Tris pH = 8 @ 15 °C, 0.1 % PEG 8000. Concentration of Na⁺

was varied while keeping the ionic strength constant by using ChCl (Ch⁺ acts as an inert cation).

The mechanism of Na⁺ binding is biphasic, with a fast phase followed by a single-exponential slow phase of fluorescence increase. The slow phase can be fit to a single exponential to obtain k_{obs} values. Figure 3.2.b shows the k_{obs} dependence on [Na⁺]. The value of k_{obs} decreases with increasing [Na⁺], proving that the slow phase precedes Na⁺ binding and pertains to the conformational transition between E* and E. Similar mechanism is observed for the thrombin mutant D102N. The continuous lines were drawn according to the Equation 1.



$$k_{obs} = k_1 + k_{-1} \frac{1}{1 + K_A[Na^+]}$$

Figure 3.2. Effect of hirugen on the dependence of k_{obs} on [Na⁺]. A. Stopped-flow fluorescence experiments reveal that Na⁺ binds to thrombin in a two-step mechanism with a rapid phase occurring within the dead time of the spectrometer (<0.5 ms) followed by a single-exponential slow

phase. The rapid phase is due to Na^+ binding to the enzyme E to generate the $\text{E}:\text{Na}^+$ form. The slow phase is due to the interconversion between E^* and E, where E^* is a form that cannot bind Na^+ . **B.** The k_{obs} values, for the single-exponential fluorescence increase, decreases hyperbolically with $[\text{Na}^+]$ (black wild-type, grey D102N mutant). Similar experiments done under saturating concentrations of exosite I binding ligand, hirugen reveals that the k_{obs} changes linearly with $[\text{Na}^+]$ (red wild-type + hirugen, cyan D102N + hirugen).

Analysis of k_{obs} dependence on $[\text{Na}^+]$ for both wild-type and D102N mutant shows that $k_1 = 115 \pm 3 \text{ s}^{-1}$, $k_{-1} = 83 \pm 6 \text{ s}^{-1}$, $K_A = 160 \pm 20 \text{ M}^{-1}$ (black circles); $k_1 = 57 \pm 5 \text{ s}^{-1}$, $k_{-1} = 64 \pm 5 \text{ s}^{-1}$, $K_A = 21 \pm 6 \text{ M}^{-1}$ (gray circles). The ratio of E^* to E, denoted by r is equal to 0.7 for wild-type and 1.1 for the D102N mutant. It can be concluded that a pre-equilibrium exists between E^* and E for both wild-type and D102N mutant. Furthermore, E^* is a form of thrombin that cannot bind Na^+ . Na^+ binds only to the E form to generate the $\text{E}:\text{Na}^+$ form of thrombin. Similar experiments were done in presence of saturating concentrations of exosite I binding ligand, hirugen (wild-type red circles and D102N blue circles). It can be observed that in presence of hirugen, k_{obs} is independent of $[\text{Na}^+]$ and that k_{-1} is negligible. This suggests that binding of hirugen shifts the equilibrium in favor of E, consistent with our x-ray structural data.

Structural identification of the pathway of long-range communication in an allosteric enzyme

Prafull S. Gandhi, Zhiwei Chen, F. Scott Mathews, and Enrico Di Cera*

Department of Biochemistry and Molecular Biophysics, Washington University School of Medicine, Box 8231, St. Louis, MO 63110

Edited by Laszlo Lorand, Northwestern University Feinberg School of Medicine, Chicago, IL, and approved December 21, 2007 (received for review November 16, 2007)

Allostery is a common mechanism of regulation of enzyme activity and specificity, and its signatures are readily identified from functional studies. For many allosteric systems, structural evidence exists of long-range communication among protein domains, but rarely has this communication been traced to a detailed pathway. The thrombin mutant D102N is stabilized in a self-inhibited conformation where access to the active site is occluded by a collapse of the entire 215–219 β -strand. Binding of a fragment of the protease activated receptor PAR1 to exosite I, 30-Å away from the active site region, causes a large conformational change that corrects the position of the 215–219 β -strand and restores access to the active site. The crystal structure of the thrombin-PAR1 complex, solved at 2.2-Å resolution, reveals the details of this long-range allosteric communication in terms of a network of polar interactions.

protease activated receptor | thrombin | x-ray crystallography

Ever since its original formulation (1, 2), the allosteric concept of enzyme regulation has captivated the interest of structural biologists. The idea that events occurring at a given site of the protein can be transmitted long-range to affect affinity or catalytic efficiency at a distant site offers an elegant explanation for linkage and cooperativity (3) but poses a challenge to the crystallographer who seeks to identify the communication pathway underlying the functional effects. Perutz (4) was the first to offer a molecular explanation for the allosteric mechanism of hemoglobin cooperativity. For multimeric proteins like hemoglobin, conformational transitions tend to affect the quaternary structure and signatures of allostery have been detected crystallographically (5–9). Allostery is not limited to multimeric assemblies and, in fact, many monomeric proteins feature conformational plasticity that translate into allosteric behavior at equilibrium and steady state (6, 10, 11). For such systems, the structural signatures of long-range communication tend to manifest themselves as small changes in tertiary structure or H-bonding connectivity (12, 13) and lack the amplification seen in large quaternary structural reorganization. Identification of the pathway of communication underlying an allosteric mechanism remains a difficult task in general and continues to receive utmost attention (11, 13). Alternative approaches have been proposed to identify such pathways based on the statistical analysis of evolutionary records of protein sequences (14) or anisotropic thermal diffusion (15). Although promising and insightful, such approaches must ultimately find validation by structural investigation.

Among Na^+ -activated allosteric enzymes (6), the serine protease thrombin has received much attention in view of its critical roles in hemostasis and thrombosis (12, 16, 17). Thrombin features considerable structural plasticity and exists predominantly in two forms at equilibrium, the Na^+ -free slow form E ($\approx 40\%$ of the molecules *in vivo*) and the Na^+ -bound fast form E: Na^+ ($\approx 60\%$ of the molecules *in vivo*) that are responsible, respectively, for the anticoagulant and procoagulant functions of the enzyme (18). A third form, E* ($\approx 1\%$ of the molecules *in vivo*), is in equilibrium with E and is unable to bind Na^+ (19).

Na^+ binds 15-Å away from residues of the active site (20, 21) and enhances activity toward fibrinogen and the protease activated receptors (PAR) PAR1 and PAR4 (18, 22). Structural details on how Na^+ binding influences allosterically the active site have emerged recently (12, 21), but mutagenesis and spectroscopic studies vouch for more extensive, global effects of Na^+ binding on the conformation of the enzyme (12, 19, 23). In addition to the allosteric effect of Na^+ , thrombin activity and specificity is influenced allosterically by binding of ligands to exosite I (24–28), a domain located 25-Å away from the active site and on the opposite pole of the molecule relative to the Na^+ site (16, 29). The exact mechanism of this long-range communication remains controversial (30, 31). A recent structure of murine thrombin bound to a fragment of PAR3 at exosite I has revealed a significant conformational change of the 60-loop that opens the active site fully for optimal substrate diffusion (32). Such structural transition is relevant to the cofactor function of PAR3 on PAR4 cleavage (33–35) and to the cofactor function of thrombomodulin on protein C activation that is at the basis of the anticoagulant activity of thrombin (36, 37). We now provide crystallographic evidence of a much larger conformational change experienced by thrombin when exosite I is bound to the extracellular fragment of PAR1, which is the primary receptor responsible for aggregation of human platelets (33, 34, 38). The findings reveal the full extent of structural flexibility accessible to this important allosteric enzyme and a precise pathway of long-range communication.

Results

Human thrombin inactivated with the single-site mutation D102N was crystallized in complex with the extracellular fragment of human PAR1, $^{42}\text{SFLLRNPNDKYEPFWEDEEKN}^{62}$, corresponding to the sequence downstream from the cleavage site at Arg-41 (38) and containing the hirudin-like motif $^{52}\text{YEPFWE}^{57}$ predicted to bind to exosite I (33, 38). Although the structure was solved at a resolution of 2.2 Å, only the sequence $^{49}\text{NDKYEPFWE}^{57}$ of the extracellular fragment of PAR1 could be traced in the electron density map, leaving the tethered ligand domain $^{42}\text{SFLLRN}^{47}$ and the acidic tail of the fragment unresolved (Fig. 1). A similar problem recently was encountered for the cleaved fragment of murine PAR3 bound to exosite I of murine thrombin (32). The tethered ligand domain presumably folds away from the thrombin surface after cleavage at Arg-41, and its conformation becomes disordered, as documented by NMR studies (39). As recently seen for the binding epitope of PAR3 (32), the PAR1 fragment engages exosite I of

Author contributions: P.S.G., Z.C., F.S.M., and E.D.C. designed research; P.S.G. and Z.C. performed research; P.S.G. contributed new reagents/analytic tools; P.S.G., Z.C., F.S.M., and E.D.C. analyzed data; and E.D.C. wrote the paper.

The authors declare no conflict of interest.

This article is a PNAS Direct Submission.

Data deposition: The atomic coordinates have been deposited in the Protein Data Bank, www.pdb.org (PDB ID code 3BEF).

*To whom correspondence should be addressed. E-mail: enrico@wustl.edu.

© 2008 by The National Academy of Sciences of the USA

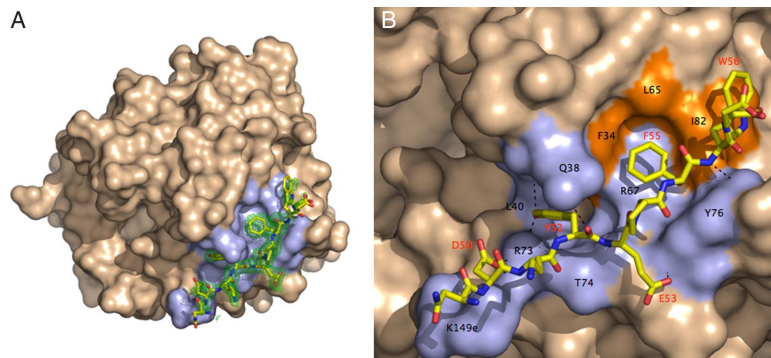


Fig. 1. Structure of the human thrombin mutant D102N in complex with the extracellular fragment of human PAR1. (A) Thrombin is rendered in surface representation (wheat) with residues $<4 \text{ \AA}</math> from the bound fragment of PAR1 (stick model) colored in light blue. The orientation is centered on the 30-loop that separates exosite I on the right from the active site (left on the left). The 60-loop occupies the upper rim of the active site. The electron density $2F_o - F_c$ map (green mesh) is contoured at 1.0σ . (B) Details of the molecular contacts at the thrombin-PAR1 interface, with hydrophobic regions of the thrombin epitope colored in orange and polar regions colored in light blue. H bonds are depicted as broken lines. Residues involved in contacts $<4 \text{ \AA}</math> are listed in Table 1 and are labeled in black for thrombin and red for PAR1. The extracellular fragment of PAR1 engages exosite I through polar and hydrophobic interactions.$$

thrombin in a number of polar and hydrophobic interactions starting with Asp-50 whose O δ 1 atom H bonds to the NH1 and NH2 atoms of Arg-73 and the N ζ atom of Lys-149e of thrombin (Table 1 and Fig. 1). Other polar interactions involve the O and OH atoms of Tyr-52 of PAR1 with the Ne2 atom of Gln-38, the NH1 atom of Arg-73, and the N atom of Leu-40 of thrombin. The O ϵ 1 and N atoms of Glu-53 H bond to the N atom of Tyr-76 and the O atom of Thr-74 of thrombin, respectively. Finally, a weak H bond couples the N atom of Trp-56 to the OH atom of Tyr-76 of thrombin. The hydrophobic interactions are substantial and involve Phe-34, Leu-65, and Ile-82 that accommodate in a cluster Tyr-52, Phe-55, and Trp-56 of PAR1. Phe-34 is edge-to-face with respect to Tyr-52 on one side and Phe-55 on the other side. Phe-55 is in van der Waals' contact with the entire hydrophobic cluster in exosite I and is also engaged in a cation- π interaction by Arg-67 of thrombin. Trp-56 interacts with Ile-82 of thrombin at the boundary of the binding epitope. The contacts documented by the crystal structure are in agreement with the results of Ala scanning mutagenesis of thrombin (40). In particular, mutagenesis studies have pointed out the peculiar contribution of Arg-67 to PAR1 recognition. The guanidinium group of Arg-67 is within $4.2 \text{ \AA}</math> from the benzene ring of Phe-55 of PAR1,$

in optimal cation- π interaction, but not so relative to Phe-50 of PAR3 (32), which could explain why the R67A mutation is far more deleterious for PAR1 binding relative to PAR3 (40). Ala scanning mutagenesis of PAR1 have singled out Tyr-52, Glu-53, and Phe-55 as important determinants of recognition by exosite I (38), in agreement with the results of the crystal structure. However, the important role of Asp-50 of PAR1 in the interaction with thrombin has been missed by previous mutagenesis studies (38, 40).

A previous structure of thrombin bound to a fragment of PAR1 revealed a nonproductive binding mode bridging two thrombin molecules in the crystal lattice without any significant conformational change in the enzyme (41). The structure of bound D102N reported here shows the fragment of PAR1 recognizing exosite I basically in the same conformation as reported previously (41). However, the structure documents a large conformational change that propagates from Phe-34 and Arg-73 in exosite I to Trp-215 in the aryl binding site and Arg-221a in the 220-loop located up to $28\text{-\AA}</math> away on the opposite side of the active site relative to exosite I. The conformational change is revealed by comparison of the structure of D102N bound to the fragment of PAR1 at exosite I with that of the free mutant solved recently (42). The free mutant D102N folds in a self-inhibited conformation with the active site occluded (Fig. 2). The 215-219 β -strand collapses into the active site, with the indole ring of Trp-215 losing its contact with Phe-227 and making hydrophobic contact with the catalytic His-57. Further downstream from Trp-215, Arg-221a relinquishes its ion-pair interaction with Glu-146 in the autolysis loop and penetrates the 220-loop to engage the carboxylate of Asp-189 in the primary specificity pocket with its guanidinium group. The drastic rearrangement of the 215-219 β -strand and the 220-loop shift the orientation of the Cys-191:Cys-220 disulfide bond and propagate the perturbation up to the oxyanion hole where the backbone N atom of Gly-193 is flipped relative to wild type (42). Binding of PAR1 to exosite I reverses all of these drastic changes and shifts the conformation of D102N into that of wild-type thrombin (21, 41) using a long-range allosteric communication between exosite I and the active site.$

The crystal structure of D102N bound to PAR1 at exosite I details a plausible, yet necessarily hypothetical pathway under-

Table 1. Interatomic contacts ($<4 \text{ \AA}</math>) between thrombin and PAR1$

| Thrombin | PAR1 | Distance, \AA |
|------------------------|-----------------------|------------------------|
| Arg-73 NH1 | Asp-50 O δ 1 | 2.94 |
| Arg-73 NH2 | Asp-50 O δ 1 | 3.06 |
| Lys-149e N ζ | Asp-50 O δ 1 | 3.07 |
| Gln-38 Ne2 | Tyr-52 O | 3.34 |
| Leu-40 N | Tyr-52 OH | 3.88 |
| Arg-73 NH1 | Tyr-52 OH | 3.13 |
| Phe-34 | Tyr-52 | vdW |
| Thr-74 O | Glu-53 N | 2.95 |
| Tyr-76 N | Glu-53 O ϵ 1 | 2.67 |
| Phe-34, Leu-65, Ile-82 | Phe-55 | vdW |
| Tyr-76 OH | Trp-56 N | 3.86 |
| Ile-82 | Trp-56 | vdW |

vdW, van der Waals' contact.

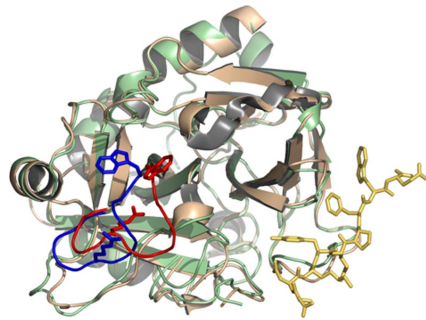


Fig. 2. Allosteric effect induced by binding of the extracellular fragment of PAR1 (stick model in gold) to exosite I of thrombin (ribbon model in light green) on the conformation of the 215–219 β -strand and the 220-loop (blue). The position of Trp-215 and Arg-221a is indicated as a stick model. Thrombin is shown in the standard Bode orientation (29) with the active site cleft in the middle and exosite I to the right. Comparison with the free structure of thrombin (ribbon model in wheat, with the 215–219 β -strand and the 220-loop, Trp-215, and Arg-221a in red) shows a drastic rearrangement that pushes the 215–219 β -strand back >6 Å. Trp-215 and Arg-221a relocate >9 Å to restore access to the active site and primary specificity pocket that was obliterated in the free form. The allosteric communication between exosite I and the 215–219 β -strand and 220-loop spans almost 30 Å across the thrombin molecule (see also Fig. 3) and reveals a possible mechanism for the conversion of thrombin from its inactive form E* into the active form E.

lying this long-range communication. In what follows, we propose a possible sequence of events consistent with the changes documented in the electron density maps. The allosteric communication is triggered by a change in the conformation of Phe-34 and Arg-73 in exosite I. The C ϵ 2 atom of Phe-34 is 4.3-Å away from the S atom of Met-32 in the free form of D102N. Upon binding of PAR1 to exosite I, the phenyl ring of Phe-34 rotates to optimize its interaction with Phe-55 and Tyr-52 of PAR1 and pulls the C ϵ atom of Met-32 along causing a 5.6-Å shift (Fig. 3). The indole ring of Trp-141 switches places with Met-32 and causes a >1 -Å concerted translation of the entire 141–146 β -strand. Contributing to this shift is the repositioning of Arg-73 for engagement of Asp-50 and Tyr-52 of PAR1 that pushes Gln-151 toward Asn-143, causing electrostatic clash between the side chain O atoms coming within 2.96 Å. Pro-152 pushes Gly-142 back, contributing to the realignment of the 141–146 and 191–193 β -strands that become stabilized by H bonds between the backbone N atom of Asn-143 with the O ϵ 1 atom of Gln-151 on one side and the backbone O atom of Glu-192 on the other side (Fig. 3). The latter H bond flips back the peptide bond with Gly-193 into the position seen in the wild type and reconstitutes the oxyanion hole with the correct orientation of the backbone N atom. As the 141–146 β -strand is pushed back, the backbone O atom of Asn-143 collides with the S atom of Cys-220. As a result, the Cys-191:Cys-220 disulfide bond twists and relocates 4.29-Å deeper inside the protein, causing a major rearrangement in the backbone of the 215–219 β -strand and the 220-loop. The shift in the 141–146 β -strand initiated at Trp-141 and amplified by Arg-73 propagates to the hinge region of the flexible autolysis loop and orders the side chain of Glu-146 for a strong ion-pair with Arg-221a in the 220-loop, whose guanidinium group moves >9 Å from the interior of the primary specificity pocket to the surface of the protein. The entire 215–219 β -strand moves back >6 Å and Trp-215 reestablishes its stacking interaction with Phe-227 moving >10 -Å away from the catalytic His-57, thereby restoring

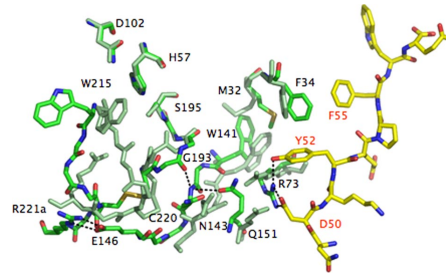


Fig. 3. Molecular basis of the allosteric communication between exosite I and the 215–219 β -strand and 220-loop spanning almost 30 Å across the thrombin molecule (see also Fig. 2). The extracellular fragment of PAR1 is rendered as a stick model with C atoms in yellow and the thrombin residues in the PAR1 bound form are rendered as stick models with C atoms in green. Residues of the free form of thrombin are rendered as stick models uniformly colored in light green. Relevant H bonds are indicated as broken lines. The allosteric communication initiates with a rotation of the benzene ring of Phe-34 and a shift in the side chain of Arg-73 (labeled in black, as all other thrombin residues) in exosite I because of binding of PAR1 via Phe-55, Tyr-52, and Asp-50 (labeled in red). The changes propagate to the 141–146 β -strand via Met-32 and Gln-151. In turn, that reestablishes H bond connections with the 191–193 β -strand and restores the oxyanion hole and the orientation/location of the Cys-191:Cys-220 disulfide bond, which relocates the entire 215–219 β -strand and 220-loop in their canonical positions to free access to the active site and the primary specificity pocket. Trp-215 folds back almost 10 Å into the aryl binding site, relinquishing its hydrophobic interaction with the catalytic His-57 (the catalytic Asp-102 and Ser-195 are also shown for completeness). Arg-221a leaves the interior of the primary specificity pocket where it binds to Asp-189 (data not shown) and moves >9 Å to the surface to engage Glu-146 in a strong bidentate ion-pair. Glu-146 is disordered in the free structure. Additional changes involving the 186-loop restoring access to the Na⁺ binding site are omitted for clarity. The allosteric communication documented in the structure of the thrombin-PAR1 complex relative to the free form of the enzyme is testimony to the flexibility of the thrombin fold and proves that the various forms of the enzyme (E*, E, and E:Na⁺) interconvert under the influence of ligand binding to distinct domains.

access to the active site. Asp-221 restores its important ion-pair interaction with Arg-187 whose guanidinium group moves away from the Na⁺ binding pocket.

Binding of PAR1 to exosite I converts the self-inhibited conformation of the mutant D102N into one that is catalytically competent, with the oxyanion hole correctly structured and access to the active site and primary specificity pocket open to substrate docking. The peculiar self-inhibited conformation documented originally for D102N (42) therefore can convert into a catalytically active conformation through a structural transition that can be traced to a set of residues organized in four layers (Fig. 3). A first layer directly in contact with ligands recognizing exosite I (Phe-34 and Arg-73), a second layer of “transducing” residues connecting to the 141–146 β -strand (Met-32 and Gln-151), a third layer comprising the interactions between the 141–146 and 191–193 β -strands (Trp-141, Asn-143, and Glu-192) and a final layer where such interactions are transmitted to the 215–219 β -strand and the 220-loop via the Cys-191:Cys-220 disulfide bond and Glu-146.

Discussion

The allosteric nature of thrombin was established more than a decade ago from functional studies (43). Two well documented pathways of allosteric regulation exist in the thrombin molecule: one involving the Na⁺ site and the other involving exosite I. Binding of Na⁺ to thrombin enhances activity toward procoagulant and prothrombotic substrates like fibrinogen and PARs (12,

44), whereas binding of thrombomodulin to exosite I enhances activity toward the anticoagulant protein C (37, 45). A significant linkage also exists between the two allosteric sites (28, 46, 47). The structural mechanism underlying these physiologically important mechanisms of allosteric regulation has been subject to intense investigation. The structure of thrombin bound to a fragment of thrombomodulin at exosite I failed to reveal significant conformational changes in the active site (30). Such changes might have been obliterated by the presence of the active site inhibitor used in the crystallization. A number of peptides targeting exosite I influence allosterically the active site of thrombin and bring about significant changes in activity and even substrate specificity (24, 27, 28, 47, 48). One of these peptides, hirugen, is derived from the C-terminal fragment of hirudin. The structure of thrombin bound to hirugen was solved with the active site free (31) but again failed to reveal any significant conformational changes as for the thrombomodulin-bound structure (30). In contrast, the recent structure of murine thrombin bound to a fragment of PAR3 at exosite I reveals a snapshot of the mechanism for the allosteric communication in terms of a shift in the indole ring of Trp-60d and upward movement of the entire 60-loop that open up the active site cleft (32). The resulting facilitated diffusion of substrate into the active site produces an enhancement of k_{cat}/K_m as found experimentally (28). Thrombomodulin binding to exosite I may open the active site fully as shown in the thrombin-PAR3 structure and produce the large change in the rate of diffusion of protein C into the active site (49) in addition to enhanced k_{cat} (50). The conformational change documented in the structure of the thrombin mutant D102N bound to a fragment of PAR1 at exosite I differs markedly from that uncovered for PAR3 binding, which opens the question as to the true extent of conformational perturbation induced by binding to exosite I. Consideration of the distinct conformational states that thrombin assumes when free and bound to Na^+ rationalizes these structural findings.

A recent kinetic analysis of the mechanism of Na^+ binding to thrombin has revealed the existence of three major states of the enzyme (19, 51). The Na^+ -bound form $E:Na^+$ is the high-activity conformation corresponding to the procoagulant fast form (18, 43), and its structural signatures are well established (21, 29). The Na^+ -free form is partitioned into two conformations, E and E^* , of which only E can interact with Na^+ and corresponds to the low-activity, anticoagulant slow form (18, 43). The structure of E reveals several differences with that of $E:Na^+$ (21), but recent mutagenesis and spectroscopic studies suggest that the $E \rightarrow E:Na^+$ transition is more global because it affects the environment of all nine Trp residues of thrombin located up to 35-Å away from the bound Na^+ (12, 19, 23). Similarly, the $E^* \rightarrow E$ transition affects the structure of the enzyme as a whole (12, 19). If E^* is indeed an inactive conformation of thrombin (47, 52), then the recent structure of the mutant D102N in the free form offers a possible representation (42). Given the current structural assignments of E^* , E, and $E:Na^+$, one can conclude that the structural changes in the 60-loop documented upon PAR3 binding to exosite I of murine thrombin (32) pertain to a conformation of the enzyme that is stabilized in the highly active $E:Na^+$ form (53, 54). In fact, murine thrombin is constitutively stabilized in the $E:Na^+$ form by the D222K replacement in the Na^+ site, where Lys-222 provides molecular mimicry of the bound Na^+ (54). However, the larger structural effects caused by binding of PAR1 to exosite I in the D102N mutant of human thrombin pertain to the E^* conformation of the enzyme that is severely compromised for both substrate and Na^+ binding. The consequences of exosite I ligation therefore would differ for the various conformations, E^* , E, and $E:Na^+$, accessible to thrombin under conditions relevant to physiological function (19). Binding to exosite I in the $E:Na^+$ form would cause a shift in the 60-loop

Table 2. Crystallographic data for the human thrombin mutant D102N bound to the extracellular fragment of human PAR1 (PDB ID 3BEF)

| | |
|---|---|
| Data Collection | |
| Wavelength, Å | 0.9 |
| Space Group | P1 |
| Unit Cell Dimension, Å | $a = 46.1, b = 50.3, c = 85.1,$ $\alpha = 76.9^\circ, \beta = 84.3^\circ, \gamma = 73.7^\circ$ |
| Molecules/Asymmetric Unit | 2 |
| Resolution Range, Å | 40.0–2.2 |
| Observations | 81,492 |
| Unique Observations | 34,055 |
| Completeness, % | 94.0 (87.7) |
| $R_{sym}, \%$ | 6.1 (22.1) |
| $I/\sigma(I)$ | 12.3 (3.1) |
| Refinement | |
| Resolution, Å | 40.0–2.2 |
| $ F /\sigma(F)$ | >0 |
| R_{cyst}, R_{free} | 0.207, 0.248 |
| Reflections (Working/Test) | 31,620/1,657 |
| Protein Atoms | 4,963 |
| Solvent Molecules | 229 |
| rmsd Bond Lengths,* Å | 0.006 |
| rmsd angles,* ° | 1.3 |
| rmsd $\Delta B, \text{Å}^2$ (mm/ms/ss) [†] | 3.12/3.58/4.64 |
| protein, Å ² | 37.9 |
| solvent, Å ² | 36.0 |
| Ramachandran Plot | |
| Most favored, % | 98.5 |
| Generously allowed, % | 1.5 |
| Disallowed, % | 0.0 |

*Root-mean-squared deviation (rmsd) from ideal bond lengths and angles and rmsd in B factors of bonded atoms.

[†]mm, main chain–main chain; ms, main chain–side chain; ss, side chain–side chain.

to open the active site fully. Binding to exosite I in the E^* form would cause a larger conformational transition with a long-range communication that can be traced from exosite I to the opposite side of the molecule almost 30-Å away. As a result of this drastic conformational change induced allosterically by binding to exosite I, access to the active site is fully restored and the self-inhibited E^* conformation of D102N is converted into a catalytically competent form similar to E or $E:Na^+$. Therefore, it is not surprising that previous structures of thrombin crystallized in the highly active $E:Na^+$ form have failed to reveal large-scale conformational changes upon binding of ligands to exosite I (31, 41), as documented here for the E^* form.

Recent studies have stressed the importance of allostery as an intrinsic property of all dynamic proteins (10), encompassing numerous examples of monomeric proteins such as thrombin. Proteins that exist in multiple states in dynamic equilibrium tend to show large conformational transitions linked to ligand binding or substrate catalysis. In the classical example of hemoglobin allostery, the initial shift in the F8 His near the heme upon O_2 binding triggers a cascade of structural changes that alter the interaction within and between the α and β chains leading to the T to R transition (4). Similarly, large-scale allosteric changes are observed in multimeric proteins like aspartate transcarbamylase (7), the nicotinic receptor (5), or GroEL (9). Evidence of long-range communication in smaller monomeric proteins is more difficult to obtain (10), but notable successes have been documented recently (8, 11) especially by NMR (55). The results reported here add an important example of how allosteric communication is channeled within a protein in the absence of

quaternary structure by using the shift in a preexisting equilibrium between two distinct conformations.

Another relevant aspect of the results reported in this study is the possibility of exploiting allostery for rational drug design. One embodiment of this exciting strategy is to screen the protein surface for potential allosteric sites (56). The equilibrium between inactive and active forms could be used to switch the enzyme on and off upon binding of suitable molecules working as activators or inhibitors. The thrombin mutant W215A/E217A features a remarkable anticoagulant and antithrombotic profile *in vitro* (57) and *in vivo* (58, 59) by expressing catalytic activity only in the presence of the cofactor thrombomodulin. The structure of W215A/E217A in the free form shows a collapse of the 215–219 β -strand (60) similar to that seen in the D102N mutant (42), indicating that it may be stabilized in the inactive E* form. Upon binding of thrombomodulin to exosite I, the W215A/E217A mutant acquires full catalytic activity toward protein C (57). Most likely, the W215A/E217A mutant bound to thrombomodulin experiences a E* \rightarrow E conformational transition similar to that seen for the D102N mutant upon binding of PAR1. Hence, the structural basis of the E* \rightarrow E transition reported here document how thrombin can be engineered as an allosteric switch to turn on optimal anticoagulant activity *in vivo* upon interaction with an effector molecule.

Materials and Methods

The human thrombin mutant D102N was constructed, expressed, and purified to homogeneity to enable cocrystallization with relevant substrates (42). The isosteric D102N mutation effectively inactivates the enzyme at pH < 8.0 and avoids drastic changes in the polarity of the active site such as those observed with the S195A mutation. A soluble fragment of human PAR1, ⁴²SFLLRNPND-

KYEPFWEDEEKN⁶², corresponding to the sequence downstream from the cleavage site at Arg-41 and containing the hirudin-like motif ⁵²YEPPFWE⁵⁷ predicted to bind to exosite I (33, 38), was synthesized by solid phase, purified to homogeneity by HPLC, and tested for purity by mass spectrometry.

Crystals of human thrombin D102N in complex with human PAR1 were obtained by using the hanging drop vapor-diffusion method. D102N and PAR1 were mixed in 1:1 molar ratio at 4°C for 2 h before crystallization. A solution of D102N (5 mg/ml in 2 μ l) in 50 mM choline chloride and 20 mM Mes (pH 6.0) was mixed with an equal volume reservoir solution containing 30% PEG 4000 and 100 mM Mes (pH 6.5) and left to equilibrate at 12°C. Crystals were triclinic, space group P1, with unit cell parameters $a = 46.1 \text{ \AA}$, $b = 50.3 \text{ \AA}$, $c = 85.1 \text{ \AA}$, $\alpha = 76.9^\circ$, $\beta = 84.3^\circ$, and $\gamma = 73.7^\circ$, and contained two molecules in the asymmetric unit. A structure of D102N in the free form also was obtained at 1.55- \AA resolution (PDB ID code 3BEI) and reproduced the self-inhibited conformation of the mutant reported previously at 1.87 \AA (42). Crystals were cryoprotected in the solution containing 15% glycerol and mother liquor for 3 min and frozen in liquid nitrogen to 100 K. X-ray data were collected to 2.2- \AA resolution on an ADSC Quantum-315 CCD detector at the Biocars Beamline 14-BM-C of the Advanced Photon Source, Argonne National Laboratories (Argonne, IL). Data processing, indexing, integration, and scaling were performed with the HKL2000 package (61). The structure was solved by molecular replacement with MOLREP from the CCP4 package (62) using the coordinates of the PPACK-inhibited form of human thrombin (PDB ID code 1SHH) (21) as a starting model. Refinement and electron density generation were performed with Crystallography and NMR System software package (63), and 5% of the reflections were randomly selected as a test set for cross-validation. Ramachandran plots were calculated with PROCHECK (64). Results of data collection, processing, and refinement are listed in Table 2. Coordinates of the structure of the human D102N–PAR1 complex have been deposited in the Protein Data Bank (PDB ID code 3BEF).

ACKNOWLEDGMENTS. We are grateful to Leslie Bush-Pelc and Alaji Bah for their valuable contribution and suggestions. This work was supported in part by the National Institutes of Health Research Grants HL49413, HL58141, and HL73813 (to E.D.C.).

- Monod J, Changeux JP, Jacob F (1963) Allosteric proteins and cellular control systems. *J Mol Biol* 6:306–329.
- Monod J, Wyman J, Changeux JP (1965) On the nature of allosteric transitions: A plausible model. *J Mol Biol* 12:88–118.
- Wyman J, Gill SJ (1990) *Binding and Linkage* (Univ Science Books, Mill Valley, CA).
- Perutz MF (1970) Stereochemistry of cooperative effects in haemoglobin. *Nature* 228:726–739.
- Changeux JP, Edelstein SJ (2006) Allosteric mechanisms of signal transduction. *Science* 308:1424–1428.
- Di Cera E (2006) A structural perspective on enzymes activated by monovalent cations. *J Biol Chem* 281:1305–1308.
- Kantrowicz ER, Lipscomb WM (1990) Escherichia coli aspartate transcarbamylase: the molecular basis for a concerted allosteric transition. *Trends Biochem Sci* 15:53–59.
- Pellicena P, Kuriyan J (2006) Protein-protein interactions in the allosteric regulation of protein kinases. *Curr Opin Struct Biol* 16:702–709.
- Xu Z, Horwich AL, Sigler PB (1997) The crystal structure of the asymmetric GroEL–GroES–(ADP) γ chaperonin complex. *Nature* 388:741–750.
- Gunasekaran K, Ma B, Nussinov R (2004) Is allostery an intrinsic property of all dynamic proteins? *Prot Struct Funct Genet* 57:433–443.
- Swain JF, Gierasch LM (2006) The changing landscape of protein allostery. *Curr Opin Struct Biol* 16:102–108.
- Di Cera E, Page MJ, Bah A, Bush-Pelc LA, Garvey LC (2007) Thrombin allostery. *Phys Chem Chem Phys* 9:1292–1306.
- Yu EW, Koshland DE, Jr (2001) Propagating conformational changes over long (and short) distances in proteins. *Proc Natl Acad Sci USA* 98:9517–9520.
- Süel GM, Lockless SW, Wall MA, Ranganathan R (2003) Evolutionarily conserved networks of residues mediate allosteric communication in proteins. *Nat Struct Biol* 10:59–69.
- Ota N, Agard DA (2007) Intramolecular signaling pathways revealed by modeling anisotropic thermal diffusion. *J Mol Biol* 351:345–354.
- Bode W (2006) Structure and interaction modes of thrombin. *Blood Cells Mol Dis* 36:122–130.
- Davie EW, Kulman JD (2006) An overview of the structure and function of thrombin. *Semin Thromb Hemost* 32(Suppl 1):3–15.
- Dang OD, Vindigni A, Di Cera E (1995) An allosteric switch controls the procoagulant and anticoagulant activities of thrombin. *Proc Natl Acad Sci USA* 92:5977–5981.
- Bah A, Garvey LC, Ge J, Di Cera E (2006) Rapid kinetics of Na⁺ binding to thrombin. *J Biol Chem* 281:40049–40056.
- Di Cera E, et al. (1995) The Na⁺ binding site of thrombin. *J Biol Chem* 270:22089–22092.
- Pineda AO, et al. (2004) Molecular dissection of Na⁺ binding to thrombin. *J Biol Chem* 279:31842–31853.
- Dang QD, Quinto ER, Di Cera E (1997) Rational engineering of activity and specificity in a serine protease. *Nat Biotechnol* 15:146–149.
- Mengwasser KE, Bush LA, Shih P, Cantwell AM, Di Cera E (2005) Hirudin binding reveals key determinants of thrombin allostery. *J Biol Chem* 280:23997–27003.
- Liu LW, Vu TK, Esmon CT, Coughlin SR (1991) The region of the thrombin receptor resembling hirudin binds to thrombin and alters enzyme specificity. *J Biol Chem* 266:16977–16980.
- Rezaie AR, He X, Esmon CT (1998) Thrombomodulin increases the rate of thrombin inhibition by BPTI. *Biochemistry* 37:693–699.
- Rezaie AR, Yang L (2003) Thrombomodulin allosterically modulates the activity of the anticoagulant thrombin. *Proc Natl Acad Sci USA* 100:12051–12056.
- Vindigni A, White CE, Komives EA, Di Cera E (1997) Energetics of thrombin-thrombomodulin interaction. *Biochemistry* 36:6674–6681.
- Ayala Y, Di Cera E (1994) Molecular recognition by thrombin. Role of the slow–fast transition, site-specific ion binding energetics and thermodynamic mapping of structural components. *J Mol Biol* 235:733–746.
- Bode W, Turk D, Karshikov A (1992) The refined 1.9- \AA X-ray crystal structure of D-Phe-Pro-Arg chloromethylketone-inhibited human alpha-thrombin: Structure analysis, overall structure, electrostatic properties, detailed active-site geometry, and structure-function relationships. *Protein Sci* 1:426–471.
- Fuentes-Prior P, et al. (2000) Structural basis for the anticoagulant activity of the thrombin-thrombomodulin complex. *Nature* 404:518–525.
- Vijayalakshmi J, Padmanabhan KP, Mann KG, Tulinsky A (1994) The isomorphous structures of prethrombin₂, hirugen-, and PPACK-thrombin: changes accompanying activation and exosite binding to thrombin. *Protein Sci* 3:2254–2271.
- Bah A, Chen Z, Bush-Pelc LA, Mathews FS, Di Cera E (2007) Crystal structures of murine thrombin in complex with the extracellular fragments of murine protease-activated receptors PAR3 and PAR4. *Proc Natl Acad Sci USA* 104:11603–11608.
- Coughlin SR (2000) Thrombin signalling and protease-activated receptors. *Nature* 407:258–264.
- Coughlin SR (2005) Protease-activated receptors in hemostasis, thrombosis and vascular biology. *J Thromb Haemost* 3:1800–1814.
- Nakanishi-Matsui M, et al. (2000) PAR3 is a cofactor for PAR4 activation by thrombin. *Nature* 404:609–613.
- Esmon CT (1995) Thrombomodulin as a model of molecular mechanisms that modulate protease specificity and function at the vessel surface. *FASEB J* 9:946–955.
- Esmon CT (2003) The protein C pathway. *Chest* 124:265–325.
- Vu TK, Wheaton VI, Hung DT, Charo I, Coughlin SR (1991) Domains specifying thrombin-receptor interaction. *Nature* 353:674–677.
- Seeley S, Covic L, Jacques SL, Sudmeier J, Baleja JD, Kuliopulos A (2003) Structural basis for thrombin activation of a protease-activated receptor: Inhibition of intramolecular liganding. *Chem Biol* 10:1033–1041.
- Ayala YM, Cantwell AM, Rose T, Bush LA, Arosio D, Di Cera E (2001) Molecular mapping of thrombin-receptor interactions. *Proteins* 45:107–116.

41. Mathews II, et al. (1994) Crystallographic structures of thrombin complexed with thrombin receptor peptides: Existence of expected and novel binding modes. *Biochemistry* 33: 3266–3279.
42. Pineda AO, Chen ZW, Bah A, Garvey LC, Mathews FS, Di Cera E (2006) Crystal structure of thrombin in a self-inhibited conformation. *J Biol Chem* 281:32922–32928.
43. Wells CM, Di Cera E (1992) Thrombin is a Na⁽⁺⁾-activated enzyme. *Biochemistry* 31:11721–11730.
44. Di Cera E (2003) Thrombin interactions. *Chest* 124:115–175.
45. Esmon CT, Mather T (1998) Switching serine protease specificity. *Nat Struct Biol* 5:933–937.
46. Kroh HK, Tans G, Nicolaes GAF, Rosing J, Bock PE (2007) Expression of allosteric linkage between the sodium ion binding site and exosite I of thrombin during prothrombin activation. *J Biol Chem* 282:16095–16104.
47. Lai MT, Di Cera E, Shafer JA (1997) Kinetic pathway for the slow to fast transition of thrombin: Evidence of linked ligand binding at structurally distinct domains. *J Biol Chem* 272:30275–30282.
48. Parry MA, Stone SR, Hofsteenge J, Jackman MP (1993) Evidence for common structural changes in thrombin induced by active-site or exosite binding. *Biochem J* 290(Pt 3): 665–670.
49. Xu H, Bush LA, Pineda AO, Caccia S, Di Cera E (2005) Thrombomodulin changes the molecular surface of interaction and the rate of complex formation between thrombin and protein C. *J Biol Chem* 280:7956–7961.
50. Esmon NL, DeBault LE, Esmon CT (1983) Proteolytic formation and properties of gamma-carboxyglutamic acid-domainless protein C. *J Biol Chem* 258:5548–5553.
51. Gianni S, Ivarsson Y, Bah A, Bush-Pelc LA, Di Cera E (2007) Mechanism of Na⁽⁺⁾ binding to thrombin resolved by ultra-rapid kinetics. *Biophys Chem* 131:111–114.
52. Carrell CJ, Bush LA, Mathews FS, Di Cera E (2006) High resolution crystal structures of free thrombin in the presence of K⁽⁺⁾ reveal the basis of monovalent cation selectivity and an inactive slow form. *Biophys Chem* 121:177–184.
53. Bush LA, Nelson RW, Di Cera E (2006) Murine thrombin lacks Na⁽⁺⁾ activation but retains high catalytic activity. *J Biol Chem* 281:7183–7188.
54. Marino F, Chen ZW, Ergenekan C, Bush-Pelc LA, Mathews FS, Di Cera E (2007) Structural basis of Na⁽⁺⁾ activation mimicry in murine thrombin. *J Biol Chem* 282:16355–16361.
55. Boehr DD, McElheny D, Dyson HJ, Wright PE (2006) The dynamic energy landscape of dihydrofolate reductase catalysis. *Science* 313:1638–1642.
56. Hardy JA, Wells JA (2004) Searching for new allosteric sites in enzymes. *Curr Opin Struct Biol* 14:706–715.
57. Cantwell AM, Di Cera E (2000) Rational design of a potent anticoagulant thrombin. *J Biol Chem* 275:39827–39830.
58. Gruber A, Cantwell AM, Di Cera E, Hanson SR (2002) The thrombin mutant W215A/E217A shows safe and potent anticoagulant and antithrombotic effects in vivo. *J Biol Chem* 277:27581–27584.
59. Gruber A, et al. (2007) Relative antithrombotic and antihemostatic effects of protein C activator versus low molecular weight heparin in primates. *Blood* 109:3733–3740.
60. Pineda AO, et al. (2004) The anticoagulant thrombin mutant W215A/E217A has a collapsed primary specificity pocket. *J Biol Chem* 279:39824–39828.
61. Otwinowski Z, Minor W (1997) Processing of x-ray diffraction data collected by oscillation methods. *Methods Enzymol* 276:307–326.
62. Bailey S (1994) The CCP4 suite. Programs for protein crystallography. *Acta Crystallogr D Biol Crystallogr* 50:760–763.
63. Brunger AT, et al. (1998) Crystallography and NMR system: A new software suite for macromolecular structure determination. *Acta Crystallogr D Biol Crystallogr* 54(Pt 5): 905–921.
64. Morris AL, MacArthur MW, Hutchinson EG, Thornton JM (1992) Stereochemical quality of protein structure coordinates. *Proteins* 12:345–364.

4. Mechanism of the anticoagulant activity of the thrombin mutant WE

4.1. Prelude

We showed that binding of three different ligands to exosite I of E* stabilizes the E form by invoking the D102N mutant. To test our model further, we chose another mutant of thrombin which stabilized in the E* form, i.e., the WE mutant. This study is a direct extension of work done with the thrombin mutant D102N. The thrombin mutant W215A/E217A (WE) is a potent anticoagulant both *in vitro* and *in vivo*. The WE mutant of thrombin has compromised activity towards fibrinogen and PAR₁ but exhibits near wild-type like activity towards protein C, in presence of thrombomodulin (exosite I ligand). Crystal structure of WE shows a collapse of the 215-217 β -strand as well as a compromised Na⁺ binding site similar to what is observed in D102N. We wanted to answer the question of whether this collapse can be restored upon exosite I occupancy. To understand the molecular basis of its anticoagulant potency, I co-crystallized WE with PAR₁. Binding of PAR₁ does not restore the active site as observed with D102N mutant. This work showed that WE is highly stabilized in the E* form and that binding of PAR₁ pulls the equilibrium towards the E form equivalent to the ratio of affinities in the E* and E forms. Further, we concluded that the anticoagulant activity displayed by WE is a consequence of thrombomodulin and protein C on thrombin. We explain our results using binding studies by calorimetry.

Mechanism of the Anticoagulant Activity of Thrombin Mutant W215A/E217A*

Received for publication, May 26, 2009, and in revised form, July 1, 2009. Published, JBC Papers in Press, July 8, 2009, DOI 10.1074/jbc.M109.025403

Prafull S. Gandhi, Michael J. Page, Zhiwei Chen, Leslie Bush-Pelc, and Enrico Di Cera¹

From the Department of Biochemistry and Molecular Biophysics, Washington University School of Medicine, St. Louis, Missouri 63110

The thrombin mutant W215A/E217A (WE) is a potent anticoagulant both *in vitro* and *in vivo*. Previous x-ray structural studies have shown that WE assumes a partially collapsed conformation that is similar to the inactive E^* form, which explains its drastically reduced activity toward substrate. Whether this collapsed conformation is genuine, rather than the result of crystal packing or the mutation introduced in the critical 215–217 β -strand, and whether binding of thrombomodulin to exosite I can allosterically shift the E^* form to the active E form to restore activity toward protein C are issues of considerable mechanistic importance to improve the design of an anticoagulant thrombin mutant for therapeutic applications. Here we present four crystal structures of WE in the human and murine forms that confirm the collapsed conformation reported previously under different experimental conditions and crystal packing. We also present structures of human and murine WE bound to exosite I with a fragment of the platelet receptor PAR1, which is unable to shift WE to the E form. These structural findings, along with kinetic and calorimetry data, indicate that WE is strongly stabilized in the E^* form and explain why binding of ligands to exosite I has only a modest effect on the E^* - E equilibrium for this mutant. The $E^* \rightarrow E$ transition requires the combined binding of thrombomodulin and protein C and restores activity of the mutant WE in the anticoagulant pathway.

Thrombin is the pivotal protease of blood coagulation and is endowed with both procoagulant and anticoagulant roles *in vivo* (1). Thrombin acts as a procoagulant when it converts fibrinogen into an insoluble fibrin clot, activates clotting factors V, VIII, XI, and XIII, and cleaves PAR1² and PAR4 on the surface of human platelets thereby promoting platelet aggregation (2). Upon binding to thrombomodulin, a receptor present on the membrane of endothelial cells, thrombin becomes unable to interact with fibrinogen and PAR1 but increases >1,000-fold

its activity toward the zymogen protein C (3). Activated protein C generated from the thrombin-thrombomodulin complex down-regulates both the amplification and progression of the coagulation cascade (3) and acts as a potent cytoprotective agent upon engagement of EPCR and PAR1 (4).

The dual nature of thrombin has long motivated interest in dissociating its procoagulant and anticoagulant activities (5–12). Thrombin mutants with anticoagulant activity help rationalize the bleeding phenotypes of several naturally occurring mutations and could eventually provide new tools for pharmacological intervention (13) by exploiting the natural protein C pathway (3, 14, 15). Previous mutagenesis studies have led to the identification of the E217A and E217K mutations that significantly shift thrombin specificity from fibrinogen toward protein C relative to the wild type (10–12). Both constructs were found to display anticoagulant activity *in vivo* (10, 12). The subsequent discovery of the role of Trp-215 in controlling the balance between pro- and anti-coagulant activities of thrombin (16) made it possible to construct the double mutant W215A/E217A (WE) featuring >19,000-fold reduced activity toward fibrinogen but only 7-fold loss of activity toward protein C (7). These properties make WE the most potent anticoagulant thrombin mutant engineered to date and a prototype for a new class of anticoagulants (13). *In vivo* studies have revealed an extraordinary potency, efficacy, and safety profile of WE when compared with direct administration of activated protein C or heparin (17–19). Importantly, WE elicits cytoprotective effects (20) and acts as an antithrombotic by antagonizing the platelet receptor GpIb in its interaction with von Willibrand factor (21).

What is the molecular mechanism underscoring the remarkable functional properties of WE? The mutant features very low activity toward synthetic and physiological substrates, including protein C. However, in the presence of thrombomodulin, protein C is activated efficiently (7). A possible explanation is that WE assumes an inactive conformation when free but is converted into an active form in the presence of thrombomodulin. The ability of WE to switch from inactive to active forms is consistent with recent kinetic (22) and structural (23, 24) evidence of the significant plasticity of the trypsin fold. The active form of the protease, E , coexists with an inactive form, E^* , that is distinct from the zymogen conformation (25). Biological activity of the protease depends on the equilibrium distribution of E^* and E , which is obviously different for different proteases depending on their physiological role and environmental conditions (25). The E^* form features a collapse of the 215–217 β -strand into the active site and a flip of the peptide bond

* This work was supported, in whole or in part, by National Institutes of Health Research Grants HL49413, HL58141, and HL73813 (to E. D. C.). The atomic coordinates and structure factors (codes 3HK3, 3HK6, 3EDX, 3HK1, 3EE0, and 3HKJ) have been deposited in the Protein Data Bank, Research Collaboratory for Structural Bioinformatics, Rutgers University, New Brunswick, NJ (<http://www.rcsb.org/>).

¹ To whom correspondence should be addressed: Dept. of Biochemistry and Molecular Biophysics, Washington University School of Medicine, P. O. Box 8231, St. Louis, MO 63110. Tel.: 314-362-4185; Fax: 314-362-4311; E-mail: enrico@wustl.edu.

² The abbreviations used are: PAR, protease-activated receptor; WE, W215A/E217A; hWE, human thrombin version of WE; mWE, murine thrombin version of WE.

between residues Glu-192 and Gly-193, which disrupts the oxyanion hole. These changes have been documented crystallographically in thrombin and other trypsin-like proteases such as α -tryptase (26), the high temperature requirement-like protease (27), complement factor D (28), granzyme K (29), hepatocyte growth factor activator (30), prostate kallikrein (31), prostatic (32, 33), complement factor B (34), and the arterivirus protease nsp4 (35). Hence, the questions that arise about the molecular mechanism of WE function are whether the mutant is indeed stabilized in the inactive E^* form and whether it can be converted to the active E form upon thrombomodulin binding.

Structural studies of the anticoagulant mutants E217K (36) and WE (37) show a partial collapse of the 215–217 β -strand into the active site that abrogates substrate binding. The collapse is similar to, but less pronounced than, that observed in the structure of the inactive E^* form of thrombin where Trp-215 relinquishes its hydrophobic interaction with Phe-227 to engage the catalytic His-57 and residues of the 60-loop after a 10 Å shift in its position (24). These more substantial changes have been observed recently in the structure of the anticoagulant mutant Δ 146–149e (38), which has proved that stabilization of E^* is indeed a molecular mechanism capable of switching thrombin into an anticoagulant. It would be simple to assume that both E217K and WE, like Δ 146–149e, are stabilized in the E^* form. However, unlike Δ 146–149e, both E217K and WE carry substitutions in the critical 215–217 β -strand that could result into additional functional effects overlapping with or mimicking a perturbation of the E^* - E equilibrium. A significant concern is that both structures suffer from crystal packing interactions that may have biased the conformation of side chains and loops near the active site (24). The collapsed structures of E217K and WE may be artifactual unless validated by additional structural studies where crystal packing is substantially different.

To address the second question, kinetic measurements of chromogenic substrate hydrolysis by WE in the presence of saturating amounts of thrombomodulin have been carried out (37), but these show only a modest improvement of the k_{cat}/K_m as opposed to >57,000-fold increase observed when protein C is used as a substrate (7, 37). The modest effect of thrombomodulin on the hydrolysis of chromogenic substrates is practically identical to that seen upon binding of hirugen to exosite I (37) and echoes the results obtained with the wild type (39) and other anticoagulant thrombin mutants (7, 9, 10, 12, 38). That argues against the ability of thrombomodulin alone to significantly shift the E^* - E equilibrium in favor of the E form. Binding of a fragment of the platelet receptor PAR1 to exosite I in the D102N mutant stabilized in the E^* form (24) does trigger the transition to the E form (23), but evidence that a similar long-range effect exists for the E217K or WE mutants has not been presented.

In this study we have addressed the two unresolved questions about the mechanism of action of the anticoagulant thrombin mutant WE. Here we present new structures of the mutant in its human and murine versions, free and bound to a fragment of the thrombin receptor PAR1 at exosite I. The structures are complemented by direct energetic assessment of the binding of ligands to exosite I and its effect on the E^* - E equilibrium.

MATERIALS AND METHODS

The human and murine thrombin versions of the mutant WE (hWE and mWE, respectively) were expressed, purified, and validated as described previously (7, 40). The soluble fragment of human PAR1, ⁴²SFLLRNPNDKYEPFWEDEEKN⁶², corresponding to the sequence downstream from the cleavage site at Arg-41 and containing the hirudin-like motif ⁵²YEPFWE⁵⁷ for binding exosite I, was synthesized by solid phase, purified to homogeneity by high pressure liquid chromatography (HPLC), and tested for purity by mass spectrometry. hWE was concentrated to 8.0 mg/ml in 50 mM choline chloride, 20 mM Tris, pH 7.4. mWE was concentrated to 9.8 mg/ml in 50 mM choline chloride, 20 mM Tris, pH 7.4. Crystallization was achieved at 22 °C by the vapor diffusion technique, with each crystallization reservoir containing 500 μ l of solution. Equal volumes of the protein sample and reservoir solution (1 μ l each) were mixed to prepare the hanging drops. The reservoir solutions are provided in Table 1. Diffraction quality crystals grew in 1–3 weeks and were cryoprotected in a solution similar to the reservoir solution but containing 15% glycerol prior to flash freezing. X-ray diffraction data for mWE-3, mWE-PAR1, hWE, and hWE-PAR1 (Table 1) were collected at the Advanced Photon Source (Beamline Biocars 14-BMC, Argonne National Laboratory), and those for mWE-1 and mWE-2 were collected with a home source RAXIS IV detector (Rigaku/MSC, The Woodlands, TX). The data were indexed, integrated, and scaled with the HKL2000 software package (41). The structures were solved by molecular replacement using MOLREP from the CCP4 suite (42) and Protein Data Bank accession code 1TQ0 (37) as a search model. Refinement and electron density generation were performed with the Crystallography and NMR System (43) for mWE-3, mWE-PAR1, hWE, and hWE-PAR1 or with REFMAC (44) for mWE-1 and mWE-2; 5% of the reflections were randomly selected as a test set for cross-validation. Ramachandran plots were calculated using PROCHECK (45). Statistics for data collection and refinement are summarized in Table 1. Atomic coordinates and structure factors have been deposited in the Protein Data Bank (accession codes: 3HK3 for mWE-1, 3HK6 for mWE-2, 3EDX for mWE-3, 3HK1 for mWE-PAR1, 3EE0 for hWE, and 3HKJ for hWE-PAR1).

Binding of the exosite I ligand hirugen was studied directly by isothermal titration calorimetry under experimental conditions of 5 mM Tris, 0.1% polyethylene glycol 8000, and 200 mM NaCl, pH 8.0 at 25 °C using an iTC200 calorimeter (MicroCal Inc., Northampton, MA) with the sample cell containing thrombin and the syringe injecting hirugen. Details of the experimental procedures have been presented elsewhere (38). Thermodynamic parameters were extracted from a curve fit to the data using software (Origin 7.0) provided by MicroCal that was consistent with a one-site binding model. Experiments were performed in triplicate with excellent reproducibility (<10% variation in thermodynamic parameters). The effect of ligand binding to exosite I on the E^* - E equilibrium can be understood in terms of the properties of the linkage scheme (Scheme 1).

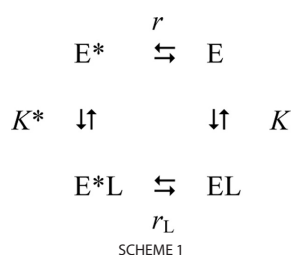
The scheme involves the four possible intermediates for an enzyme existing in two states, E^* and E , binding an allosteric

Structures of W215A/E217A Thrombin

effector, L , such as hirugen or thrombomodulin with an equilibrium association constant, K^* or K . The equilibrium distribution of E^* and E is reflected by the constant $r = [E^*]/[E]$ in the absence of L and $r_L = [E^*L]/[EL]$ in the presence of L . Conservation of energy in Scheme 1 requires (46, 47)

$$\frac{r}{r_L} = \frac{K}{K^*} \quad (\text{Eq. 1})$$

which implies that the original distribution of E^* and E forms quantified by the equilibrium constant r can only be affected to an extent r/r_L equal to the ratio K/K^* . If L binds to E with an affinity x -fold higher than that of E^* , then the relative population of E^* relative to E will decrease x -fold in the presence of L . In other words, the transition of E^* to E is never complete upon binding of an allosteric effector (unless $K/K^* \rightarrow \infty$) but obeys in magnitude the constraints imposed by Equation 1.



RESULTS

Six crystal structures of hWE and mWE were obtained, four in the absence of any ligands and two bound to the extracellular fragment of human PAR1. The six models vary in number of molecules per asymmetric unit, space group, and crystallization conditions including pH (Table 1), as well as in a number of critical residues that confer murine thrombin high catalytic activity in the absence of Na^+ activation (40). Yet the structures present a common active site architecture differing significantly from the wild type in the E form (48). Each of the 11 hWE or mWE protein monomers shows collapse of the 215–217 β -strand into the active site, and the majority show disruption of the oxyanion hole (Fig. 1). Binding of PAR1 to exosite I does not correct the collapsed conformation.

Only one molecule is present in the asymmetric unit of the new structure of hWE, unlike the previous structure, 1TQO (37). The $P2_12_12_1$ space group differs from the previous $P2_13$ lattice and has smaller cell dimensions. In the new hWE structure, the 215–217 β -strand collapses into the S1 pocket (Fig. 1) and is accompanied by complete disorder of the 186- and 220-loops responsible for Na^+ binding. Although the electron density does not enable definition of the autolysis loop and the 220-loop in hWE, the conformational state of what can be observed suggests solvent exposure of the Na^+ binding site and increased solvent accessibility of the normally buried $^{187}\text{RGD}^{189}$ sequence. Such a conformation bears similarity to the K^+ -bound form of thrombin (49, 50) as well as to the structure of the thrombin mutant E217K (36). The new structure

TABLE 1
Crystallographic data for the thrombin mutant W215A/E217A (human and murine) free and bound to a fragment of PAR1

| | mWE-1 | mWE-2 | mWE-3 | mWE-PARI | hWE | hWE-PARI |
|---|--|--|--|---|---|---|
| Buffer/salt | 0.2 M NH_4Cl | 0.2 M $\text{NH}_4\text{H}_2\text{PO}_4$ | 0.2 M Na_2SO_4 | 100 mM Tris | 100 mM MES | 100 mM HEPES |
| pH | 6.3 | 4.6 | 6.6 | 8.5 | 6.5 | 7.5 |
| Polyethylene glycol | 3,350 (20%) | 3,350 (14%) | 3,350 (20%) | 10,000 (20%) | 400 (30%) | 10,000 (20%) |
| PDB* ID | 3HK3 | 3HK6 | 3EDX | 3HK1 | 3EE0 | 3HKJ |
| Data collection | | | | | | |
| Wavelength (Å) | 1.54 | 1.54 | 0.9 | 0.9 | 0.9 | 0.9 |
| Space group | $P2_12_12_1$ | $P4_12_12_1$ | $P2_12_12_1$ | $P2_12_12_1$ | $P2_12_12_1$ | $P1$ |
| Unit cell dimensions (Å) | $a = 48.6$ $b = 63.9$ $c = 95.0$ | $a = 70.4$ $b = 70.4$ $c = 293.1$ | $a = 97.7$ $b = 105.8$ $c = 176.8$ | $a = 231.4$ $b = 51.0$ $c = 80.5$ | $a = 40.1$ $b = 60.0$ $c = 120.0$ | $a = 53.1, \alpha = 98.9^\circ$ $b = 61.8, \beta = 110.3^\circ$ $c = 67.8, \gamma = 92.9^\circ$ |
| Molecules/asymmetric unit | 1 | 2 | 3 | 2 | 1 | 2 |
| Resolution range (Å) | 40–1.94 | 40–3.2 | 40–2.4 | 40–2.2 | 40–2.75 | 40–2.6 |
| Observations | 124,234 | 80,314 | 380,536 | 311,467 | 43,454 | 69,365 |
| Unique observations | 21,296 | 12,201 | 67,622 | 45,052 | 7,810 | 22,864 |
| Completeness (%) | 94.9 (87.0) | 93.3 (72.8) | 94.5 (79.9) | 90.9 (80.9) | 97.5 (85.3) | 93.4 (79.3) |
| R_{sym} (%) | 8.1 (28.0) | 10.5 (37.8) | 5.9 (46.1) | 5.1 (36.5) | 9.0 (32.3) | 5.2 (19.9) |
| $I/\sigma(I)$ | 17.2 (3.3) | 14.6 (3.5) | 21.2 (2.5) | 28.6 (4.9) | 15.4 (2.9) | 18.5 (4.2) |
| Refinement | | | | | | |
| Resolution (Å) | 40–1.94 | 40–3.2 | 40–2.4 | 40–2.2 | 40–2.75 | 40–2.6 |
| $ F /\sigma(F)$ | >0 | >0 | >0 | >0 | >0 | >0 |
| $R_{\text{cryst}}, R_{\text{free}}$ | 0.181, 0.235 | 0.222, 0.314 | 0.214, 0.244 | 0.227, 0.261 | 0.239, 0.323 | 0.195, 0.234 |
| Reflections (working/test) | 20,160/1,098 | 11,572/583 | 62,795/3,371 | 40,411/3,592 | 7,683/418 | 21,050/1,079 |
| Protein atoms | 2,289 | 4,882 | 7,353 | 5,041 | 2,218 | 4,714 |
| Solvent molecules | 240 | 0 | 227 | 217 | 0 | 154 |
| r.m.s.d. bond lengths ^b (Å) | 0.013 | 0.019 | 0.007 | 0.011 | 0.008 | 0.007 |
| r.m.s.d. angles ^c (°) | 1.4 | 1.9 | 1.3 | 1.8 | 1.3 | 1.5 |
| r.m.s.d. ΔB (Å ²) (mm/ms/ss) ^c | 0.76/0.55/2.17 | 0.74/0.37/1.72 | 3.45/4.18/5.55 | 2.32/2.63/3.22 | 1.57/1.76/2.01 | 1.24/1.19/1.60 |
| (B) protein (Å ²) | 25.6 | 44.9 | 54.6 | 41.2 | 38.4 | 40.6 |
| (B) solvent (Å ²) | 34.8 | | 48.9 | 40.4 | | 37.7 |
| Ramachandran plot | | | | | | |
| Most favored (%) | 98.8 | 97.1 | 97.4 | 98.5 | 99.2 | 99.0 |
| Generously allowed (%) | 1.2 | 2.4 | 1.8 | 1.3 | 0.9 | 0.2 |
| Disallowed (%) | 0.0 | 0.5 | 0.8 | 0.2 | 0.0 | 0.8 |

* PDB, Protein Data Bank.

^b Root-mean-squared deviation (r.m.s.d.) from ideal bond lengths and angles and in B-factors of bonded atoms.

^c mm, main chain-main chain; ms, main chain-side chain; ss, side chain-side chain.

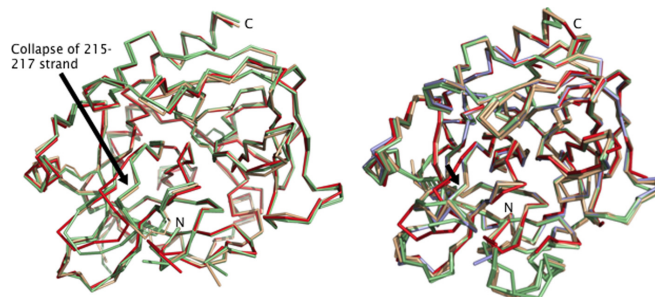


FIGURE 1. α traces of engineered proteases hWE and mWE compared with native thrombin. Left, new hWE structure with only one molecule in the asymmetric unit (*wheat*) is nearly identical to the previous structure, 1TQ0 (*light green*), and differs from the active E form (1SGT (*red*)) (48) for the collapse of the 215–217 β -strand (arrow) into the active site. Right, mWE-1 (*light blue*), mWE-2 (*wheat*), and mWE-3 (*light green*) differ from wild-type murine thrombin (20CV (*red*)) (51) at both the 215–217 β -strand (arrow) and the oxyanion hole.

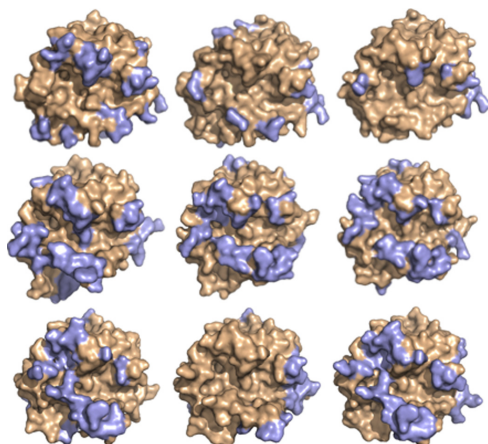


FIGURE 2. Surface representation of the nine free monomers of hWE and mWE (*wheat*). The wide variety of crystal contacts <4 Å (*light blue*) documented in the data sets proves that the collapse of the 215–217 β -strand (arrow) is not an artifact of crystal packing. Top row, hWE, 1TQ0 molecule A, 1TQ0 molecule B. Middle row, mWE-1, mWE-2 molecule A, mWE-2 molecule B. Bottom row, mWE-3 molecules A, B, and C.

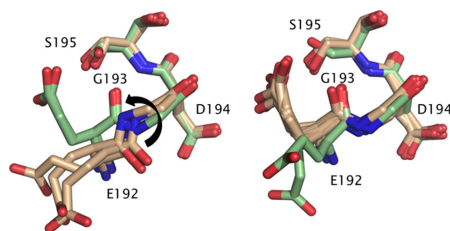


FIGURE 3. Comparison of the oxyanion hole in hWE and mWE in the presence and absence of PAR1. Left, PAR1 binding in hWE (*light green*) induces rotation of the Glu-192–Gly-193 peptide bond such that the backbone O atom is in H-bonding distance of both the OH and backbone N atom of the catalytic Ser-195. Right, in all mWE structures the Glu-192–Gly-193 peptide bond is flipped whether free (*wheat*) or bound to the PAR1 peptide (*light green*).

confirms the collapsed conformation under different crystallization conditions, space groups, and crystal packing (Fig. 2) lending support to the validity of the three-dimensional architecture of the mutant WE first observed in the structure 1TQ0 (37).

Crystals of mWE in the free form were obtained with one, two, and three molecules in the asymmetric unit (mWE-1, mWE-2, and mWE-3). As in the hWE, the 215–217 β -strand collapses into the active site (Fig. 1) although the structures were solved under different crystallization conditions, space groups, and crystal packing (Fig. 2). The

oxyanion hole is disrupted in all monomers because of a flip of the Glu-192–Gly-193 peptide bond (Fig. 3). The ψ angle of Glu-192 decreases by 75° , and the φ angle of Gly-193 decreases by 180° . In this altered conformation, the carbonyl O atom of Glu-192 is placed within H-bonding distance to both the OH and backbone N atoms of the catalytic Ser-195, resulting in an architecture of the triad and oxyanion hole that is incompatible with stabilization of the catalytic transition state (Fig. 3). In turn, the stretch of residues from Glu-192 to Asp-194 assumes a short helical geometry. Overall, the conformational change is less drastic than that observed in the E^* form documented in the D102N (24) and $\Delta 146$ –149e (38) mutants of human thrombin, although it goes in the same direction.

All six monomers of mWE are highly similar to one another throughout their entire structures with the exception of the surface exposed 145-, 186-, and 220-loops. All monomers show the 186-loop flipped toward the active site with only slight variations, which exposes the Na^+ binding site to solvent. Molecule B of hWE-3 is unique in presenting a more extended 145-loop because of packing between adjacent molecules (Fig. 2). Unlike the hWE crystal structure and 1TQ0, the Na^+ -binding loops are well defined due in part to the recruitment of Arg-187 as an intramolecular cation mimic and favorable electrostatics due to the presence of the critical Lys-222 in the murine enzyme. In wild-type murine thrombin, and unlike human thrombin, Lys-222 buries into the Na^+ binding site and effectively mimics the Na^+ activation mechanism (40, 51). In all mWE structures, Lys-222 is dislodged from its position between the 186- and 220-loops and rotates upward to become stabilized by Glu-146 from the autolysis loop, albeit in slightly different orientations in each monomer. In all three monomers of mWE-3, Arg-187 substitutes into the Na^+ site and recruits polar contacts from the backbone O atoms of Phe-184a, Lys-185, and Lys-224. Arg-187 assumes a similar buried conformation in the D102N mutant of thrombin (23, 24). In molecule B of mWE-3, the backbone O atom of Lys-222 is also recruited into the ligand shell of Arg-187. In contrast, the other three monomers from mWE-1 and mWE-2 present Arg-187 in an orientation more similar to wild-type murine thrombin, leaving the Na^+ binding site exposed to solvent. All three structures of mWE support the conclusion

Structures of W215A/E217A Thrombin

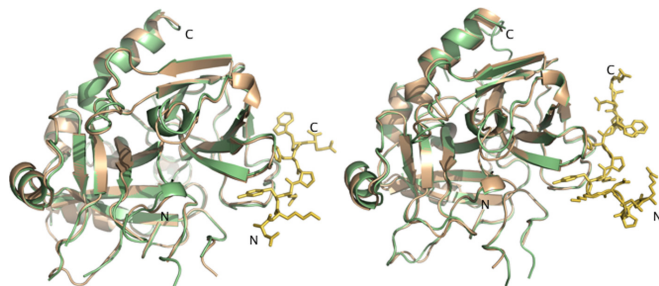


FIGURE 4. PAR1 binding to hWE and mWE does not restore active site architecture. Left, hWE free (wheat) and hWE bound (light green) to the PAR1 peptide (gold) are nearly identical with the exception of the oxyanion hole (see legend for Fig. 3). Right, mWE free (wheat) is nearly identical to the PAR1 (gold) bound state (light green).

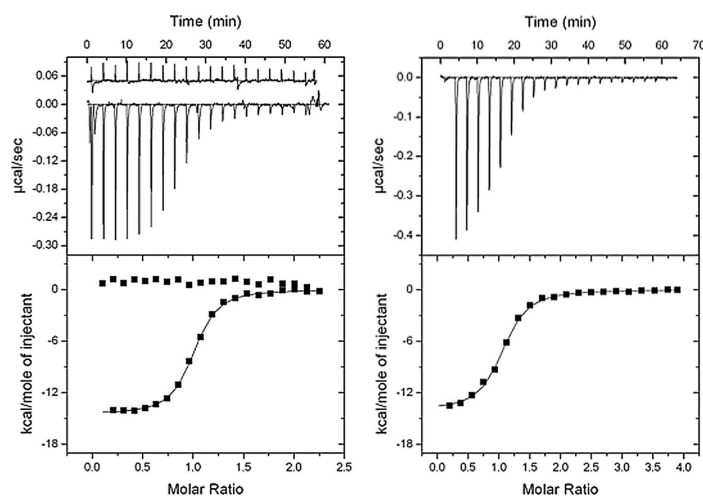


FIGURE 5. Hirugen binding to thrombin wild type (left) and WE (right) measured by isothermal titration calorimetry. The top panel shows the heat exchanged in each individual titration for the thrombin sample (lower trace) and the hirugen buffer control (upper trace, left). The bottom panel is the integration of the data to yield the overall heat exchanged as a function of the ligand/protein molar ratio. Experimental conditions are: 5 mM Tris, 0.1% polyethylene glycol 8000, 200 mM NaCl, pH 8.0, 25 °C. The enzyme and hirugen concentrations are: 10 and 105 μM (thrombin wild type); 12 and 220 μM (WE). Titration curves were fit using the Origin software of the iTC200, with best-fit parameter values: thrombin wild type, $K = 7.4 \pm 0.1 \cdot 10^6 \text{ M}^{-1}$, $\Delta G = -9.4 \pm 0.1 \text{ kcal/mol}$, $\Delta H = -14.5 \pm 0.1 \text{ kcal/mol}$, $T\Delta S = -5.1 \pm 0.1 \text{ kcal/mol}$; WE, $K = 2.1 \pm 0.5 \cdot 10^6 \text{ M}^{-1}$, $\Delta G = -8.6 \pm 0.1 \text{ kcal/mol}$, $\Delta H = -14.0 \pm 0.1 \text{ kcal/mol}$, $T\Delta S = -5.4 \pm 0.1 \text{ kcal/mol}$. The value of the stoichiometric constant, N , was 0.97 ± 0.01 for thrombin wild type and 1.02 ± 0.01 for the WE mutant.

that the disrupted active site architecture is the dominant conformation in solution that is generated by the double Ala substitution at residues 215 and 217.

To test whether the structural defects of the WE conformation are corrected upon ligand binding to exosite I, as documented recently for the E^* form (23), both hWE and mWE were crystallized in complex with an extracellular fragment of PAR1. In the hWE-PAR1 complex, eight residues of the peptide are visible bound to molecule A, whereas seven residues are visible bound to molecule B (Fig. 4). In the mWE-PAR1 complex, the peptide bound to molecule A is defined as being over 15

residues in length, whereas in the peptide bound to molecule B only 9 residues are visible in the electron density (Fig. 4). In both structures the PAR1 fragment engages exosite I of thrombin through a number of polar and hydrophobic interactions. Residue Tyr-52 and Phe-55 of PAR1 interlock with Phe-34 of thrombin, and this complementary hydrophobic packing is assisted by a cation- π interaction between Arg-67 in thrombin and the aromatic ring of Phe-55 of PAR1. Additional H-bond contacts link Asp-50, Tyr-52, and Thr-54 of PAR1 to Leu-40, Arg-73, and Tyr-76 of thrombin. Lack of distinct contacts in the C-terminal portion of PAR1 is unlike that found in hirudin (52) or PAR3 (53) binding, which present additional C-terminal acidic moieties to extend the reach of these peptides farther back into exosite I. The paucity of contacts by the C-terminal residues of PAR1 forces the peptide to adopt two different binding poses to pack Trp-56 against the surface of thrombin. These peptide conformations are similar to that observed in the previously determined complex with the D102N mutant of thrombin (23). However, PAR1 binding to hWE or mWE restores neither the collapse of the 215–217 β -strand (Fig. 4) nor the disruption of the oxyanion hole (Fig. 3). The PAR1-bound structures are nearly identical to those in the free state.

The integrity of exosite I in the WE mutant is supported by calorimetric measurements of the binding of hirugen (Fig. 5). Hirugen binding to exosite I in the wild type elicits changes in activity toward chromogenic substrates that are practically identical to those elicited by thrombomodulin (39). Calorimetry provides a direct and highly informative method of studying binding interactions that, in the case of ligands like hirugen, have thus far relied on indirect kinetic assays (37, 39, 54) or fluorescence probes added to the ligand or the enzyme (55). The binding of hirugen to the wild type is characterized by an equilibrium association constant of $K = 7.4 \cdot 10^6 \text{ M}^{-1}$ and an enthalpy of -14.5 kcal/mol , underscoring a significant entropy loss in the interaction. The binding of hirugen to the mutant WE features an equilibrium association constant $K = 2.1 \cdot 10^6 \text{ M}^{-1}$, which is <4 -fold lower than that of the wild type. The enthalpy change associated with

binding is -14.0 kcal/mol, practically identical to that of the wild type. These results support the conclusion that exosite I is affected modestly by the WE mutation or the collapse in the 215–217 β -strand. It follows from linkage Scheme 1 that binding of ligands to exosite I of the mutant WE should have only a modest effect on the E^* - E equilibrium. If the mutant WE is stabilized in the E^* form, binding of ligands such as thrombomodulin and hirugen to exosite I are expected to have only a modest effect on the catalytic activity of the enzyme toward small chromogenic substrates, as indeed was found when measured experimentally (37).

DISCUSSION

The anticoagulant thrombin mutant WE has little activity toward substrate but features significant activity toward the anticoagulant protein C in the presence of the cofactor thrombomodulin (7). Because of its remarkable success in preclinical studies (17–19, 21), elucidation of the molecular mechanism underlying the function of WE is necessary to eventually remove any residual activity toward fibrinogen and PAR1 in future thrombin variants. A new paradigm, which emerged from the analysis of recent crystal structures of trypsin-like proteases (23, 24, 26–35), offers a context in which to interpret the peculiar properties of WE and other anticoagulant thrombin mutants (9, 10, 12, 38). Trypsin-like proteases such as thrombin exists in equilibrium between two forms, E^* (inactive) and E (active) (25). The biological activity of the protease is determined by the exact partitioning between the inactive E^* and active E forms. The allosteric equilibrium may be shifted using *ad hoc* cofactors or small molecules as well as site-directed mutations. The mutant $\Delta 146-149e$ carrying a deletion of nine residues in the autolysis loop of thrombin has been shown recently to adopt the E^* conformation (38), and its anticoagulant profile has been explained in terms of stabilization of E^* until binding of protein C and thrombomodulin restore activity by triggering the conversion to the E form. The mutant WE features a collapse of the 215–217 β -strand and disruption of the oxyanion hole, which resembles the conformation of E^* (24). This collapse is not artifactual, as it is observed in structures of the human and murine enzymes obtained under different experimental conditions, space groups, and crystal packing (Fig. 2) lending support to the validity of the conformation first observed in the structure 1TQ0 (37). It is likely that the collapsed conformation of WE is indeed the E^* form biased by the effect of removing the indole of Trp-215. The side chain of Trp-215 is critical in maintaining the open conformation of the active site in the E form through a strong hydrophobic interaction with Phe-227 (48). Likewise, in the E^* form, the hydrophobic interaction of Trp-215 with His-57 and Tyr-60a in the 60-loop produces the collapsed conformation that obliterates substrate access to the active site (24). When the side chain of Trp-215 is eliminated with the W215A substitution, the 215–217 β -strand loses a key structural element to stabilize either E or E^* . Hence, it is not surprising that the conformation of the 215–217 β -strand in the WE mutant occupies a position that is intermediate to the two limiting positions in the E and E^* forms. The collapse is sufficient to compromise substrate binding to

the active site even though it does not move the 215–217 β -strand fully to the position seen in the E^* form.

The crystal structures of human and murine thrombin mutant WE bound to a fragment of PAR1 in exosite I show no conversion to the E form and no change in the collapsed 215–217 β -strand as observed in the free form. These observations seem to contradict recent crystallographic evidence that the D102N mutant assumes the E^* form when free and the E form when bound to a fragment of PAR1 at exosite I (23). However, attention to the principles embodied by scheme 1 shows that the results are not in contradiction. Linkage Scheme 1 establishes that an allosteric effector can only shift the E^* - E equilibrium in favor of E by an amount equal to the ratio of affinities of the two forms. Because exosite I, unlike the active site, is similarly accessible in the E^* and E forms (1, 23, 24, 48), binding of thrombomodulin, hirugen, or fragments of PAR1 to the two forms is unlikely to result in extreme perturbations of the E^* - E equilibrium. In fact, binding of hirugen to exosite I in the WE mutant takes place with an affinity that is <4 -fold lower than that of the wild type, confirming that the collapsed conformation of the mutant that compromises access to the active site has little effect on the architecture of exosite I. The available structures of D102N do not imply an all-or-none distribution of E^* and E in solution. Kinetic studies in which the E^* - E equilibrium distribution can be measured directly (22) prove that $r = 1.1$ for D102N free in solution (24). Therefore, it would have been equally likely for this mutant to crystallize in the E form when free, but E^* predominated under the crystallization conditions explored thus far (23, 24). If binding to exosite I takes place with 4-fold higher affinity in the E form, as suggested by the hirugen binding data reported in this study (Fig. 5), then a value of $r_L = 0.28$ is obtained for the mutant D102N bound to exosite I (see Equation 1). Under these conditions, the fraction of D102N in the active E form would be 78% of the total. It is not surprising, then that the structure of D102N bound to a fragment of PAR1 to exosite I has revealed the active E form (23). However, future crystallization studies may trap the D102N-PAR1 complex with the enzyme in the E^* form because of the significant fraction (22%) of this inactive conformation still present in solution. The value of r for the WE mutant cannot be estimated directly from kinetic studies because Trp-215 is a major fluorophore reporting the E^* - E interconversion (22). However, a lower boundary of $r = 200$ can be inferred from the functional properties of the mutant $\Delta 146-149e$ that crystallizes in the E^* form when free (38) and is a less potent anticoagulant compared with WE. Binding of ligands to exosite I of WE should give a value of $r_L = 50$ (see Equation 1), which translates into 2% of the enzyme in the E form when bound. Under these conditions, it would be very difficult to trap the WE-PAR1 complex with the enzyme in the E form, and the E^* form documented in the present study reflects the conformation of 98% of the molecules in solution.

The foregoing argument also explains why thrombomodulin and hirugen have little effect on the hydrolysis of chromogenic substrates by the mutants WE (37) and $\Delta 146-149e$ (38) as well as why physiological substrates like fibrinogen and PAR1 are not cleaved efficiently by the mutants WE and $\Delta 146-149e$ (7, 38). Assuming that these substrates bind to exosite I before

Structures of W215A/E217A Thrombin

contacting the active site, the interaction with exosite I would be insufficient to energetically move the E^* - E equilibrium completely in favor of the active E form. On the other hand, when protein C and thrombomodulin are present in solution, then most of the activity of the mutant WE is restored. The thrombomodulin-protein C complex acting as a substrate may have a more profound effect on E^* - E equilibrium by accessing additional regions of the thrombin surface beyond exosite I (56). In that case, the change in affinity between the E^* and E forms shown in Scheme 1 may be substantial and could ensure significant repopulation of the E form that is not possible with either protein C or thrombomodulin alone.

We conclude that the mutant WE is stabilized in the E^* form, but the complete collapse of the 215–217 β -strand is impeded by the absence of the side chain of Trp-215. Binding to exosite I fails to shift substantially the E^* - E equilibrium in favor of the E form unless protein C and thrombomodulin act in combination. The result of this mechanism is a mutant that acts efficiently in the anticoagulant pathway and retains minimal activity toward the procoagulant substrate fibrinogen and the prothrombotic substrate, PAR1. The intriguing functional properties of the mutant WE (20, 21), its well established potency as an anticoagulant in non-human primates (17, 19), and the current elucidation of the role of E^* in switching thrombin into an anticoagulant (38) should make it possible to engineer a thrombin mutant with exclusive activity toward protein C for therapeutic applications.

REFERENCES

- Di Cera, E. (2008) *Mol. Aspects Med.* **29**, 203–254
- Davie, E. W., and Kulman, J. D. (2006) *Semin. Thromb. Hemost.* **32**, Suppl. 1, 3–15
- Esmon, C. T. (2003) *Chest* **124**, 265–325
- Riewald, M., Petrovan, R. J., Donner, A., Mueller, B. M., and Ruf, W. (2002) *Science* **296**, 1880–1882
- Le Bonniec, B. F., and Esmon, C. T. (1991) *Proc. Natl. Acad. Sci. U.S.A.* **88**, 7371–7375
- Wu, Q. Y., Sheehan, J. P., Tsiang, M., Lentz, S. R., Birktoft, J. J., and Sadler, J. E. (1991) *Proc. Natl. Acad. Sci. U.S.A.* **88**, 6775–6779
- Cantwell, A. M., and Di Cera, E. (2000) *J. Biol. Chem.* **275**, 39827–39830
- Dang, Q. D., Guinto, E. R., and Di Cera, E. (1997) *Nat. Biotechnol.* **15**, 146–149
- Dang, Q. D., Sabetta, M., and Di Cera, E. (1997) *J. Biol. Chem.* **272**, 19649–19651
- Gibbs, C. S., Coutré, S. E., Tsiang, M., Li, W. X., Jain, A. K., Dunn, K. E., Law, V. S., Mao, C. T., Matsumura, S. Y., Mejza, S. J., Paborsky, L. R., and Leung, L. L. (1995) *Nature* **378**, 413–416
- Tsiang, M., Jain, A. K., Dunn, K. E., Rojas, M. E., Leung, L. L., and Gibbs, C. S. (1995) *J. Biol. Chem.* **270**, 16854–16863
- Tsiang, M., Paborsky, L. R., Li, W. X., Jain, A. K., Mao, C. T., Dunn, K. E., Lee, D. W., Matsumura, S. Y., Matteucci, M. D., Coutré, S. E., Leung, L. L., and Gibbs, C. S. (1996) *Biochemistry* **35**, 16449–16457
- Bates, S. M., and Weitz, J. I. (2006) *Br. J. Haematol.* **134**, 3–19
- Di Cera, E. (2007) *J. Thromb. Haemost.* **5**, 196–202
- Griffin, J. H. (1995) *Nature* **378**, 337–338
- Arosio, D., Ayala, Y. M., and Di Cera, E. (2000) *Biochemistry* **39**, 8095–8101
- Gruber, A., Cantwell, A. M., Di Cera, E., and Hanson, S. R. (2002) *J. Biol. Chem.* **277**, 27581–27584
- Gruber, A., Fernández, J. A., Bush, L., Marzec, U., Griffin, J. H., Hanson, S. R., and Di Cera, E. (2006) *J. Thromb. Haemost.* **4**, 392–397
- Gruber, A., Marzec, U. M., Bush, L., Di Cera, E., Fernández, J. A., Berny, M. A., Tucker, E. I., McCarty, O. J., Griffin, J. H., and Hanson, S. R. (2007) *Blood* **109**, 3733–3740
- Feistritz, C., Schuepbach, R. A., Mosnier, L. O., Bush, L. A., Di Cera, E., Griffin, J. H., and Riewald, M. (2006) *J. Biol. Chem.* **281**, 20077–20084
- Berny, M. A., White, T. C., Tucker, E. I., Bush-Pelc, L. A., Di Cera, E., Gruber, A., and McCarty, O. J. (2008) *Arterioscler. Thromb. Vasc. Biol.* **18**, 329–334
- Bah, A., Garvey, L. C., Ge, J., and Di Cera, E. (2006) *J. Biol. Chem.* **281**, 40049–40056
- Gandhi, P. S., Chen, Z., Mathews, F. S., and Di Cera, E. (2008) *Proc. Natl. Acad. Sci. U.S.A.* **105**, 1832–1837
- Pineda, A. O., Chen, Z. W., Bah, A., Garvey, L. C., Mathews, F. S., and Di Cera, E. (2006) *J. Biol. Chem.* **281**, 32922–32928
- Di Cera, E. (2009) *IUBMB Life* **61**, 510–515
- Rohr, K. B., Selwood, T., Marquardt, U., Huber, R., Schechter, N. M., Bode, W., and Than, M. E. (2006) *J. Mol. Biol.* **357**, 195–209
- Krojer, T., Garrido-Franco, M., Huber, R., Ehrmann, M., and Clausen, T. (2002) *Nature* **416**, 455–459
- Jing, H., Babu, Y. S., Moore, D., Kilpatrick, J. M., Liu, X. Y., Volanakis, J. E., and Narayana, S. V. (1998) *J. Mol. Biol.* **282**, 1061–1081
- Hink-Schauer, C., Estébanez-Perpiñá, E., Wilharm, E., Fuentes-Prior, P., Klinkert, W., Bode, W., and Jenne, D. E. (2002) *J. Biol. Chem.* **277**, 50923–50933
- Shia, S., Stamos, J., Kirchofer, D., Fan, B., Wu, J., Corpuz, R. T., Santell, L., Lazarus, R. A., and Eigenbrot, C. (2005) *J. Mol. Biol.* **346**, 1335–1349
- Carvalho, A. L., Sanz, L., Baretino, D., Romero, A., Calvete, J. J., and Romão, M. J. (2002) *J. Mol. Biol.* **322**, 325–337
- Rickert, K. W., Kelley, P., Byrne, N. J., Diehl, R. E., Hall, D. L., Montalvo, A. M., Reid, J. C., Shipman, J. M., Thomas, B. W., Munshi, S. K., Darke, P. L., and Su, H. P. (2008) *J. Biol. Chem.* **283**, 34864–34872
- Spraggon, G., Hornsby, M., Shipway, A., Tully, D. C., Bursulaya, B., Danahy, H., Harris, J. L., and Lesley, S. A. (2009) *Protein Sci.* **18**, 1081–1094
- Ponnuraj, K., Xu, Y., Macon, K., Moore, D., Volanakis, J. E., and Narayana, S. V. (2004) *Mol. Cell* **14**, 17–28
- Barrette-Ng, I. H., Ng, K. K., Mark, B. L., Van Aken, D., Cherney, M. M., Garen, C., Kolodenko, Y., Gorbalenya, A. E., Snijder, E. J., and James, M. N. (2002) *J. Biol. Chem.* **277**, 39960–39966
- Carter, W. J., Myles, T., Gibbs, C. S., Leung, L. L., and Huntington, J. A. (2004) *J. Biol. Chem.* **279**, 26387–26394
- Pineda, A. O., Chen, Z. W., Caccia, S., Cantwell, A. M., Savvides, S. N., Waksman, G., Mathews, F. S., and Di Cera, E. (2004) *J. Biol. Chem.* **279**, 39824–39828
- Bah, A., Carrell, C. J., Chen, Z., Gandhi, P. S., and Di Cera, E. (2009) *J. Biol. Chem.* **284**, 20034–20040
- Vindigni, A., White, C. E., Komives, E. A., and Di Cera, E. (1997) *Biochemistry* **36**, 6674–6681
- Bush, L. A., Nelson, R. W., and Di Cera, E. (2006) *J. Biol. Chem.* **281**, 7183–7188
- Otwinowski, Z., and Minor, W. (1997) *Methods Enzymol.* **276**, 307–326
- Bailey, S. (1994) *Acta Crystallogr. D Biol. Crystallogr.* **50**, 760–763
- Brünger, A. T., Adams, P. D., Clore, G. M., DeLano, W. L., Gros, P., Grosse-Kunstleve, R. W., Jiang, J. S., Kuszewski, J., Nilges, M., Pannu, N. S., Read, R. J., Rice, L. M., Simonson, T., and Warren, G. L. (1998) *Acta Crystallogr. D Biol. Crystallogr.* **54**, 905–921
- Murshudov, G. N., Vagin, A. A., and Dodson, E. J. (1997) *Acta Crystallogr. D Biol. Crystallogr.* **53**, 240–255
- Morris, A. L., MacArthur, M. W., Hutchinson, E. G., and Thornton, J. M. (1992) *Proteins* **12**, 345–364
- Di Cera, E. (1995) *Thermodynamic Theory of Site-specific Binding Processes in Biological Macromolecules*, Cambridge University Press, Cambridge, UK
- Wyman, J., and Gill, S. J. (1990) *Binding and Linkage*, University Science Books, Mill Valley, CA
- Pineda, A. O., Carrell, C. J., Bush, L. A., Prasad, S., Caccia, S., Chen, Z. W., Mathews, F. S., and Di Cera, E. (2004) *J. Biol. Chem.* **279**, 31842–31853
- Carrell, C. J., Bush, L. A., Mathews, F. S., and Di Cera, E. (2006) *Biophys. Chem.* **121**, 177–184
- Papaconstantinou, M. E., Carrell, C. J., Pineda, A. O., Bobofchak, K. M., Mathews, F. S., Flordellis, C. S., Maragoudakis, M. E., Tsopanoglou, N. E.,

Structures of W215A/E217A Thrombin

- and Di Cera, E. (2005) *J. Biol. Chem.* **280**, 29393–29396
51. Marino, F., Chen, Z. W., Ergenekan, C., Bush-Pelc, L. A., Mathews, F. S., and Di Cera, E. (2007) *J. Biol. Chem.* **282**, 16355–16361
52. Rydel, T. J., Tulinsky, A., Bode, W., and Huber, R. (1991) *J. Mol. Biol.* **221**, 583–601
53. Bah, A., Chen, Z., Bush-Pelc, L. A., Mathews, F. S., and Di Cera, E. (2007) *Proc. Natl. Acad. Sci. U.S.A.* **104**, 11603–11608
54. Ayala, Y., and Di Cera, E. (1994) *J. Mol. Biol.* **235**, 733–746
55. Kroh, H. K., Tans, G., Nicolaes, G. A., Rosing, J., and Bock, P. E. (2007) *J. Biol. Chem.* **282**, 16095–16104
56. Xu, H., Bush, L. A., Pineda, A. O., Caccia, S., and Di Cera, E. (2005) *J. Biol. Chem.* **280**, 7956–7961

5. Expression of thrombin catalytic domain in

E. coli

5.1. Need for a new recombinant expression system: Crystal structures of D102N-PAR₁, D102N-hirugen, and D102N-PAR₃ document a massive conformational change upon binding of different ligands at exosite I. Such extreme conformational transitions have never been documented in the multitude of thrombin crystal structures solved to date. Lack of conformational transitions in previous x-ray structural studies was interpreted as thrombin fold being rather rigid (Stubbs & Bode, 1993). Lack of conformational changes in previous structures can be attributed to a variety of reasons ranging from crystal contacts to the presence of thrombin effectors in the crystallization conditions. To directly address the question of whether this flexibility is experienced by thrombin in solution, we pursued solution based structural studies using Nuclear Magnetic Resonance (NMR).

Our current protein expression system using mammalian (Baby Hamster Kidney) cells does not allow labeling for NMR purposes. Protein expression in *E. coli* has been the expression of choice for ¹⁹F-NMR purposes (Bann *et al.*, 2002; Schuler *et al.*, 2002; Frieden *et al.*, 2004). I have, therefore, developed a recombinant thrombin expression system using *E. coli* (DiBella *et al.*, 1995; Soejima *et al.*, 2001; Johnson *et al.*, 2005). Induction of *E. coli* cells using 1 mM IPTG results in inclusion

body that is mostly composed of prethrombin-2. I was successful in resuspending thrombin from the inclusion bodies followed by refolding it in its canonical fold. I was able to purify it and have tested the construct for activity and structure.

5.2. *E. coli* expression protocol:

The cDNA corresponding to prethrombin-2 sequence was cloned into pET21a vector (Novagen) using the EcoRI and the XhoI restriction sites. The prethrombin-2 vector was transformed into BL21(DE3) *E. coli* cells. The *E. coli* cells were grown overnight in 10 mL of LB media with 100 µg/mL ampicillin at 37 °C and 225 rpm. The next morning, 3 L of LB media with 100 µg/mL of ampicillin was inoculated with the 10 mL overnight culture. Growth was continued at 37 °C and 225 rpm until the cells reached OD₆₀₀ = 0.6. Prethrombin-2 expression was initiated by adding IPTG to a final concentration of 1 mM. The *E. coli* cells were cultured for an additional 4 hours. The cultures were spun at 3500 rpm for 20 minutes at 4 °C. The supernatant was discarded and the cell paste, from 1 L of LB media, was resuspended in 50 mL of resuspension buffer, 50 mM Tris pH = 8.0 @ 25 °C, 20 mM EDTA. The suspension was combined and spun again at 3500 rpm for 20 minutes at 4 °C. The supernatant was discarded and the cell paste was stored at -80 °C.

The cell paste was thawed at 37 °C and resuspended in 50 mL of 50 mM Tris pH = 8.0 at 25 °C, 20 mM EDTA, 0.1 % Triton X-100, 20 mM DTE. Cells were further

sonicated on ice for 30 sec x 5 (~ 1 minute rest) at constant duty, 5 ½ output, and time - hold. The well-homogenized cells were ultracentrifuged for 30 minutes at 4 °C, 30,000 rpm, using a Ti45 rotor. The supernatant was discarded and the pellet was resuspended in 40 ml of 50 mM Tris pH = 8.0 at 25 °C, 20 mM EDTA, 2 % Triton X-100, 20 mM DTE using gentle vortexing and a spatula. The homogenate was centrifuged for 30 minutes, 30,000 rpm, 4 °C. Supernatant was discarded and the pellet was suspended in 40 ml of 50 mM Tris pH = 8.0 at 25 °C, 20 mM EDTA, 1 M NaCl, 20 mM DTE prior to centrifugation for 30 minutes, 30000 rpm at 4 °C. The supernatant was discarded and the pellet was re-suspended in 25 ml of 50 mM Tris pH = 8 @ 25 °C, 20 mM EDTA, 6 M GdnHCl, 20 mM DTE overnight. The suspension was spun at 30000 rpm at 4 °C for 45 minutes. The supernatant was dialyzed against 20 mM Tris pH = 8 @ 25 °C, 6 M GdnHCl, 5 mM EDTA three times at 4 °C. Post-dialysis, the unfolded protein was incubated with 5 mM GSH and 2 mM GSSG for 3 hours at room temperature. The supernatant was then dialyzed against two changes of 6 M GdnHCl, 20 mM EDTA, pH = 5 at 4 °C.

Refolding of prethrombin-2 was initiated by adding 1 mL, every 1 hr, of the unfolded protein in 500 mL of refolding buffer, 0.6 M L-Arginine, 10 % Glycerol, 25 mM CaCl₂, 0.2 % Brij58, 50 mM Tris pH = 8 at 25 °C. The refolded protein was concentrated from 2 L to 150 mL using Quickstand, from Amersham Biosciences, with a 10 kDa hollow fiber cartridge. The 150 mL of refolded protein was dialyzed against three changes of 10 mM Tris pH = 8 at 25 °C, 0.1 M NaCl. A final dialysis

was done against a buffer of 10 mM Tris pH = 8 at 25 °C. Precipitate was removed by centrifugation. Protein solution was loaded onto a 5 mL heparin column, from GE Healthcare, at 3 mL/minute. The bound protein was extensively washed by 100 mM NaCl, 10 mM Tris pH = 8 at 25 °C before elution with a linear gradient of 100 mM to 1 M NaCl in 10 mM Tris, pH 8 @ 25 °C. The elution was monitored by UV spectroscopy. Fractions that showed activity were combined and re-purified on heparin column for a second time. Prethrombin-2 was activated using 10 uL of ecarin (50 EU/mL) per 1 mL of protein solution. Activation was monitored by cleaving a synthetic substrate, FPR-pNA, and following the absorbance of the p-nitroanilide at 405 nm. The activated protein was diluted 4-fold and loaded on the heparin column. Bound protein was extensively washed by 100 mM ChCl, 10 mM Tris pH = 8 at 25 °C before elution with a linear gradient of 100 mM to 1 M ChCl in 10 mM Tris, pH 8 @ 25 °C. The active site concentration was determined by using a tight binding inhibitor hirudin.

5.3. Functional and structural characterization of thrombin expressed in the

***E. coli* expression system:** *E. coli* does not have the capability to introduce glycosylation at the sole site in human thrombin at position N60g. It is, therefore, important to characterize the properties of thrombin expressed using the *E. coli* expression system. Refolding results are consistent with previous work by other labs (DiBella *et al.*, 1995; Johnson *et al.*, 2005). Relevant parameters for a small synthetic substrate hydrolysis, FPR-pNA, are listed in table 1.

| Solution conditions | | k_{cat}/K_m | $k_{cat}(\text{sec}^{-1})$ | $K_m(\mu\text{M})$ | $K_p(\mu\text{M})$ |
|---------------------|----------------|---------------|----------------------------|--------------------|--------------------|
| 200 mM NaCl | BHK | 80±10 | 27±2 | 0.34±0.03 | 1.49±0.03 |
| | <i>E. coli</i> | 80.3±1.7 | 28.7±0.5 | 0.358±0.007 | 1.56±0.004 |
| 200 mM ChCl | BHK | 3±0.1 | 5.4±0.4 | 1.8±0.09 | 11±3 |
| | <i>E. coli</i> | 3.16±0.05 | 4.54±0.03 | 1.44±0.02 | 4.69±0.1 |

Table 5.1. Catalytic efficiency of thrombin expressed in BHK and *E. coli* expression systems towards FPR. Solution conditions are 5 mM Tris pH = 8 @ 25 deg. C, 0.1 % PEG 8000, **200 mM NaCl/ChCl**

The k_{cat}/K_m values of thrombin expressed in *E. coli* towards physiological substrates like fibrinogen, PAR₁ and protein C cleavage are identical to the values that are obtained from mammalian expressed thrombin. Furthermore to test our *E. coli* expression system, I crystallized the wild-type thrombin free of any active site inhibitors and other effectors at 1.55-Å. The structural alignment to the wild-type (R77aA mutant, PDB: 1SGI) expressed in the mammalian expression system is shown in figure 5.1. For the purpose of clarity only the active site residues are shown. The structure is identical to the one that was published earlier (Johnson *et al.*, 2005).

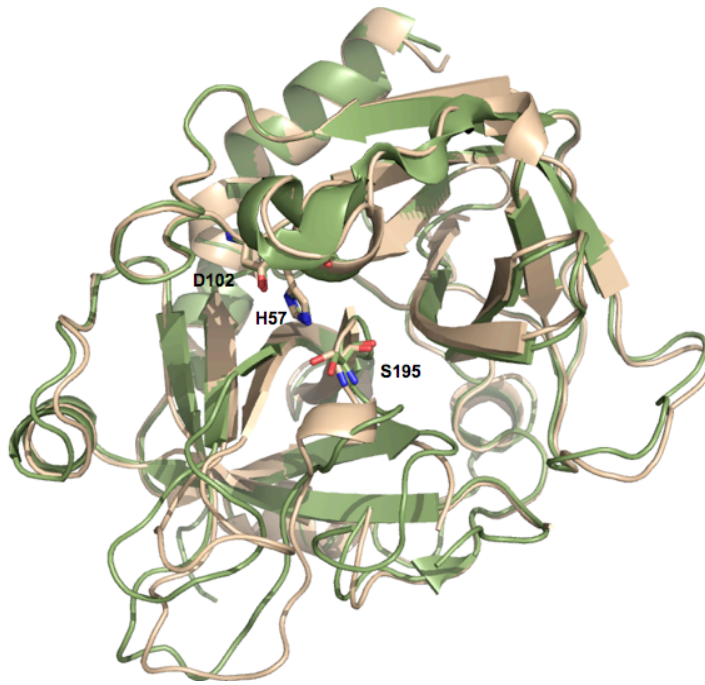


Figure 5.1. Crystal structure of α -thrombin expressed in *E. coli*. Structural alignment of *E. coli* expressed thrombin (wheat) with thrombin (R77aA, PDB: 1SGI) expressed using the mammalian expression system. For clarity, only the three active site residues (H57, D102, S195) are shown.

6. Application of ^{19}F -NMR to study thrombin structure and allostery

6.1. Prelude:

Substantial progress has been achieved in understanding thrombin properties using x-ray crystallography and variety of functional studies. X-ray crystallography has revealed how thrombin recognizes various cofactors, ligands, inhibitors and substrates. Probing conformational change in the thrombin scaffold upon ligand binding by x-ray crystallography is still challenging. To test our long-range allosteric model and to test whether apo wild-type α -thrombin is similar to prethrombin-2, I have employed ^{19}F -NMR. NMR has been successfully applied to thrombin substrates including PAR₁ (Seeley *et al.*, 2003), PAR₄ (Cleary *et al.*, 2002), fXIII activation peptide (Trumbo & Maurer, 2003; Isetti & Maurer, 2004a & 2004b), and γ' peptide (Sabo *et al.*, 2006) and also on thrombomodulin (TM), a thrombin cofactor (Wood *et al.*, 2000; Prieto *et al.*, 2005). NMR studies on PAR₁ documented a major conformational transition in PAR₁ peptide upon thrombin cleavage while studies on γ' peptide revealed formation of a significant secondary structure upon binding to thrombin exosite II. NMR studies of TM revealed the correlation between backbone dynamics and anticoagulant cofactor activity. NMR studies on thrombin substrates and cofactor have elegantly captured the conformational transitions upon thrombin binding/cleavage and have underscored the role of protein dynamics in macromolecular recognition.

6.2. Introduction:

Thrombin is a Na^+ -activated (1), allosteric serine protease that plays procoagulant, prothrombotic, and anticoagulant functions in blood. In the presence of the monovalent cation Na^+ , thrombin acts as a procoagulant converting fibrinogen into fibrin and activates platelets through protease-activated receptors 1 and 4 (PAR_1 and PAR_4). In contrast, in complex with the endothelial receptor thrombomodulin (TM), thrombin acts as an anticoagulant activating protein C (2-4). Two well-documented allosteric pathways form the basis of thrombin's opposing function, a) one employing the Na^+ binding site, and b) the other employing exosite I (5, 6). The central role played by thrombin in hemostasis and thrombosis has generated immense interest in elucidating how thrombin is endowed with substrate specificity and allosteric regulation. In particular, what is the full extent of conformational flexibility, if any, experienced by the thrombin scaffold and its role in thrombin function. At physiological conditions, thrombin exists predominantly in two forms at equilibrium, the Na^+ free form, E and the Na^+ bound form, $\text{E}:\text{Na}^+$. X-ray crystal structures of E and $\text{E}:\text{Na}^+$ have been solved and display subtle structural differences (7-9). In addition to the two forms, it was proposed that there is a third form of the enzyme, E^* , in equilibrium with the free form, E, that can neither bind/cleave substrates nor bind Na^+ (10, 11). Crystal structure of the E^* form of thrombin shows a collapse of the 215-217 β -strand in the active site region and a compromised Na^+ binding site. Several mutants, including

the anticoagulant thrombin mutants WE (12) and E217K (13), have been identified that document occluded active site, compromised Na⁺ binding site and a non-optimal oxyanion hole. Such structural features signal the presence of the E* form and help rationalize the functional properties of these thrombin variants (14-17).

Functional and biophysical data vouch for extensive and global effects upon ligand binding to thrombin (1, 10, 18, 19). Several crystal structures of apo-thrombin as well as thrombin bound to various ligands and cofactors have been reported but lack significant conformational differences (8, 20, 21). While x-ray crystallography has revealed the molecular basis of thrombin macromolecular recognition (20-25) and substrate specificity (26), tracking allosteric changes in the thrombin scaffold has remained challenging. A recent x-ray structural study from our lab revealed that binding of cleaved fragment of PAR₁ to exosite I of E* causes massive conformational change in the active site cleft and stabilizes the enzyme in the canonical E form (27). Such extreme large-scale conformational transitions have never been documented in the multitude of thrombin crystal structures solved to date. More recently, it was suggested that apo α -thrombin is zymogen-like and relies on ligand binding to achieve a fully active conformation (28-31). To address the question of whether this structural plasticity is experienced by wild-type α -thrombin in solution and to test the hypothesis that wild-type α -thrombin and its immediate zymogen form, prethrombin-2, share similar structural and biophysical signatures, we have employed solution based structural studies using ¹⁹Fluorine-

Nuclear Magnetic Resonance (^{19}F -NMR). Here we report the ^{19}F -NMR spectra of α -thrombin and prethrombin-2 that reveal the signatures of structural differences between the two forms of thrombin. We have used argatroban to further probe the biophysical differences between the two forms using isothermal titration calorimetry (iTC₂₀₀) experiments. Together, our data indicate that wild-type apo α -thrombin is an extremely dynamic molecule with high conformational flexibility. The structural and biophysical signatures of apo α -thrombin and prethrombin-2 are dramatically distinct from each other. In the apo form, prethrombin-2 also experiences E^* to E equilibrium but has a higher population of E^* when compared to wild-type α -thrombin. Although flexible, prethrombin-2 lacks the same extent of dynamics that is conferred upon apo α -thrombin.

6.3. Results:

6.3.1. Assignment of ^{19}F -tryptophan resonances.

We have recorded the ^{19}F -NMR spectra of wild-type α -thrombin in four states: apo-thrombin, thrombin in presence of hirugen, in the presence of Na^+ , and bound to PPACK in the presence of both hirugen and Na^+ . In order to assign all the peaks, we have expressed, purified, and obtained ^{19}F -NMR spectra of all single tryptophan mutants to a phenylalanine (except W29F) in the apo form of α -thrombin as well as bound to different ligands. A similar strategy to assign the peaks in the prethrombin-2 spectra did not work as a result of extensive overlap between tryptophan chemical shifts.

¹⁹F-NMR spectra of wild-type α -thrombin, figure 6.2, shows one broad peak (-43.7 ppm) and three clusters of peaks (-46.5 ppm to -51.5 ppm). A single tryptophan mutation to phenylalanine, W₁₄₁F, establishes unambiguously that the broad peak at -43.7 ppm corresponds to W₁₄₁. The downfield chemical shift of W₁₄₁ is significantly different when compared to the free ¹⁹F-tryptophan suggesting that the 5th position on the indole ring of W₁₄₁ is experiencing a chemical environment that is very different from being solvent exposed and is consistent with several crystal structures. The broad nature of the peak suggests that it is experiencing a slow exchange between at least two different conformations. Tryptophans 51 and 207 show overlapping chemical shifts in cluster 1 (-46.5 ppm to -48 ppm) suggesting that they are experiencing similar environments. Their chemical shifts are significantly shifted from the free ¹⁹F-tryptophan suggesting that W₅₁ and W₂₀₇ are not solvent exposed consistent with the crystal structures. The spectrum of the apo form of W₅₁F shows that W₂₀₇ displays one sharp peak (-47.2 ppm) with a shoulder (-47.5 ppm) suggesting that W₂₀₇ is in equilibrium with at least two populations. Similar interpretation for W₅₁ is difficult to make because of the overall changes in the spectrum of the W₂₀₇F mutant. The chemical shifts of tryptophans 96 and 237 are overlapped in cluster 2 (-48 ppm to -49 ppm). The relatively narrow linewidths of these two tryptophans suggest that there is little ring motion associated with these two tryptophans. Cluster 3 (-49 ppm to -51.5 ppm) gives a large number of overlapped shifts belonging to tryptophans 29, 60d,

148, and 215. Single site mutations of W60d, W148, and W215 to a phenylalanine affects the overall architecture and preclude clear assignment of the peaks but it is straightforward to prove that these tryptophans show resonances very close to each other. Several crystal structures show that these three tryptophans are solvent exposed and therefore it is not surprising that they may experience similar environment and similar chemical shifts. Replacing W29 with the hydrophobic phenylalanine side chain results in an incorrectly folded protein. This is surprising because the crystal structures show that the only H-bond that the indole ring makes is with the backbone O of S27 upstream. Our failure to express a correctly folded W29F mutant is testament to the fact that the indole ring of W29 is not occupying a hydrophobic environment. Our assignment of this tryptophan very close to the free ^{19}F -tryptophan spectra is therefore not surprising. Similar strategy was used to assign resonances in different ligand bound forms of α -thrombin and is summarized in figure 6.2.

6.3.2. Binding of Na^+ , exosite I ligand hirugen, and an irreversible inhibitor PPACK induce significant and distinct structural and dynamic changes

We chose hirugen as our exosite I binding ligand and PPACK as our irreversible active site inhibitor. Figure 6.3 shows the ^{19}F -NMR spectra of α -thrombin and prethrombin-2 in the presence of Na^+ , in the presence of hirugen, and in the presence of hirugen, Na^+ and PPACK. Each spectrum is distinct from one another and from the apo form of α -thrombin. In general, change in fluorine chemical shift

is suggestive of change in the tryptophan environment most likely associated with conformational change upon ligand binding. Furthermore, sharpening of linewidth is suggestive of stripping the tryptophan of some degree of freedom. For example, binding of Na^+ causes major rearrangement in the chemical shifts of the labeled tryptophans. When compared to the apo-form, binding of Na^+ sharpens the linewidth of W_{141} at -43.7 ppm. W_{141} resonance does not change in terms of the frequency suggesting that binding of Na^+ does not change the chemical environment of W_{141} but only changes its dynamics. Cluster 1 harbors W_{51} and W_{207} . As observed in the apo-form, there is a shoulder at -47.5 ppm corresponding to W_{207} . This shoulder merges into the main peak at -47.2 ppm and results in a sharper combined peak of W_{51} and W_{207} . It can be interpreted that binding of Na^+ locks down the conformation of W_{207} residue. Cluster 2 which harbors W_{96} and W_{237} displayed sharp resonances in the apo-form suggesting little ring motion associated with these two tryptophans. Binding of Na^+ results in even sharper resonances suggesting further loss in ring motion. Cluster 3 that harbors four tryptophans (W_{29} , W_{60d} , W_{148} , and W_{215}) responds the most to the binding of Na^+ . Binding of Na^+ results in splitting of the cluster 3 into three different peaks (-49 ppm, -49.3 ppm, and -50 ppm). W_{148} and W_{215} combine to give one sharp peak at -49 ppm while W_{60d} display resonance at -50 ppm. These 3 tryptophans display a huge change in their resonances in two aspects, a) Binding of Na^+ makes them more solvent exposed as their resonance is observed very close to -49.5 ppm (chemical shift for free $^{19}\text{F-W}$), b) their resonance becomes sharp

suggesting that these tryptophans undergo a dynamic change from a state where they were sampling different conformations to rigid conformation. W29 display a slightly broad resonance suggesting that it is still able to sample few degrees of freedom. Overall, binding of Na⁺ locks the enzyme such that it cannot sample multiple conformations.

Similar observations regarding structural and dynamic changes upon hirugen and PPACK binding can be made based on figure 6.2. In general, binding of ligands disperse and sharpen the chemical shifts compared to the apo form of α -thrombin suggesting that binding of ligands induce conformational changes and strip thrombin of its degrees of freedom respectively. This effect is seen when hirugen binds, a larger effect is observed when Na⁺ binds and the largest effect is observed when all the three ligands are bound.

6.3.3. ¹⁹F-NMR spectra of Prethrombin-2

Figures 6.2 and 6.3 show the ¹⁹F-NMR spectra of prethrombin-2 in our standard buffer, in presence of Na⁺, in presence of hirugen, and bound to PPACK in presence of hirugen and Na⁺. Spectra of apo forms of prethrombin-2 and α -thrombin unequivocally point out the differences between the two forms. Spectra of prethrombin-2 in presence and in absence of Na⁺ are almost identical suggesting that 200 mM of Na⁺ has little or no effect on the prethrombin-2 architecture at the level of tryptophan sidechains. Spectrum of prethrombin-2 in presence of hirugen

or PPACK and hirugen show differences when compared to apo prethrombin-2. This is consistent with the knowledge that prethrombin-2 binds hirugen as well as PPACK. The differences in these two spectra clearly show that binding of hirugen and PPACK in presence of hirugen induce distinct changes in the prethrombin-2 scaffold. These changes fade when compared to similar binding in α -thrombin scaffold. This suggests that changes in prethrombin-2 may not be global and widespread as seen for α -thrombin.

6.3.4. Thermodynamics of ligand induced allostery in thrombin

To test the hypothesis that apo α -thrombin is zymogen like, we have probed α -thrombin, prethrombin-1, prethrombin-2 and several thrombin mutants by argatroban using iTC₂₀₀. Thrombin variants were selected such that the mutated site did not interact with argatroban. We have measured the apparent association binding constant and the related thermodynamics parameters, figure 6.4. In all our binding experiments, the stoichiometry is 1:1 as expected. Thrombin mutant loopless and D194N define the upper limit while the wild-type define the lower limit of enthalpic interaction with argatroban. All thrombin variants, including prethrombin-1 and prethrombin-2, fall between these two extremes. Thrombin mutant loopless has been shown to exhibit exclusive anticoagulant activity and was more recently crystallized in the E* form. It has been conclusively shown that wild-type experiences the E* to E equilibrium. The Y-axis of such a plot can thus be thought of as a scale of relative population of E*. A value of $\Delta H = 0$ will signify

an entirely E* population, whereas a value of $\Delta H \leq -13$ kcal/mole will signify a wild-type like situation. Thrombin mutant N143P, loopless, and thrombin variant prethrombin-1 have crystallized in the E* like conformation with a collapsed active site. Because these variants bind to argatroban, it proves that these variants also have a significant population with the active site accessible to argatroban. These isotherms are closer to the upper limit suggesting that the relative population of E* is more compared to wild-type. It can be concluded that these variants experience E* to E equilibrium. Binding isotherm for I16A variant, prethrombin-2 and prethrombin-1 are between the two extremes suggesting similar E* to E equilibrium but with higher E* content compared to wild-type and lower E* content when compared to the loopless variant of thrombin. Recently, it was proposed that ligand binding shuttles thrombin from zymogen-like to proteinase-like states (30). In their work, fragment 2 was used a ligand to probe thrombin structure. Fragment 2 does not interact with the active site and hence cannot perturb the E* to E equilibrium. Argatroban is a more suitable probe which penetrates the primary specificity pocket. We show with the iTC data that the zymogen form of thrombin (prethrombin-1 and prethrombin-2) does not lie at the extremes.

6.4. Discussion:

X-ray crystallography has been widely used to study allosteric regulation and substrate selectivity in thrombin. Although it has revealed a great deal about this

protease, tracking conformational changes associated with ligand binding has proven to be tricky. The reasons could be, a) It is very difficult to predict the correct and optimum buffer conditions that aid in the initiation of crystal nucleation and its growth, b) Often, crystallization conditions need to include functionally unnecessary reagents to induce crystallization with little information on their effects on the enzyme properties, c) a homogeneous protein sample does not guarantee diffraction quality crystals, which is often the bottleneck in structural studies based on x-ray crystallography, d) unavoidable crystal packings can potentially mask the true conformation of the enzyme, and e) explaining protein dynamics using x-ray crystallography is non-trivial and is still in a nascent phase. We, therefore, chose to study ligand induced conformational change using solution-based techniques. In this study, ligand induced allosteric changes in thrombin structure were elucidated with ^{19}F -NMR combined with calorimetric studies.

6.4.1. ^{19}F -tryptophan as a probe to study thrombin allostery.

Mature thrombin, denoted as α -thrombin, is a 33.8 kDa monomeric serine protease susceptible to self-cleavage at millimolar concentrations at room temperature. To avoid self-cleavage, thrombin has to be engineered with an exosite I mutant which necessitates studying a thrombin mutant. α -thrombin is a highly allosteric protease as exemplified by numerous functional and biophysical studies. Studying a mutant thrombin and correlating it to wild-type α -thrombin

should be undertaken with caution. Therefore, conventional NMR has proved unsuitable, as of yet, for solution based structural studies of wild-type α -thrombin. Fluorine NMR has proven to be a powerful technique in the study of protein structure and dynamics (32-34) and it offers a unique advantage in the case of α -thrombin. Fluorine NMR experiments typically call for sample concentrations of around 50 μ M. Wild-type α -thrombin is resistant to autolysis at low concentrations of 50 μ M for more than three days allowing us to work with physiologically relevant wild-type α -thrombin in solution. Furthermore, the ^{19}F nucleus is extremely sensitive to structural changes in the local environment, including van der Waals packing interactions and local electrostatic fields and can provide site-specific dynamical information (32, 33). This provides us with a unique tool to study the effect of ligand binding on thrombin structure and dynamics as probed by changes in the ^{19}F environment.

We chose the tryptophan sidechain as our labeling site for various reasons as three (W60d, W148, and W215) of the nine tryptophans are located strategically around the thrombin active site while the remaining tryptophans are conveniently distributed throughout the thrombin structure. Tryptophan residues play a key role in thrombin allostery and substrate selectivity. Previous studies involving these three tryptophans have shown that mutation/deletion affects the allosteric effect of Na^+ on thrombin active site (35, 36). Mutation of residue W60d, located 17-Å from the Na^+ binding site, suppresses Na^+ binding and the functional differences

between the slow and the fast forms (37-39). Spectroscopic studies indicate Na^+ binding induces extensive and global conformational change in thrombin (10). Mutagenesis of tryptophans has revealed that W₁₄₁ and W₂₁₅ contribute significantly and W₁₄₈, W₂₀₇, and W₂₃₇ contribute to a lesser extent to the fluorescence change associated with E* to E transition. These studies vouch for the involvement of tryptophans in ligand recognition and substrate selectivity. Tracking conformational transitions of tryptophans as a result of ligand binding in solution will allow us to monitor the allosteric effect of the ligand on the active site as well as the involvement of different domains of thrombin in macromolecular recognition.

6.4.2. Is the thrombin scaffold flexible?

¹⁹F-NMR spectra of thrombin in the free form show a broad resonance for W₁₄₁ as well as W₂₉, W_{60d}, W₁₄₈, and W₂₁₅. Broad resonances signify that the tryptophan is undergoing intermediate exchange between at least two states. Furthermore, W₂₀₇ shows two peaks suggesting that this tryptophan is undergoing slow exchange between at least two states. This bodes well with our current understanding that in absence of ligands, wild-type α -thrombin exists in two forms E* and E. Ability of apo wild-type α -thrombin to interchange between at least two different states is evidence to the fact that this molecule is in a dynamic state.

While functional and biophysical data has vouched for ligand induced extensive conformational change in thrombin scaffold, such structural transitions have remained elusive to x-ray crystallographic studies. Crystal structures of thrombin in presence of Na⁺, thrombomodulin, PAR₁, hirudin, hirugen, and PPACK have only revealed subtle changes when compared to apo thrombin. This has made it problematic to explain thrombin function in a structural framework. We recently proposed that Na⁺ activates thrombin by securing the correct orientation of the Glu¹⁹²-Gly¹⁹³ peptide bond, which is likely flipped in the absence of cation. In absence of Na⁺, flip in the Glu¹⁹²-Gly¹⁹³ peptide bond precludes the H-bond between backbone N of N₁₄₃ and backbone O of E₁₉₂. Loss of crucial H-bond renders the autolysis loop (harboring W₁₄₁ and W₁₄₈) in a flexible and dynamic state. This explains why in absence of Na⁺, we observe broad peaks for W₁₄₁ and most likely W₁₄₈. In presence of Na⁺, the H-bond between N₁₄₃ and E₁₉₂ secures the conformation of the autolysis loop thereby stabilizing W₁₄₁ and W₁₄₈ resulting in their sharp peaks. In addition to the overall sharpening of resonances, binding of Na⁺ results in one single resonance for W₂₀₇ starting from two distinct resonances in the apo form. W₂₀₇ and W₂₁₅ reside on the two ends of the 207-215 β-strand. It is quite possible that in absence of Na⁺, the E* to E equilibrium renders the entire β-strand flexible allowing tryptophans to sample two different states. This explains the two resonances observed for W₂₀₇. Binding of Na⁺ shifts the equilibrium in favor of E and stabilizes the entire β-strand thus sharpening the peaks. Recently, we provided crystallographic evidence of massive conformational

change in the thrombin mutant D102N scaffold upon binding of cleaved PAR₁ fragment to exosite I. We hypothesized that binding of PAR₁ induces changes in at least three tryptophans W₁₄₁, W₁₄₈, and W₂₁₅. To test this extreme flexibility observed once in the entire gamut of thrombin crystal structures, we obtained ¹⁹F-NMR spectra of thrombin bound to hirugen. Our ¹⁹F-NMR spectra of wild-type α -thrombin bound to hirugen and in the apo form clearly show that conformational changes are not restricted to these three tryptophans. In fact, binding of hirugen is felt throughout the molecule as evidenced by change in chemical shifts. Besides conformational change, hirugen also affects the residue dynamics as evidenced from change in the linewidth of resonances. This shows that binding of ligand at exosite I induces drastic conformational and dynamic changes in the wild-type α -thrombin scaffold.

Binding of Na⁺ and hirugen induces changes in the chemical environment as observed by changes in the chemical shifts as well as induces dramatic change in the residue dynamics as observed by sharpening of the peaks. Both these ligands induce distinct changes in the thrombin architecture, as the spectra of thrombin in presence of Na⁺ and that in presence of hirugen are significantly different. While binding of Na⁺ enhances the catalytic efficiency of the procoagulant and the prothrombotic substrates it is dispensable for the anticoagulant substrate protein C. Instead, binding of thrombomodulin to exosite I enhances the catalytic efficiency towards protein C by three orders of magnitude and shuts down the

procoagulant and prothrombotic activity. While previous crystal structure of thrombin bound to thrombomodulin did not show conformational changes because of cofactor binding, it was generally agreed that binding of Na^+ or exosite I ligand brought about similar conformational changes. Our NMR results show that binding of exosite I ligand and Na^+ induce distinct conformational changes and may be the basis of the opposing function in thrombin. Binding of both these ligands lock down the enzyme to different levels as observed by the differences in the linewidths of the peaks. While peaks in the Na^+ bound spectra are sharper compared to those in the hirugen bound spectra which in turn are sharper when compared to those in the apo form suggesting that binding of Na^+ is associated with higher entropy loss when compared to hirugen binding. Indeed, from stopped flow analysis, under similar conditions, binding of Na^+ is associated with ~ -16 kcal/mole whereas binding of hirugen is associated with -7 kcal/mole as observed from our calorimetry results. It was proposed that loss in entropy is due to uptake and ordering of water molecules along with binding of Na^+ based on the crystal structure observations. We show for the first time that in addition to the ordering of water molecules, loss in entropy is a direct consequence of loss in protein dynamics at the level of tryptophans. The drastic changes in the spectra of α -thrombin as a result of ligand binding are testament to the fact that the apo α -thrombin is in a highly dynamic state and that ligand binding induces major conformational and dynamic changes.

6.4.3. How different is the zymogen from the α -thrombin?

We have reported the ^{19}F -NMR spectra of prethrombin-2 and probed allostery using iTC₂₀₀. We chose to study prethrombin-2 as this zymogen precursor of thrombin has similar molecular weight when compared to α -thrombin. Cleavage between R15 and I16 in the catalytically inactive prethrombin-2 irreversibly transforms the zymogen to α -thrombin and renders enzyme activity. There are three crystal structures of prethrombin-2 (21, 40, 41), one bound to hirugen, the second bound to PPACK and staphylocoagulase and the third bound to fragment 2. When compared with the α -thrombin bound to PPACK, all four structures show highly similar overall architecture and identical conformations at the level of tryptophan side chains (data not shown). In prethrombin-2 crystal structures, the peptide bond between R15 and I16 is intact and hence the interaction between I16 and D194 is missing when compared to α -thrombin. This important missing H-bond interaction, albeit, has no effect on conformation of residues belonging to the catalytic triad that assume the canonical architecture as observed in the α -thrombin. In addition, it was recently proposed that prethrombin-2 is structurally same as the α -thrombin in the free form (29-31).

Although the catalytic residues adopt the correct orientation, with the O γ atom of S195 within 2.5 Å of the N ϵ 2 atom of H57 and the O δ 2 atom of D102 within 2.8 Å of the N ϵ 1 atom of H57, prethrombin-2 is catalytically inactive. It is known that prethrombin-2 has little or no significant Na⁺ effect on binding of ligands at the

exosite I (42). We have done similar experiments and have extended the prethrombin-2 characterization to show that there is little or no allosteric communication between the active site, Na⁺ binding site, and the exosite I in prethrombin-2. Furthermore, binding of hirudin is compromised ~ 6 orders of magnitude and is almost entirely mimicked by binding of hirugen. This suggests that the C-terminal fragment of hirudin is able to bind to exosite I as observed by binding of hirugen, but the N-terminal fragment of hirudin is not able to bind optimally as seen for wild-type α -thrombin. Crystal structure of thrombin bound to hirudin (43) documents a number of interactions between the N-terminus of hirudin and the catalytic S195. It is likely that these interactions are missing which can explain the huge loss in affinity for hirudin. It is difficult to reconcile properties of prethrombin-2 with the available crystal structures. There is no crystal structure of prethrombin-2 in the free form. It could be possible that a) binding of hirugen, PPACK or fragment 2 biases the true conformation of prethrombin-2, and b) there is more than one dominant conformation of prethrombin-2 in solution. Recently, our lab showed that prethrombin-1, another zymogen precursor of thrombin adopts an E* like conformation (manuscript under review). It could be hypothesized that prethrombin-2 also adopts an E* like conformation and there is an E* to E equilibrium in prethrombin-2 as was shown for prethrombin-1, meizothrombin (44), α -thrombin (10), and other serine proteases (45). Binding of argatroban employs a different mechanism as compared to hirudin. While the N-terminus of hirudin makes H-bond contacts with S195,

argatroban penetrates the primary specificity pocket and makes substrate like H-bonds with D189 of thrombin. Ability to penetrate the primary specificity pocket makes argatroban a favorable ligand to probe the E^* to E equilibrium. Our data shows that argatroban binds to prethrombin-2 with 22 fold lower affinity when compared to wild-type α -thrombin. This results in an r value ($r = E^*/E$) of 22 at 25 °C. The value of r , under similar conditions, for wild-type α -thrombin is 0.15. Such high value of r signifies that prethrombin-2 has a higher population of E^* in solution when compared to wild-type thrombin and that it exists in a similar E^* to E equilibrium. ^{19}F -NMR spectra of prethrombin-2 show sharp resonances when compared to apo wild-type α -thrombin suggesting that prethrombin-2 is less dynamic than α -thrombin. Furthermore, spectras of the apo forms of prethrombin-2 and α -thrombin show unequivocally that the chemical environments of tryptophans are drastically different especially in the regions of -46 to -48 ppm and -49 to -51 ppm. This suggests that the microenvironments of at least the tryptophans are not similar in the two forms of thrombin. ^{19}F -NMR results show that there is little or no effect of Na^+ on the properties of prethrombin-2. This is consistent with the calorimetric data presented in this work as well as previous fluorescence spectroscopic study. In their work, Bock et. al., reported that linkage between the Na^+ binding site and the exosite I is only expressed in the active form of the enzyme (meizothrombin and α -thrombin). On the other hand, hirugen and PPACK bind to prethrombin-2 as observed from the crystal structures of prethrombin-2. We have extended the analysis using

calorimetric data to show that there is little or no communication between exosite I, the Na⁺ binding site and the active site in the prethrombin-2 form of the enzyme. This is in sharp contrast to what is seen with the α -thrombin form where all the three domains are energetically linked. It can be concluded that prethrombin-2 and α -thrombin exhibit drastically different structural and functional properties.

6.4.4. Conundrum of substituting wild-type by mutant thrombin.

Allosteric interactions form the basis of thrombin's function with various substrates, cofactors, ligands, and inhibitors. Such interactions have been difficult to probe and frequently come in our way to use thrombin mutants instead of wild-type thrombin for a given assay. In a recent NMR work on thrombin (31), the authors used a variant form of thrombin, E217K, to assign the chemical shifts of thrombin in the unliganded form. Although a remarkable achievement, it should be pointed out that properties of E217K are distinctly different than wild-type α -thrombin. Functional characterization of this variant form of thrombin has revealed that the procoagulant and prothrombotic properties are compromised to an extent that this mutant was pursued as a potential anticoagulant (39, 46). Later structural characterization of this mutant revealed a collapse in the active site (13), which now has been assigned as a unique signature for the E* like properties. It is then not a surprise that any interpretation of the E217K mutant is not a true interpretation of the wild-type α -thrombin. Instead, the E217K mutant represents

the E* form of thrombin. Similar E*-like collapse has been documented for the thrombin mutant WE, which is also a very potent anticoagulant. Comparison of ¹⁹F-NMR spectra of the wild-type and the thrombin mutant WE confirms that it is not a good reagent to substitute as wild-type enzyme for solution based studies. In conclusion, one has to employ wild-type protein to probe the wild-type structure in solution.

6.5. Materials and Methods:

Functional and structural properties of ¹⁹F-tryptophan labeled thrombin.

Protein expression in *E. coli* has been the expression of choice for ¹⁹F-NMR purposes (32, 34, 47). We have developed a recombinant thrombin expression system using *E. coli* (48-50). All proteins, except W29F, were expressed and purified to homogeneity. All attempts to express the W29F mutant failed suggesting a) a role for W29 in refolding prethrombin-2, and b) that substitution of tryptophan sidechain with a phenylalanine is not a good choice although crystal structures suggest the indole ring to be occupying a hydrophobic environment. *E. coli* does not have the capability to introduce glycosylation at the sole site in human thrombin at position N60g. To characterize the properties of thrombin expressed using the *E. coli* expression system, we report the catalytic efficiency of the labeled thrombin for all the relevant substrates. We have also crystallized labeled thrombin in the presence of PPACK. Table 1 shows that functional and structural properties of labeled thrombin are identical to the mammalian

expressed thrombin. This suggests that neither the glycosylation nor the labeling affect catalytic efficiency and specificity of thrombin for different substrates. Figure 6.1 shows the crystal structure of ^{19}F -thrombin bound to PPACK overlaid with thrombin bound to PPACK expressed in the mammalian expression system. The C_{α} rmsd between the two structures is 0.3 Å suggesting an overall architecture of labeled thrombin highly similar to that from mammalian expressed thrombin. Electron density for the ^{19}F atom was detected at the fifth position of all the nine tryptophans. Table 6.2. summarizes the relevant parameters of the crystal structure.

^{19}F -NMR Spectroscopy. NMR spectra were recorded on a Varian Unity-Plus 500 MHz spectrometer operating at 470.3 MHz with Varian Cryo-Q dedicated 5-mm ^{19}F probe. The cryoprobe was maintained at 20°K with the Varian Cryo-Q Open Cycle Cryogenic system. The temperature of the sample was maintained at 25°C with the XR11851 Air-Jet Crystal Cooler heat exchanger (FTS Systems, Stone Ridge, NY). The 90° pulse width was 13 ms for the room temperature probe and 6.3 ms for the cryoprobe, and all spectra processed with 5 Hz line broadening. The T_1 relaxation times were determined by the inversion recovery method. All spectra were referenced to an internal standard of 5-fluorotryptophan (0.3 mM), and all samples contained 10% (vol/vol) D_2O and 10 mM Tris, pH 8.0. No correction to pH with D_2O in the sample was made. The NMR spectrum of free 5-fluorotryptophan (^{19}F -W) in solution with our standard buffer lies at a chemical shift of -49.5 ppm.

Addition of Na⁺ or PPACK does not affect the chemical shift of free 5-fluorotryptophan. Addition of hirugen does not affect the chemical shift of free 5-fluorotryptophan but gives an additional peak at -44.2 ppm. We believe that the additional peak at -44.2 ppm in presence of hirugen is a result of contaminating tri-fluoroacetic acid (TFA) used during the purification of the peptide (personal communication with Sigma-Aldrich).

iTC. Binding of the active site inhibitor argatroban was studied directly by isothermal titration calorimetry under experimental conditions of 5 mM Tris, 0.1% PEG 8000, 200 mM ChCl, pH 8.0, at 25 °C, using an iTC200 calorimeter (MicroCal Inc., Northampton, MA) with the sample cell containing thrombin and the syringe injecting argatroban. The sample volume for iTC200 was 204.6 µl, and the total volume of injected ligand was 39.7 µl. The thermal equilibration step at 25 °C was followed by an initial 60-s delay step and subsequently an initial 0.2-µl injection. Typically, 19 serial injections of 2 µl and 1 last injection of 1.5 µl of ligand were performed at an interval of 180 s. The stirring speed was maintained at 1000 rpm, and the reference power was kept constant at 5 microcalories/s. The heat associated with each injection of ligand was integrated and plotted against the molar ratio of ligand to macromolecule. Thermodynamic parameters were extracted from a curve fit to the data using the software (Origin 7.0) provided by MicroCal according to a one-site binding model.

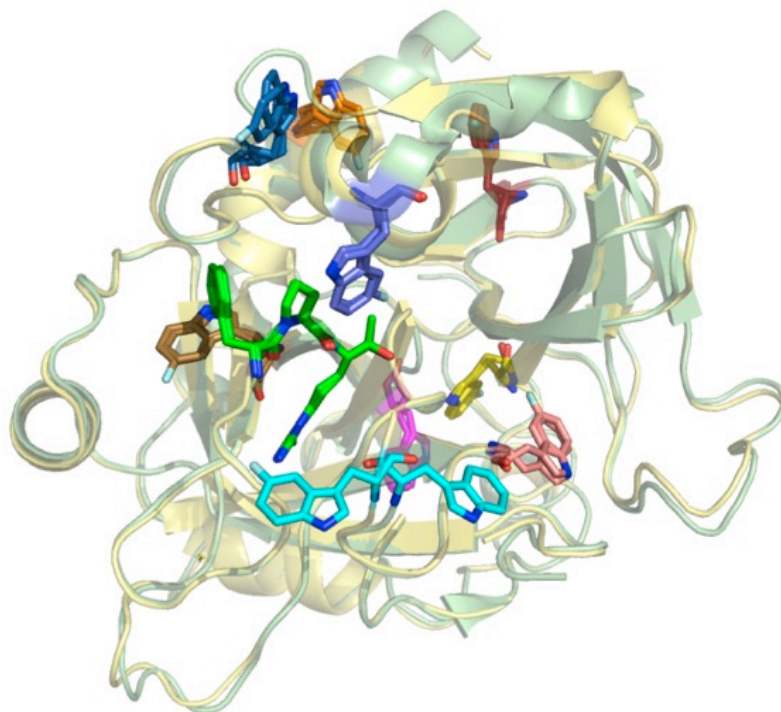


Figure 6.1. Alignment of *E. coli* expressed wild-type ^{19}F -thrombin and BHK expressed wild-type thrombin bound to PPACK. $C\alpha$ rmsd is 0.3 Å. PPACK (green) and tryptophans are shown in sticks. Except for W₁₄₈ (cyan) all the tryptophan's overlay on top of each other suggesting that labeling does not affect thrombin architecture.

| Substrates | ^{19}F-WT | BHK_WT |
|--------------------|--------------------------------------|---------------|
| FPK: Na^+ | 6.76 | 4.59 |
| FPK: Ch^+ | 0.44 | 0.44 |
| Protein C | 0.12 | 0.19 |
| Fibrinogen | 13.09 | 13.51 |
| PAR ₁ | 22.86 | 20.94 |

Table 6.1. Catalytic efficiency, k_{cat}/K_m ($\mu\text{M}^{-1}\cdot\text{sec}^{-1}$), of ^{19}F labeled wild-type and unlabeled wild-type for different substrates. FPK is a synthetic substrate, while protein C, fibrinogen, and PAR₁ are physiological substrates. All errors are within 10 % of the absolute value.

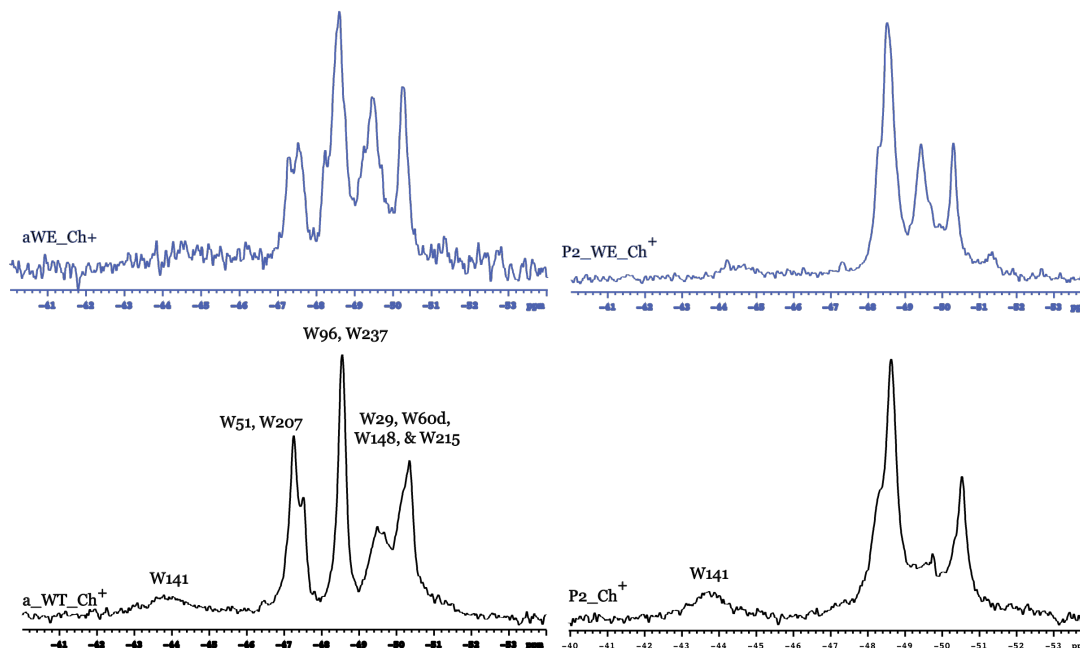


Figure 6.2. ^{19}F -NMR spectra of apo wild-type (black) and WE mutant (blue) in α -thrombin and prethrombin-2 forms. The two wild-type spectras show significant differences between -46.5 ppm to -48 ppm and -49 ppm to -50 ppm suggesting significant differences in the two structures in solution. The two spectra of WE mutant also show significant differences when compared to wild-type thrombin emphasizing the importance of using the wild-type construct for assignments in any solution based structural studies.

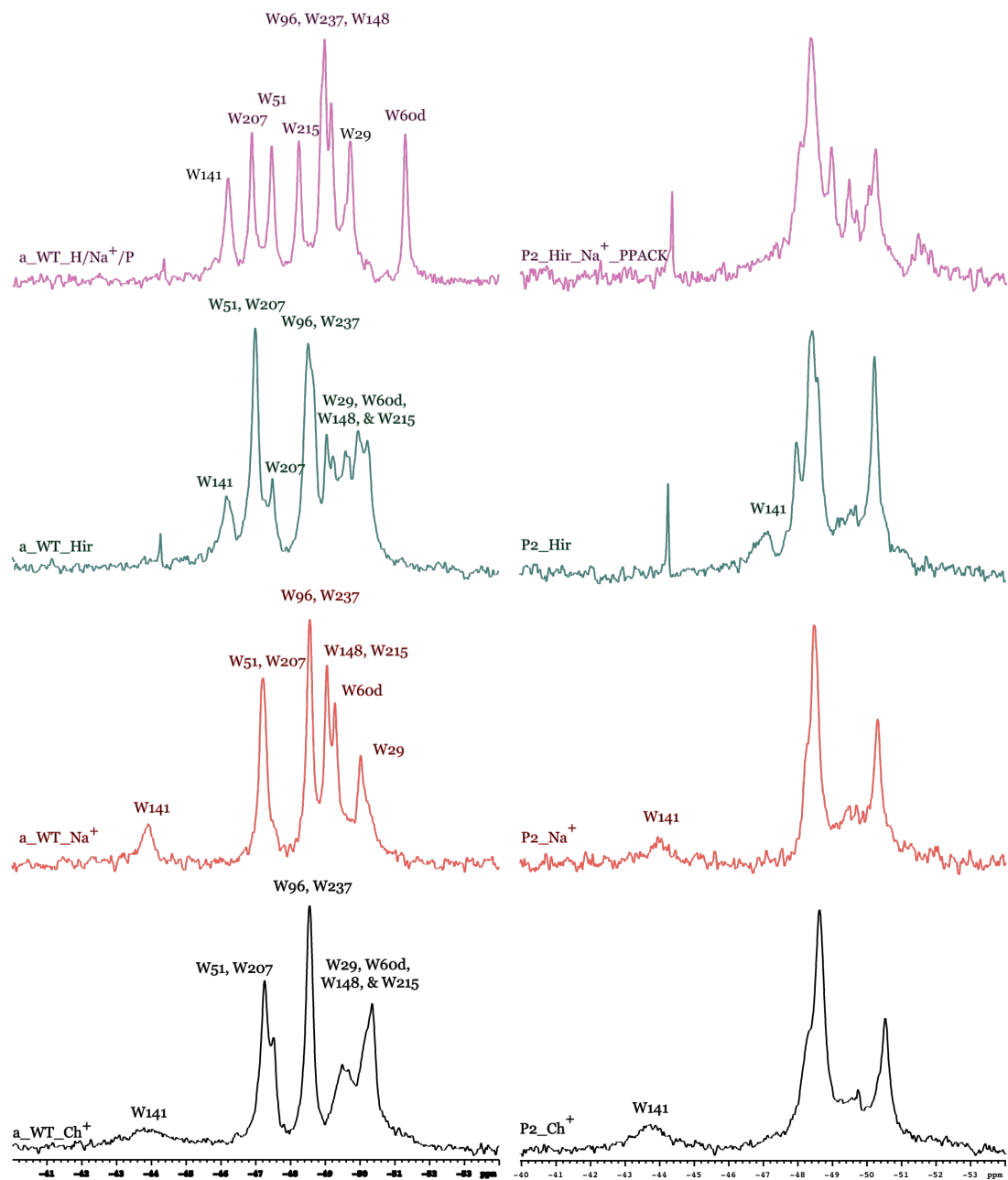


Figure 6.3. ^{19}F -NMR spectra of wild-type α -thrombin and prethrombin-2 in the apo form (black), in presence of Na^+ (red), in presence of hirugen (green), and in presence of Na^+ , hirugen and PPACK (magenta).

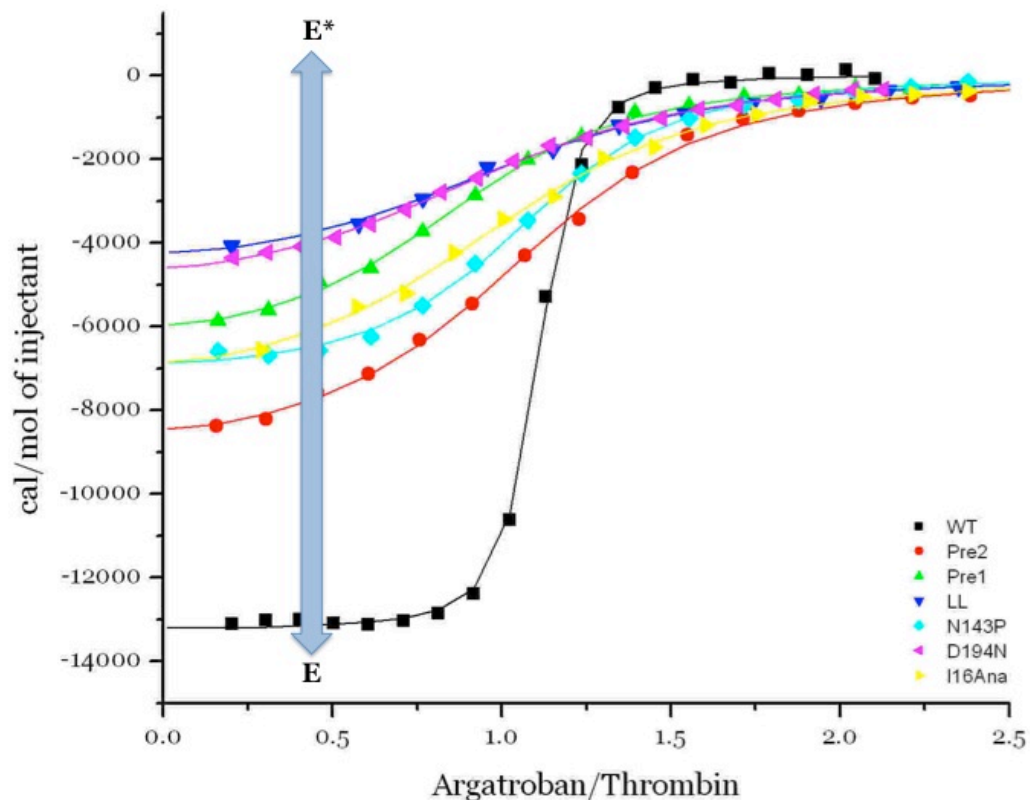


Figure 6.4. Argatroban binding to thrombin variants using isothermal titration calorimetry. Binding isotherms for argatroban binding to wild-type ($K_d = 0.04 \mu\text{M}$, $\Delta H = -13.2$ kcal/mole, $T\Delta S = -3.07$ kcal/mole), prethrombin-1 ($K_d = 2.7 \mu\text{M}$, $\Delta H = -6.58$ kcal/mole, $T\Delta S = 1.02$ kcal/mole), prethrombin-2 ($K_d = 0.71 \mu\text{M}$, $\Delta H = -9.12$ kcal/mole, $T\Delta S = -0.74$ kcal/mole), loopless ($K_d = 3.2 \mu\text{M}$, $\Delta H = -4.81$ kcal/mole, $T\Delta S = 2.69$ kcal/mole), and N₁₄₃P ($K_d = 1 \mu\text{M}$, $\Delta H = -7.2$ kcal/mole, $T\Delta S = 3.32$ kcal/mole), D₁₉₄N ($K_d = 9.5 \mu\text{M}$, $\Delta H = -5.19$ kcal/mole, $T\Delta S = 1.65$ kcal/mole) and I_{16A}_Na⁺ ($K_d = 0.35 \mu\text{M}$, $\Delta H = -9.38$ kcal/mole, $T\Delta S = -0.57$ kcal/mole) mutants of thrombin.

| Species | 29 | 51 | 60d | 96 | 141 | 148 | 207 | 215 | 237 |
|---|----------|----------|----------|----------|----------|----------|----------|----------|----------|
| Dasyus Novemcinctus, Armadillo | X | W | W | W | X | X | W | W | W |
| Loxodonta Africana, Elephant | X | W | W | X | W | W | W | W | W |
| Spermophilus Tridecemlineatus, Squirrel | X | W | W | W | W | W | W | W | W |
| Danio Rerio, Zebrafish | W | W | W | W | W | W | W | W | W |
| ACITR | X | W | W | W | W | W | W | W | W |
| Oncorhynchus my Kiss, Fish | W | W | W | W | W | W | W | W | W |
| Fugu Rubripes, Fish | W | W | W | W | W | F | W | W | W |
| Tetraodon Nigroviridis, Fish | W | W | W | W | W | Y | W | W | W |
| Gasterosteus Aaculeatus, Fish | W | W | W | W | W | W | W | W | W |
| Eptatretus Stoutii, Hagfish | W | W | W | W | W | W | W | W | W |
| Gecko Gecko, Lizard | X | W | W | W | W | W | W | W | W |
| Xenopus Laevis, Frog | W | W | W | W | W | W | W | W | W |
| Xenopus Tropicalis, Frog | W | W | W | W | W | W | W | W | W |
| Cynops Pyrrhogaster, Newt | X | W | W | W | W | W | W | W | W |
| Gallus Gallus, Chicken | W | W | W | W | W | W | W | W | W |
| Struthio Camelus, Ostrich | W | W | W | W | W | W | W | W | W |
| Human | W | W | W | W | W | W | W | W | W |
| Pan Troglodytes, Monkey | W | W | W | W | W | W | W | W | W |
| T_PON | W | W | W | W | W | W | W | W | W |
| Macaca Mulatta, Monkey | W | W | W | W | W | W | W | W | W |
| Mouse | W | W | W | W | W | W | W | W | W |
| Rat | W | W | W | W | W | W | W | W | W |
| Oryctolagus Cuniculus, Rabbit | X | W | W | W | W | W | W | W | W |
| Equus Caballus, Horse | W | W | W | W | W | W | W | W | W |
| Bovine | W | W | W | W | W | W | W | W | W |
| Pig | W | W | W | W | W | W | W | W | W |
| Erinaceus Europaeus, Hedgehog | X | W | W | W | W | W | W | W | W |

Table 6.3. Sequence alignment of thrombin from 27 different species. Human thrombin is marked in red. X (blue) represents that the amino acid was not determined. In only two instances (green), the tryptophan at that position is not conserved. Even in that situation, there is a presence of an aromatic residue similar to a tryptophan.

6.6. References:

1. Wells CM & Di Cera E (1992) Thrombin is a Na(+)-activated enzyme. *Biochemistry* 31(47):11721-11730.
2. Adams TE & Huntington JA (2006) Thrombin-cofactor interactions: structural insights into regulatory mechanisms. *Arteriosclerosis, thrombosis, and vascular biology* 26(8):1738-1745.
3. Davie EW & Kulman JD (2006) An overview of the structure and function of thrombin. *Seminars in thrombosis and hemostasis* 32 Suppl 1:3-15.
4. Di Cera E (2008) Thrombin. *Molecular aspects of medicine* 29(4):203-254.
5. Di Cera E, Page MJ, Bah A, Bush-Pelc LA, & Garvey LC (2007) Thrombin allostery. *Phys Chem Chem Phys* 9(11):1291-1306.
6. Huntington JA (2005) Molecular recognition mechanisms of thrombin. *J Thromb Haemost* 3(8):1861-1872.
7. Huntington JA & Esmon CT (2003) The molecular basis of thrombin allostery revealed by a 1.8 Å structure of the "slow" form. *Structure* 11(4):469-479.
8. Pineda AO, *et al.* (2004) Molecular dissection of Na⁺ binding to thrombin. *The Journal of biological chemistry* 279(30):31842-31853.
9. Pineda AO, Savvides SN, Waksman G, & Di Cera E (2002) Crystal structure of the anticoagulant slow form of thrombin. *The Journal of biological chemistry* 277(43):40177-40180.

10. Bah A, Garvey LC, Ge J, & Di Cera E (2006) Rapid kinetics of Na⁺ binding to thrombin. *The Journal of biological chemistry* 281(52):40049-40056.
11. Lai MT, Di Cera E, & Shafer JA (1997) Kinetic pathway for the slow to fast transition of thrombin. Evidence of linked ligand binding at structurally distinct domains. *The Journal of biological chemistry* 272(48):30275-30282.
12. Pineda AO, *et al.* (2004) The anticoagulant thrombin mutant W₂₁₅A/E₂₁₇A has a collapsed primary specificity pocket. *The Journal of biological chemistry* 279(38):39824-39828.
13. Carter WJ, Myles T, Gibbs CS, Leung LL, & Huntington JA (2004) Crystal structure of anticoagulant thrombin variant E₂₁₇K provides insights into thrombin allostery. *The Journal of biological chemistry* 279(25):26387-26394.
14. Niu W, *et al.* (2009) Mutant N₁₄₃P reveals how Na⁺ activates thrombin. *The Journal of biological chemistry* 284(52):36175-36185.
15. Gandhi PS, Page MJ, Chen Z, Bush-Pelc L, & Di Cera E (2009) Mechanism of the anticoagulant activity of thrombin mutant W₂₁₅A/E₂₁₇A. *The Journal of biological chemistry* 284(36):24098-24105.
16. Bah A, Carrell CJ, Chen Z, Gandhi PS, & Di Cera E (2009) Stabilization of the E* form turns thrombin into an anticoagulant. *The Journal of biological chemistry* 284(30):20034-20040.
17. Pineda AO, *et al.* (2006) Crystal structure of thrombin in a self-inhibited conformation. *The Journal of biological chemistry* 281(43):32922-32928.

18. Liu LW, Vu TK, Esmon CT, & Coughlin SR (1991) The region of the thrombin receptor resembling hirudin binds to thrombin and alters enzyme specificity. *The Journal of biological chemistry* 266(26):16977-16980.
19. Xu H, Bush LA, Pineda AO, Caccia S, & Di Cera E (2005) Thrombomodulin changes the molecular surface of interaction and the rate of complex formation between thrombin and protein C. *The Journal of biological chemistry* 280(9):7956-7961.
20. Fuentes-Prior P, *et al.* (2000) Structural basis for the anticoagulant activity of the thrombin-thrombomodulin complex. *Nature* 404(6777):518-525.
21. Vijayalakshmi J, Padmanabhan KP, Mann KG, & Tulinsky A (1994) The isomorphous structures of prethrombin₂, hirugen-, and PPACK-thrombin: changes accompanying activation and exosite binding to thrombin. *Protein Sci* 3(12):2254-2271.
22. Celikel R, *et al.* (2003) Modulation of alpha-thrombin function by distinct interactions with platelet glycoprotein Ibalpha. *Science* 301(5630):218-221.
23. Dumas JJ, Kumar R, Sehra J, Somers WS, & Mosyak L (2003) Crystal structure of the GpIbalpha-thrombin complex essential for platelet aggregation. *Science* 301(5630):222-226.
24. Rydel TJ, *et al.* (1990) The structure of a complex of recombinant hirudin and human alpha-thrombin. *Science* 249(4966):277-280.

25. Skrzypczak-Jankun E, Rydel TJ, Tulinsky A, Fenton JW, 2nd, & Mann KG (1989) Human D-Phe-Pro-Arg-CH₂-alpha-thrombin crystallization and diffraction data. *J Mol Biol* 206(4):755-757.
26. Bah A, Chen Z, Bush-Pelc LA, Mathews FS, & Di Cera E (2007) Crystal structures of murine thrombin in complex with the extracellular fragments of murine protease-activated receptors PAR₃ and PAR₄. *Proceedings of the National Academy of Sciences of the United States of America* 104(28):11603-11608.
27. Gandhi PS, Chen Z, Mathews FS, & Di Cera E (2008) Structural identification of the pathway of long-range communication in an allosteric enzyme. *Proceedings of the National Academy of Sciences of the United States of America* 105(6):1832-1837.
28. Huntington JA (2005) Slow thrombin in solution. *The Biochemical journal* 390(Pt 2):e1-3.
29. Huntington JA (2009) Slow thrombin is zymogen-like. *J Thromb Haemost* 7 Suppl 1:159-164.
30. Kamath P, Huntington JA, & Krishnaswamy S (2010) Ligand binding shuttles thrombin along a continuum of zymogen-like and proteinase-Like states. *The Journal of biological chemistry* .
31. Lechtenberg BC, Johnson DJ, Freund SM, & Huntington JA (2010) NMR resonance assignments of thrombin reveal the conformational and dynamic

- effects of ligation. *Proceedings of the National Academy of Sciences of the United States of America* 107(32):14087-14092.
32. Bann JG, Pinkner J, Hultgren SJ, & Frieden C (2002) Real-time and equilibrium ¹⁹F-NMR studies reveal the role of domain-domain interactions in the folding of the chaperone PapD. *Proceedings of the National Academy of Sciences of the United States of America* 99(2):709-714.
 33. Danielson MA & Falke JJ (1996) Use of ¹⁹F NMR to probe protein structure and conformational changes. *Annu Rev Biophys Biomol Struct* 25:163-195.
 34. Frieden C, Hoeltzli SD, & Bann JG (2004) The preparation of ¹⁹F-labeled proteins for NMR studies. *Methods in enzymology* 380:400-415.
 35. Arosio D, Ayala YM, & Di Cera E (2000) Mutation of W215 compromises thrombin cleavage of fibrinogen, but not of PAR-1 or protein C. *Biochemistry* 39(27):8095-8101.
 36. Dang QD, Sabetta M, & Di Cera E (1997) Selective loss of fibrinogen clotting in a loop-less thrombin. *The Journal of biological chemistry* 272(32):19649-19651.
 37. Guinto ER & Di Cera E (1997) Critical role of W60d in thrombin allostery. *Biophysical chemistry* 64(1-3):103-109.
 38. Tsiang M, *et al.* (1995) Functional mapping of the surface residues of human thrombin. *The Journal of biological chemistry* 270(28):16854-16863.

39. Tsiang M, *et al.* (1996) Protein engineering thrombin for optimal specificity and potency of anticoagulant activity in vivo. *Biochemistry* 35(51):16449-16457.
40. Adams TE, Li, W., Freund, S.M.V., Huntington, J.A. (2010) Zymogenizing a Zymogen - The Crystal Structure of the F2-Prethrombin₂ Complex. (Translated from English) *To be published* (in English).
41. Friedrich R, *et al.* (2003) Staphylocoagulase is a prototype for the mechanism of cofactor-induced zymogen activation. *Nature* 425(6957):535-539.
42. Kroh HK, Tans G, Nicolaes GA, Rosing J, & Bock PE (2007) Expression of allosteric linkage between the sodium ion binding site and exosite I of thrombin during prothrombin activation. *The Journal of biological chemistry* 282(22):16095-16104.
43. Rydel TJ, Tulinsky A, Bode W, & Huber R (1991) Refined structure of the hirudin-thrombin complex. *J Mol Biol* 221(2):583-601.
44. Papaconstantinou ME, Gandhi PS, Chen Z, Bah A, & Di Cera E (2008) Na⁺ binding to meizothrombin desF1. *Cell Mol Life Sci* 65(22):3688-3697.
45. Vogt AD, Bah A, & Di Cera E (2010) Evidence of the E*-E Equilibrium from Rapid Kinetics of Na(+) Binding to Activated Protein C and Factor Xa* (dagger). *J Phys Chem B*.
46. Gibbs CS, *et al.* (1995) Conversion of thrombin into an anticoagulant by protein engineering. *Nature* 378(6555):413-416.

47. Schuler B, Kremer W, Kalbitzer HR, & Jaenicke R (2002) Role of entropy in protein thermostability: folding kinetics of a hyperthermophilic cold shock protein at high temperatures using ^{19}F NMR. *Biochemistry* 41(39):11670-11680.
48. DiBella EE, Maurer MC, & Scheraga HA (1995) Expression and folding of recombinant bovine prethrombin-2 and its activation to thrombin. *The Journal of biological chemistry* 270(1):163-169.
49. Johnson DJ, Adams TE, Li W, & Huntington JA (2005) Crystal structure of wild-type human thrombin in the Na^+ -free state. *The Biochemical journal* 392(Pt 1):21-28.
50. Soejima K, *et al.* (2001) An efficient refolding method for the preparation of recombinant human prethrombin-2 and characterization of the recombinant-derived alpha-thrombin. *Journal of biochemistry* 130(2):269-277.
51. Fredenburgh JC, Stafford AR, & Weitz JI (1997) Evidence for allosteric linkage between exosites 1 and 2 of thrombin. *The Journal of biological chemistry* 272(41):25493-25499.

7. Conclusions and Future directions

Kinetic, thermodynamic and structural data from the present work vouches for an extremely plastic thrombin scaffold. Crystallographic studies have shown that while the E* to E transition is associated with massive conformational change, transition from the E form to the E:Na⁺ form is rather subtle in terms of conformational change. We have elucidated the allosteric pathway, in a first of its kind, between the active site and the exosite I of thrombin in terms of a network of polar interactions. We have complemented our crystallographic studies with solution based structural studies using ¹⁹F-NMR. We report the first ¹⁹F-NMR spectra of wild-type thrombin. Our results conclusively show that apo α -thrombin is a highly dynamic and flexible molecule. Apo α -thrombin is in equilibrium with at least two states. Binding of ligands strips thrombin of its dynamic property. It also reveals that the closest zymogen from of thrombin, prethrombin-2, is not similar to the wild-type apo α -thrombin in solution. This new information has enormous implications on our understanding of thrombin function and allostery. In addition, we have also solved the crystal structure of thrombin bound to uncleaved extracellular fragment of PAR₁ that documents a productive binding mode. Data from current thesis reveals novel insights into thrombin macromolecular recognition and the underlying allosteric interactions. Four lines of future investigations are outlined that take advantage of the current findings.

7.1. Protein Engineering. Tremendous success has been achieved by elucidating the role of W₂₁₅, E₂₁₇, and autolysis loop in thrombin function. Thrombin mutant W₂₁₅A/E₂₁₇A (WE) has been documented to show potent anticoagulant activity *in vitro* and *in vivo*. On going aggressive permutation and combination mutation strategy coupled with saturation mutagenesis of these important residues should facilitate in the discovery of second generation of anticoagulant thrombin molecules (ATM). Nevertheless, dissociating thrombin functions remains challenging and high priority. An important property that any next generation ATM should possess is the negligible activity towards procoagulant and prothrombotic substrates while retaining the wild-type like anticoagulant activity. The three physiological substrates that thrombin interacts with share Arg at the P₁ site. Therefore, differences in thrombin activity towards these substrates should come from interactions beyond the primary specificity pocket of the enzyme. Identifying novel thrombin-substrate interactions beyond active site region should reveal important targets for mutagenesis. Such efforts have been hampered in part because of little or no relevant structural data on thrombin-substrate interaction. We have presented the crystal structure of thrombin bound to uncleaved extracellular fragment of PAR₁ in a productive binding mode. Our model reveals novel intermolecular interactions in and beyond the active site region that could be exploited by protein engineering for therapeutic purposes.

7.2. Crystal structure of thrombin bound to PAR₄. Human platelet expresses PAR₁ and PAR₄ on its surface. Activation of platelets can occur through PAR₁ and/or PAR₄. In case of drugs targeting PARs for therapeutic intervention in patients with acute coronary syndromes, it is therefore obvious that both PAR₁ and PAR₄ should be targeted for better efficacy. There is currently no crystal structure of human thrombin bound to human PAR₄. Mutagenesis studies have revealed that PAR₄ does not interact with exosite I of thrombin. In such a case, is the interaction of PAR₄ similar to what was observed with the murine thrombin complexed with murine PAR₄ crystal structure? To have a thorough understanding of how thrombin interacts with PARs, it is essential to solve the crystal structure of thrombin bound to the uncleaved extracellular fragment of PAR₄. In mouse studies, it was shown that cleaved PAR₁ can act as a cofactor and assist in the cleavage of the nearby PAR₄ receptor. How does thrombin accommodate cleaved PAR₁ and uncleaved PAR₄ fragments is of significant mechanistic importance. These studies will complement our recent thrombin-PAR₁ crystal structure and open the doors for protein engineering studies to completely abolish thrombin-PARs interaction.

7.3. Structural studies of E* and E. Three mutants including D102N, N143P, and autolysis loop deletion mutant have crystallized in the E* conformation. Our hypothesis states that in absence of any ligands or cofactors, thrombin exists in equilibrium between two forms E* and E. While it was shown for D102N that at 15

°C, the E* to E ratio is 1. This suggests that either forms of thrombin are likely to be crystallized when working with D102N. We have crystallized the E* form using the D102N construct. To provide a proof of concept, it would be ideal to crystallize the E form using the same reagent. Similar analysis of the E* to E content cannot be applied to N143P and the autolysis loop deletion mutant because of lack of slow phase and loss of W148 respectively. Nevertheless, similar arguments apply to these mutants and their equivalent E form should be crystallized using the same reagent. We have had preliminary success in crystallizing the N143P form in absence of any ligands or effectors in a conformation more akin to the E form of thrombin. This crystal structure came from a protein obtained from the *E. coli* expression system. Efforts are on to crystallize the E* form of the N143P from the *E. coli* expressed protein.

7.4. NMR studies of thrombin. ¹⁹F-NMR data has added to the wealth of structural information already obtained from x-ray crystallography studies. ¹⁹F-NMR studies have convincingly shown that a) apo wild-type α -thrombin is a dynamic molecule and in absence of any ligands is in equilibrium with at least two states, b) binding of Na⁺ and hirugen induce distinct, global, and significant conformational change in the thrombin scaffold suggesting that the thrombin scaffold is very flexible, c) In presence of saturating amount of hirugen, wild-type thrombin is in equilibrium between at least two states, d) apo wild-type α -thrombin is distinct from its closest zymogen form, prethrombin-2. Overall, ¹⁹F-

NMR studies presented in this thesis have revealed data not amenable to other techniques. This should warrant full-scale NMR experiments of wild-type α -thrombin and other important mutants with an emphasis on the role of protein dynamics in thrombin allostery and function. Such experiments will not limit information to few residues and may reveal novel insights. Furthermore, an emphasis should be given to track the E* conformation in solution. Three distinct signatures of E* including collapsed active site, compromised Na⁺ binding site and non-optimal oxyanion hole could be exploited to specifically label for NMR purposes. Similar strategy was used by labeling thrombin with ¹⁹F-tryptophans. The E* conformation depicts W215 and W60d within 3.5 Å of each other. It was thought that NOESY experiments with labeled thrombin should show a cross peak. Indeed, resonances similar to a cross peak populated the 2D spectrum. The problem arose because of the proximity of the 2D resonance and the individual resonances. This has made it difficult to assign the cross peak with high confidence. Future work should be attempted to avoid similar situation and different sites should be chosen for labeling purposes.

Curriculum Vitae Prafull S. Gandhi

Washington University - School of Medicine

Department of Biochemistry and Molecular Biophysics

St. Louis, MO 63110

E-mail: prafullsg@gmail.com

Cell: (314) 229 - 2980

Education & Training

- **Ph.D. in Molecular Biophysics**, 2004 - 2010
Washington University - School of Medicine, St. Louis, USA

Academic Advisor: Prof. Enrico Di Cera
Chairman, Department of Biochemistry and Molecular Biology
Saint Louis University, St. Louis, USA

- **M.S. in Chemical Engineering**, 2002 - 2004
Missouri University of Science and Technology, Rolla, USA

Academic Advisor: Prof. Philip D. Whitefield
Chairman, Chemistry Department,
Missouri University of Science and Technology, Rolla, USA

- **Bachelors in Chemical Engineering**, 1997 - 2001
Pune University, India

Academic Advisor: Prof. Avinash G. Patil
CEO, Synergy Process Systems, Pune, India

Research Skills

- Protein engineering, expression, refolding and purification: Site-directed mutagenesis and molecular biology. Experience with *E. coli*, yeast, and mammalian expression systems. Isolating protein from the inclusion bodies and refolding. Develop and execute protocols for protein purification using standard FPLC/HPLC chromatographic separation techniques including ion exchange, affinity, size exclusion, and hydrophobic interaction chromatography. Analytical techniques such as SDS-PAGE and Western blot.
- Enzyme kinetics: UV/VIS spectroscopy & High Pressure Liquid Chromatography (HPLC)

- Macromolecular interactions: Extensive experience with Isothermal titration calorimeter (iTC200), Differential scanning calorimeter (DSC), Fluorescence spectroscopy, and Stopped-flow fluorescence.
- Structural biology: X-ray crystallography and 1D NMR. Hands-on experience with crystallography dispenser robot; Phoenix, Art Robbins Instruments. Experience with software to process crystallographic data including HKL-2000, CCP4 suite, Coot, and PyMol.

Awards & Honors:

- International Alumni Association of Shri Mahavir Jain Vidyalaya (IAAMJV) scholarship for outstanding graduate students.
2002 – 2004, <http://www.iaamjv.org/>

Presentations

- **Gandhi, P.S.**, Chen, Z., Mathews, F. S. & Di Cera, E. (2008) Structural and functional studies of thrombin allostery. Biochemistry and Molecular Biophysics Retreat.
- **Gandhi, P.S.**, Chen, Z., Mathews, F. S. & Di Cera, E. (2008) Structural and functional studies of thrombin allostery. Gibbs conference on Biothermodynamics, Carbondale, IL.
- **Gandhi, P. S.**, Chen, Z., & Di Cera, E. (2010) Structural studies of thrombin-PAR₁ interaction. American Crystallographic Association, Chicago, IL.
- **Gandhi, P.S.**, Zapata, F., DeKoster, G., Chen, Z., Frieden, C., Di Cera E., (2010) ¹⁹F-NMR studies of thrombin allostery. Gibbs conference on Biothermodynamics, Carbondale, IL.
- Numerous departmental and journal club presentations.

Publications

- Marino, F., Bush-Pelc, L., Vogt, A., **Gandhi, P.S.**, Di Cera, E. (2010) Engineering thrombin for selective specificity toward protein C and PAR₁. *J. Biol. Chem.*, 285(25): 19145-52.
- **Gandhi, P.S.**, Chen, Z., Di Cera, E. (2010) Crystal structure of thrombin bound to the uncleaved extracellular fragment of PAR₁. *J. Biol. Chem.*, 285(20): 15393-8.

- Niu, W., Chen, Z., Bah, A., Bush-Pelc, L., **Gandhi, P.S.**, Di Cera, E., (2009) Mutant N143P reveals how Na⁺ activates thrombin. *J. Biol. Chem.*, 284(52): 36175-85.
- **Gandhi, P.S.**, Page, M. J., Chen, Z., Bush-Pelc, L., Di Cera, E. (2009) Mechanism of the anticoagulant activity of the thrombin mutant W215A/E217A. *J. Biol. Chem.*, 284(36): 24098-105.
- Bah, A., Carrell, C.J., Chen, Z., **Gandhi, P.S.**, Di Cera, E. (2009) Stabilization of the E* form turns thrombin into an anticoagulant. *J. Biol. Chem.*, 284(30): 20034-40.
- Papaconstantinou, M., **Gandhi, P.S.**, Chen, Z., Bah, A., Di Cera, E. (2008) Na⁺ binding to meizothrombin desF1. *Cellular and Mol. Life Sci.*, 65(22): 3688-97.
- **Gandhi, P.S.**, Chen, Z., Mathews, F. S. & Di Cera, E. (2008) Structural identification of the pathway of long-range communication in an allosteric enzyme. *Proceedings of National Academy of Sciences*, 105(6): 1832-7.